

## ABSTRACT

Title of Document:                    BIOLOGICAL CHARACTERIZATION OF  
TWO PUTATIVE DNA METABOLIZING  
ENZYMES IN *DEINOCOCCUS*  
*RADIODURANS*

Charles W. Mueller, Doctor of Philosophy, 2014

Directed By:                            Dr. Douglas Julin, Department of Chemistry and  
Biochemistry

HerA proteins are members of the FtsK-HerA superfamily of P-loop ATPases. FtsK is a bacterial protein that translocates double-stranded DNA during cell division. In archaea, *herA* is an essential gene that encodes an enzyme believed to be important for recombinational DNA repair. It is typically found in an operon with a gene that codes for a nuclease, *nurA*. Homologs of *herA* and *nurA* are found in a few bacterial genomes. In most cases, these bacteria lack an *ftsK* homolog. The functions of NurA and HerA in bacteria are not known. We chose to investigate the roles of NurA and HerA in *Deinococcus radiodurans*, typically studied for its extreme resistance to double-strand DNA breaks. The *D. radiodurans* genome has homologs of *nurA* and *herA* in an operon, and it also has an *ftsK* gene. We made strains with deletions of either *herA* or *nurA* and characterized their sensitivity to DNA damaging agents and basic growth properties. The results indicate that neither gene is essential in *D. radiodurans*, and deletions of the genes do not cause significant sensitivity to DNA

damaging agents. The *herA* deletion strain displayed a distinct phenotype consisting of slower growth and larger cell types. The *herA* phenotype in *D. radiodurans* is similar to that of mutation of *ftsK* homologs in *Escherichia coli* and *Bacillus subtilis*. The results suggest that HerA has an FtsK-like function in cell division, rather than acting in DNA repair, in *D. radiodurans*.

BIOLOGICAL CHARACTERIZATION OF TWO PUTATIVE  
DNA METABOLISM ENZYMES IN *DEINOCOCCUS*  
*RADIODURANS*.

By

Charles William Mueller

Dissertation submitted to the Faculty of the Graduate School of the  
University of Maryland, College Park, in partial fulfillment  
of the requirements for the degree of  
Doctor of Philosophy  
2014

Advisory Committee:  
Dr. Douglas Julin, Chair  
Dr. Theodore Dayie  
Dr. Steven Hutcheson  
Dr. Jason Kahn  
Dr. Hermon Sintim

© Copyright by  
Charles William Mueller  
2014

## Dedication

I dedicate this work, the culmination of almost six years of hard work, little sleep and questionable hygiene, to the people, who without, I could have never accomplished this incredible educational adventure.

First and foremost I dedicate this work to my Nana, the late Sylvia Mallory, and my Papa, the late Charles Mallory. They provided me with an opportunity to pursue any intellectual path I wanted without any restrictions and for that I am forever grateful. I miss you both and I'm sorry you are no longer here to see this work.

Secondly, I'd like to dedicate this work to my late Grandpa Dale and my Grandma Ann, who without, I most certainly would never have been able to maintain the necessary mental fortitude to keep pursuing this degree. They both listened for hours as I explained to them my frustrations, my amazements and my successes regardless if they could truly comprehend or relate to the experiences I was sharing.

It would be great injustice if I didn't also dedicate this work to my wife, Theresa Ann Mueller. She has felt the wrath of the Ph. D. process more than anyone and has embraced every single second of it. Well maybe not every single second, but a lot. She is my rock and has sacrificed so much over the years for my pursuit of knowledge. There are not appropriate words to describe what that means to me. We did this together and I cannot wait to see what our future holds. KissKiss TuvTuv

Lastly, I'd like to dedicate this work to my late Father-in-law, John F. Mencarini Sr. He was a father to me during a time I needed it the most and I'll always hold precious the many memories we made together during the time I was able to know him.

## Acknowledgements

After almost six years in pursuit of this Ph. D. there are many people I believe I need to acknowledge, because without their support and guidance at times, this entire process would have been “the worst”.

Although I’m sure they will be saddened to see their names appear on this page instead of the previous, my mother, Kathy Schulberg, and my father, Donald Mueller, are two people I hold dear to my heart and literally helped me at every stage in my life. Each instilled in me a willingness to seek the unknown and to not be afraid of the things which I don’t understand. To them I owe everything.

I would like to thank my advisor, Dr. Julin. Nobody has put up with me more during his time (except for maybe my wife) than him. He has entertained my spontaneous visits to his office, upon which I often talked his ear off for hours (yes hours) about the wonders of the universe, the hypocrisies of our times and even sometimes what was going on with my project. His mentorship has been instrumental in my maturation as a young scientist.

Secondly, I’d like to thank my committee: Dr. Jason Kahn, Dr. Hermon Sintim, Dr. Theodore Dayie and my Dean’s Representative Dr. Steven Hutcheson. They have provided me at times with a much needed listening ear and have always challenged me on the things I believe, which has been critical to my learning process.

I’d like to thank several past graduate students for the friendship and companionship that they offered me during my time here and I look forward to our many years ahead. Thank you: Dong Yang, Jen Buss, Zheng Cao, Lucas Tricoli and William Shadrick.

In addition, I'd like to thank several mentors in my life, who without, I likely would never have pursued this degree. Thank you: Dr. Dolph Hatfield, Brad Carlson, Dr. Joel Karty, Dr. Eugene Grimley and Dr. Jo Grimley.

Without my brother, Thomas Mueller, the Plasters DGs and the great men who filled out my wedding party I would have forgotten what fun was during the last 6 years. Thanks for keeping me, me. WWCCD.

To all my the other friends and family that I have not mentioned in this; thank you for being a part of my life and helping shape me into the person I am today.

Lastly, and this one likely will seem most odd and signal red flags on some peoples radar, I'd like to thank my dog Dinero (aka Pug). During the many hours it has taken to contemplate, analyze and write up the data in this study, he has spent almost all of them laying patiently by my side; making me smile when I needed it most and nobody else was around.

# Table of Contents

Dedication .....	ii
Acknowledgements .....	iii
Table of Contents .....	v
List of Tables .....	vii
List of Figures .....	viii
Chapter 1: Introduction .....	1
1.1 Studying DNA Repair in <i>D. radiodurans</i> .....	4
1.2 Homologous Recombination in <i>D. radiodurans</i> .....	9
1.3 The Role of NurA and HerA in Archaea .....	15
1.4 The Role of NurA and HerA in <i>D. radiodurans</i> .....	22
1.5 Specific Aims .....	26
1.5.1 Specific Aim 1: Biological Characterization of NurA from <i>D. radiodurans</i> .....	26
1.5.2 Specific Aim 2: Biological Characterization of HerA from <i>D. radiodurans</i> .....	27
Chapter 2: ASSESSMENT OF DNA REPAIR PHENOTYPES OF NURA AND HERA MUTANT STRAINS .....	28
2.1 INTRODUCTION .....	28
2.2 MATERIALS AND METHODS .....	30
2.2.1 Bacterial Strains, Plasmids and Culturing .....	30
2.2.2 Isolation of Genomic DNA .....	31
2.2.3 Transformation of <i>D. radiodurans</i> .....	33
2.2.4 Restriction Digestions, Ligations and Transformations in <i>E. coli</i> .....	33
2.2.5 Polymerase Chain Reactions .....	35
2.2.6 Cloning and Sequencing of <i>nurA</i> and $\Delta nurAKO$ Fragment .....	36
2.2.7 Generation of $\Delta nurA::strep$ ( $\Delta nurA$ ) .....	39
2.2.8 Cloning and Sequencing of <i>herA</i> and $\Delta herAKO$ Fragment .....	40
2.2.9 Generation of $\Delta herA::strep$ ( $\Delta herA$ ) .....	42
2.2.10 <i>In vivo</i> Survival Assays with Treatments of DNA Damaging Agents .....	48
2.2.10.1 Treatment with H <sub>2</sub> O <sub>2</sub> .....	48
2.2.10.2 Treatment with MMC .....	49
2.2.10.3 Treatment with UV-C .....	49
2.2.10.4 Treatment with Phleomycin .....	50
2.2.11 Expression and Purification of Putative HerA Enzyme .....	50
2.2.12 Micro-Bradford Assay .....	52
2.2.13 ATPase Activity Assay .....	52
2.3 RESULTS .....	53
2.3.1 Confirmation of <i>nurA</i> and <i>herA</i> deletion .....	53
2.3.2 <i>In vivo</i> survival assay results for mutant strains .....	56
2.3.3 <i>In vivo</i> survival assay results: UV-C .....	57
2.3.4 <i>In vivo</i> survival assay results: Phleomycin .....	57
2.3.5 <i>In vivo</i> survival assay results: MMC .....	59



2.3.6 <i>In vivo</i> survival assay results: H <sub>2</sub> O <sub>2</sub> .....	59
2.3.7 Expression and purification of putative HerA enzyme from <i>E. coli</i> .....	60
2.3.8 Initial ATPase activity measurements on putative HerA enzyme .....	61
2.4 DISCUSSION.....	64
2.4.1 <i>In vivo</i> Survival Analysis.....	64
2.4.2 <i>In vivo</i> Survival Analysis: Future Work.....	68
2.4.3 Concluding Remarks about NurA and HerA in DNA repair in <i>D. radiodurans</i> .....	69
Chapter 3: ASSESSMENT OF GROWTH PHENOTYPES OF NURA AND HERA MUTANT STRAINS.....	71
3.1 INTRODUCTION .....	71
3.2 MATERIALS AND METHODS.....	76
3.2.1 Bacterial Strains and Culturing.....	76
3.2.2 Growth and Morphology Assessment.....	76
3.2.3 Growth Assay: Cell Concentration Determination .....	77
3.2.4 Growth Assay: Culture Density and Cell Mass Determination .....	77
3.2.5 Phase Contrast and Low Resolution Fluorescence Microscopy .....	78
3.2.6 High Resolution Fluorescence Microscopy .....	80
3.2.7 Flow Cytometry .....	82
3.2.8 <sup>3</sup> H-Thymidine Incorporation Assay .....	83
3.3 RESULTS .....	85
3.3.1 Growth analysis of $\Delta nurA$ and $\Delta herA$ strains .....	85
3.3.2 Morphology analysis: Phase contrast and low resolution fluorescence microscopy.....	89
3.3.3 Morphology assessment: Flow cytometry .....	92
3.3.4 Effect of <i>herA</i> mutation on cell cycle .....	98
3.3.5 Measurement of DNA synthesis rates in $\Delta herA$ strain .....	100
3.3.6 Morphology Assessment: High resolution fluorescence microscopy.....	101
3.4 DISCUSSION.....	108
3.4.1 <i>Growth and Morphology Analysis</i> .....	108
3.4.2 <i>The nurA and herA genes in D. radiodurans</i> .....	113
3.4.3 <i>Growth and Morphology Analysis: Future Work</i> .....	115
3.4.4 <i>Concluding Remarks Regarding NurA and HerA in D. radiodurans</i> .....	117
Appendices.....	121
Appendix 1: Partial <i>In vivo</i> Characterization of the $\Delta herA^*$ Strains .....	121
Appendix 1.1: Generation of $\Delta herA^*$ mutant strains with <i>nurA</i> mutation.....	121
Appendix 1.2: Summary of all $\Delta herA^*$ mutant strains.....	123
Appendix 1.3: Partial growth analysis of selected $\Delta herA^*$ strains.....	127
Appendix 1.4: Partial morphology assessment of selected $\Delta herA^*$ strains.....	129
Appendix 1.5: Partial DNA damage sensitivity analysis for selected $\Delta herA^*$ strains .....	132
Appendix 1.6: Concluding remarks on $\Delta herA^*$ strains .....	135
Appendix 2: References to Work on RecJ Nuclease in <i>D. radiodurans</i> .....	138
Bibliography .....	139

## List of Tables

	Page
Table 1: Comparison of enzymes involved in Homologous Recombination (HR) in <i>D. radiodurans</i> (DR) and <i>E. coli</i> .....	8
Table 2 DNA oligonucleotides used for $\Delta nurA$ strain.....	38
Table 3: DNA oligonucleotides used for $\Delta herA$ strain.....	42
Table 4: Growth properties of wild-type, $\Delta nurA$ and $\Delta herA$ strains. ....	87
Table 5: Summary of morphology data in wild-type, $\Delta nurA$ and $\Delta herA$ strains.....	90
Table A1: Summary of $\Delta herA^*$ Phenotypes.....	124

## List of Figures

	Page
Figure 1-1: The repair of DSB in bacteria by HR.....	3
Figure 1-2 <i>D. radiodurans</i> cells grown on TGY agar plates at 30°C.....	5
Figure 1-3: Survival curves of <i>D. radiodurans</i> following DNA damage.....	6
Figure 1-4: Initiation of HR in <i>D. radiodurans</i> by RecFOR pathway.....	13
Figure 1-5: The repair of DSB through the SSA and ESDA models in <i>D. radiodurans</i> .....	14
Figure 1-6: The crystal structure of NurA from <i>Sulfolobus solfataricus</i> .....	16
Figure 1-7: The HerA-NurA complex and models of DNA end resection.....	21
Figure 1-8: Multiple Alignment of HAS-barrel domain of the HerA Superfamily....	24
Figure 1-9: Multiple Alignment of NurA Superfamily.....	25
Figure 2-1: Making pCRBlunt_Δ <i>nurA</i> . ....	39
Figure 2-2: Making pCRBlunt_Δ <i>herA</i> *.....	44
Figure 2-3: Generation of pCRBlunt_Δ <i>herA</i> *.....	45
Figure 2-4: Genotype PCR reactions for wild-type, Δ <i>nurA</i> and Δ <i>herA</i> strains.....	55
Figure 2-5. Effect of DNA damaging agents on viability of wild-type, Δ <i>nurA</i> and Δ <i>herA</i> cells.....	56
Figure 2-6: Expression and Purification of Putative HerA Enzyme.....	61
Figure 2-7: ATPase assays with HerA enzyme from <i>D. radiodurans</i> .....	63
Figure 3-1: Domain architecture of selected FtsK-like proteins.....	73
Figure 3-2: The process of generating binary images to count cell areas.....	79
Figure 3-3: The process of generating overlay images.....	82

Figure 3-4: Growth of wild-type and $\Delta nurA$ cells. ....	86
Figure 3-5: Growth of wild-type and $\Delta herA$ cells. ....	88
Figure 3-6: Images of wild-type during late exponential phase of growth. ....	91
Figure 3-7: Size Distributions of wild-type, $\Delta herA$ and $\Delta nurA$ cells. ....	92
Figure 3-8: 2-D scatter plots of FSC-A and FITC-A signals from flow cytometry of wild-type and $\Delta nurA$ strains. ....	94
Figure 3-9: 2-D scatter plots of FSC-A and FITC-A signals from flow cytometry of wild-type and $\Delta herA$ strains. ....	95
Figure 3-10: Histogram overlays of FSC-A and FITC-A signals from flow cytometry of wild-type and $\Delta nurA$ strains. ....	96
Figure 3-11: Histogram overlays of FSC-A and FITC-A signals from flow cytometry of wild-type and $\Delta herA$ strains. ....	97
Figure 3-12: Growth data and representative phase-contrast images of wild-type and $\Delta herA$ cells upon treatment with hydroxyurea. ....	100
Figure 3-13: The various growth states of <i>D. radiodurans</i> . ....	103
Figure 3-14: Fluorescence image overlays showing septum and nucleoid abnormalities. ....	106
Figure 3-15: The average cell size per growth state for wild-type and $\Delta herA$ cells. ....	107
Figure 3-16: The loss of ClpPX activity results in a chromosome segregation defect following DNA damage in <i>D. radiodurans</i> . ....	113
Figure A-1: Alignment of pCRBlunt_ $\Delta herA^*$ and <i>nurA</i> from <i>D. radiodurans</i> ....	122
Figure A-2: A family tree of the $\Delta herA^*$ strains made from $\Delta herA^*KO$ . ....	125
Figure A-3: PCR Genotype reactions for select $\Delta herA^*$ strains. ....	126

Figure A-4: Growth Curves for wild-type and  $\Delta herA^*$  strains..... 129

Figure A-5: *D. radiodurans* imaged at 400x magnification using phase contrast...130

Figure A-6: 2-D scatter plots of FSC-A and PI-A signals from flow cytometry of wild-type and  $\Delta herA^*$  strains.....131

Figure A-7: Histograms of FSC-A and PI-A signals from flow flow cytometry of wild-type and  $\Delta herA^*$  strains.....132

Figure A-8: Effect of DNA damaging agents on viability of wild-type and  $\Delta herA^*$  cells.....134

## List of Abbreviations

6-4 PPs	Pyrimidine-(6-4)-pyrimidone photoproducts
ATP	Adenosine triphosphate
BER	Base excision repair
BSA	Bovine serum albumin
CFU/mL	Colony forming units per mL
CPD	Cyclobutane pyrimidine dimer
D	Downstream region of <i>herA</i> gene
DAPI	4',6-diamidino-2-phenylindole
DMSO	Dimethyl Sulfoxide
dNTP	Deoxyribonucleic acid triphosphate
DSB	Double strand break
dsDNA	Double strand DNA
EDTA	Ethylenediaminetetracetic acid
ESDSA	Extended synthesis dependent strand annealing
FITC-A	Area of SYTO9 emission signal from flow cytometry
FSC-A	Area of Forward SCatter signal from flow cytometry
gDNA	Genomic DNA
G	Generation time
HR	Homologous Recombination
HU	Hydroxyurea
IPTG	Isopropyl- $\beta$ -D-thiogalactopyranoside
KO	Knockout
LB	Luria-Bertani
MMC	Mitomycin C
MMR	Mismatch repair
MMS	Methyl methanesulfonate
NER	Nucleotide excision repair
NHEJ	Non-homologous end joining
PAGE	Polyacrylamide gel electrophoresis
PCR	Polymerase chain reaction
PI	Propidium iodide
PI-A	Area of propidium iodide emission signal from flow cytometry
ROS	Reactive oxygen species
SDS	Sodium dodecyl sulfate
SDSA	Synthesis dependent strand annealing
SSB	Single strand binding protein
ssDNA	Single strand DNA
SSG	Single strand gap
<i>Strep</i>	Streptomycin

TGY	Tryptone-glucose-yeast
U	Upstream region of <i>herA</i> gene
UA	Upstream region of <i>herA</i> ligated to <i>addA</i>
UV	Ultraviolet
$\Delta herA$	<i>herA</i> mutant strain with no mutations in <i>nurA</i>
$\Delta herA^*$	<i>herA</i> mutant strain with mutations in <i>nurA</i>
$\Delta herA\#$	<i>herA</i> mutant strain with <i>nurA</i> mutation colony number
$\Delta herA\#\_ \#$	<i>herA</i> mutant strain with <i>nurA</i> mutation colony number after transformation with <i>herA</i> mutation strain KO fragment
$\Delta herA\#\_ Letter$	<i>herA</i> mutant strain with <i>nurA</i> mutation colony number after transformation with <i>herA</i> mutation strain gDNA
$\Delta herAKO$	<i>herA</i> knockout fragment
$\Delta herA^*KO$	<i>herA</i> knockout fragment with mutations in <i>nurA</i>
$\Delta nurA$	<i>nurA</i> mutant strain
$\Delta nurAKO$	<i>nurA</i> knockout fragment

## Chapter 1: Introduction

Double strand breaks (DSBs) in an organism's genome can occur through a variety of processes. In the lab they can be produced through exposure to ionizing radiation such as UV or gamma radiation, DNA damaging agents such as mitomycin C (MMC), and environmental conditions like those that promote desiccation or mechanical stress (1). They can also occur naturally when the DNA replication machinery encounters damaged DNA, other replication fork barriers or as a result of spontaneous damage from reactive oxygen species formed during aerobic metabolism (1, 2). Their repair is critical because the cell cannot replicate and remain viable without an intact genome.

The major pathway for DSB repair in prokaryotes is homologous recombination (HR), as opposed to eukaryotes that favor the error prone non-homologous end joining (NHEJ). HR is relatively error free, but requires an intact template, unlike NHEJ (1). The process of DSB repair by HR in bacteria typically occurs in four steps (**Figure 1-1**). The first, termed pre-synapsis, is the processing of an end of a DSB by a helicase and nuclease to generate a 3' single strand DNA (ssDNA) tail for subsequent loading of the ubiquitous bacterial recombinase RecA (3, 4). The second step (synapsis) involves a RecA-dependent homology search that culminates in the formation of a joint molecule between the damaged strand and a homologous template strand known as a D-loop. This structure can be used as a template for DNA synthesis and ultimately results in the formation of a Holliday junction (4). The final steps (post-synapsis/resolution) involves branch migration of the Holliday junction by



proteins such as RuvAB followed by resolution of this intermediate by a resolvase like RuvC resulting in either crossover or non-crossover products (4).

The mechanism for processing DNA ends for RecA loading and subsequent HR has been extensively studied in *E. coli* and *B. subtilis* (1, 5). In *E. coli*, the RecBCD multi-enzyme complex is responsible for initiating recombination 90% of the time in response to DSBs (3, 4). RecB is a SF1A helicase which passes ssDNA along its RecA-like folds in the 3'-5' direction and RecD is a SF1B helicase which moves ssDNA in the opposite direction (5'-3'). Each of these helicases interacts with one of the two strands and both utilize the hydrolysis of ATP to promote their translocation along the ssDNA generating a bipolar helicase activity (3). RecB is also the active nuclease in this complex and degrades both strands as it unwinds the duplex DNA until the RecC subunit detects a particular sequence known as a Chi-sequence (crossover *hotspot instigator*; 5'-GCTGGTGG-3') (6). RecC binds to this Chi sequence preventing the 3'-5' strand from reaching the RecB nuclease domain. Thus as the RecB and RecD helicase domains continue to unwind the duplex DNA, only the 5'-3' strand is degraded resulting in a 3'-5' single strand loop which can be utilized for RecA loading (1). The overall process occurs similarly in *B. subtilis* except that the AddAB complex is utilized. This complex has a single helicase-dual nuclease activity where both strands of duplex DNA are digested by the nuclease activities of AddA and AddB until they reach a Chi site (5-AGCGG-3') (1).

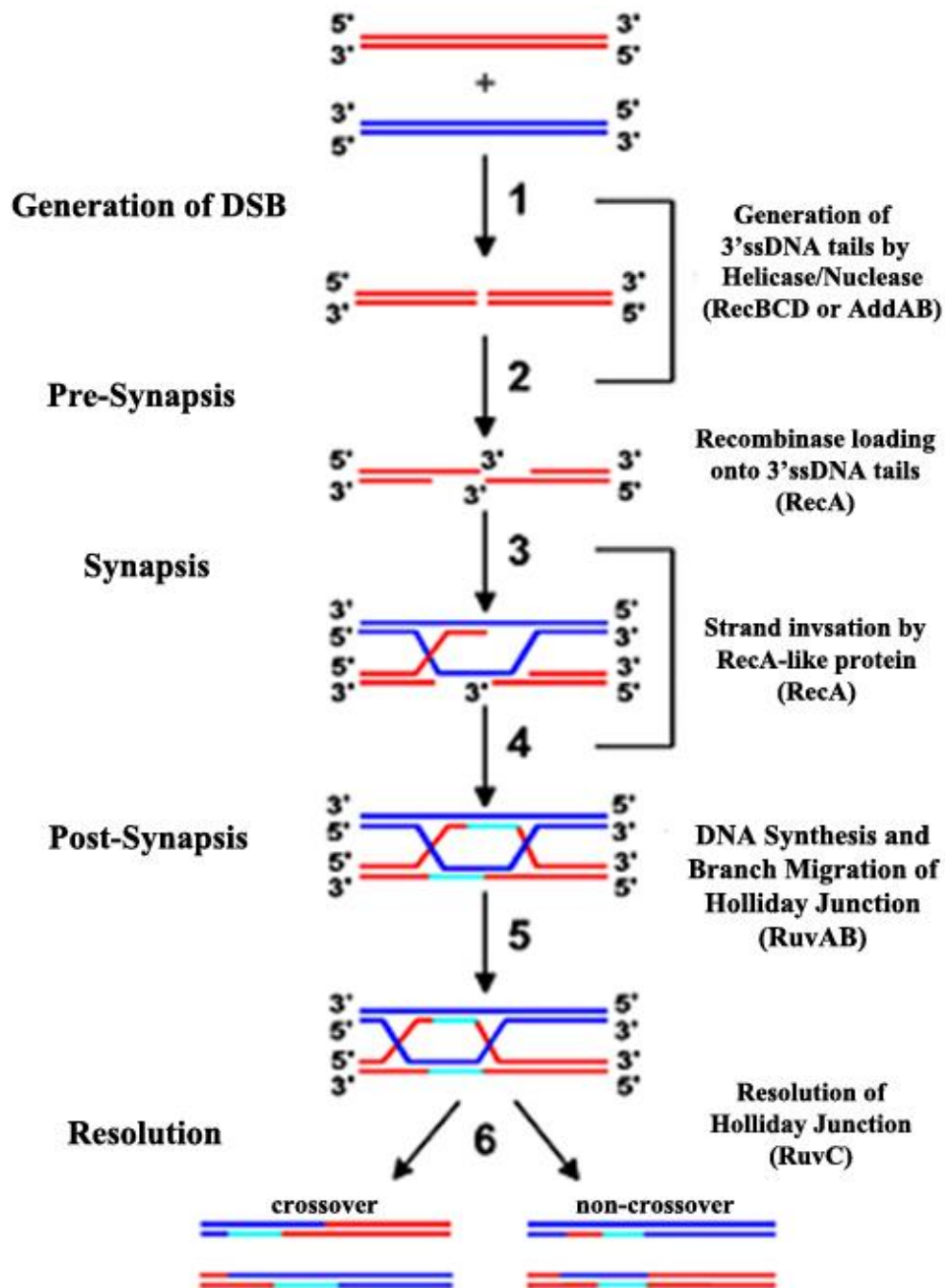


**Figure 1-1: The repair of DSB in bacteria by HR.**

An event occurs inside a bacterial cell resulting in a DSB (1). Following the DSB, helicases and nucleases, such as the RecBCD or AddAB complexes, generate 3' ssDNA tails for RecA loading (2; pre-synapsis). RecA-dependent homology pairing and subsequent strand exchange then occurs forming a D-loop (3; synapsis). Following DNA synthesis, branch migration of the Holliday junction occurs, facilitated by proteins such as RuvAB (4; post-synapsis). This is followed by resolution (5) of this intermediate by a resolvase, like RuvC, resulting in crossover or non-crossover products. Figure was adapted from Bianco, 1999 (7).

### 1.1 Studying DNA Repair in *D. radiodurans*

*Deinococcus radiodurans* is an unusual bacterium known for its extreme resistance to DNA damage and is typically utilized as a model organism for studying DNA repair. It was first isolated in 1956, when cans of meat irradiated with 4000 Gray (Gy) of gamma rays, were found to contain a living, coccus bacteria (8). This amount of radiation is capable of producing hundreds of DSBs and is more than enough to kill *E. coli* (9, 10). Since its discovery, researchers have been trying to learn everything they can about this bacterium in hopes of one day understanding how and why it is so resistant to DNA damage (9).

We now know that it is an aerobic, non-motile, red-pigmented, nonpathogenic mesophile, that stains Gram-positive even though its cell envelope is similar to that of Gram-negative bacteria (9). Its optimal growth conditions are between 30°-32° C and because its preferred source of carbon is amino acids (proteolytic) it is typically cultured in TGY medium which is a mixture of tryptone (0.5%), yeast extract (0.3%) and glucose (0.1%) (9). *D. radiodurans* does not form spores and depending on its stage of growth contains between 2-10 copies of its 3.28 megabase genome consisting of two chromosomes and two plasmids (9). Its growth state and culture medium also give rise to a range of morphologies, but it is typically found as a mixture of diads and tetrads between 0.5 to 3.5 µm in diameter (9). These different morphologies arise due to the unusual division pattern of *D. radiodurans* whereby the cells divide in alternating planes (**Figure 1-2**), such that the new division sites are orthogonal to each other (9). This division process is further distinct from other cocci because two septa converge from opposite sides of the cell to form a slit closure and during rapid

growth new septation can begin before the previous cycle finishes giving rise to cells with multiple (>2) communicating compartments (9). Although the physical processes that occur during cell division are understood, the enzymatic mechanisms for how this is accomplished are not known (9).

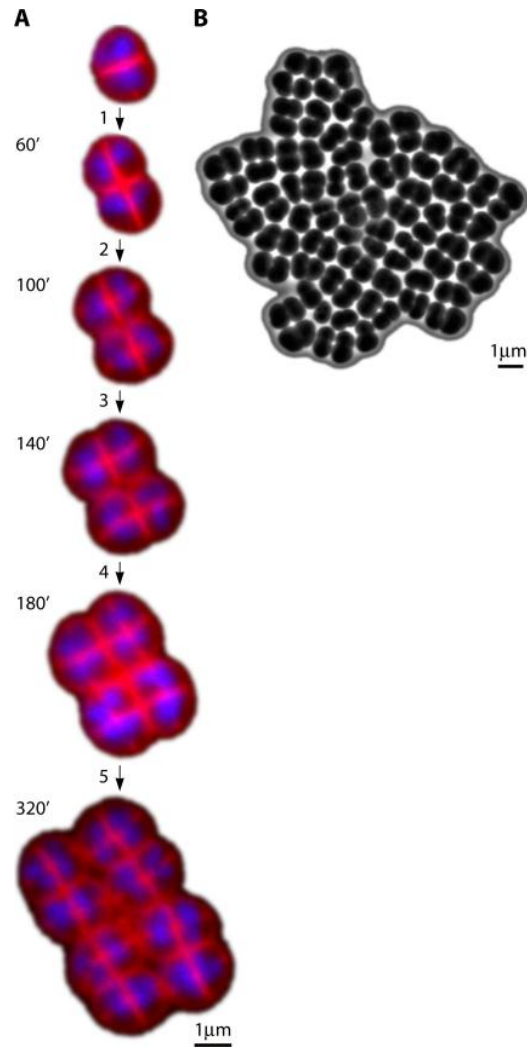


**Figure 1-2 *D. radiodurans* cells grown on TGY agar plates at 30°C.**

(A) *D. radiodurans* cells were stained with the cell membrane stain FM4-64 (red) and nucleic acid stain DAPI (blue). A single diad was monitored via time-lapse fluorescent microscopy until it reached a cell basically consisting of 8 connected diads. (B) A phase contrast image of a *D. radiodurans* microcolony started from a single diad. Figure is adapted from Slade, 2011 (9).

*D. radiodurans* is most famously known for its extremely high tolerance to ionizing radiation (9). It is capable of repairing up to 200 ionizing radiation induced DSBs in its genome without any significant loss in viability (9). For comparison, *E. coli* and most other bacteria succumb to death after only about 10 radiation-induced DSBs per chromosome (10, 11). In addition to its unparalleled resistance to ionizing radiation it also has great resistance (Figure 1-3) to various types of oxidative stresses (e.g. H<sub>2</sub>O<sub>2</sub>), agents that can cause direct damage to DNA (e.g. mitomycin C; MMC) and environmental conditions which can induce DSBs (e.g. desiccation). As a result, the primary focus for studying this bacterium has been centered on elucidating the enzymatic mechanisms that allow it to recover from such types of DNA damage (9).

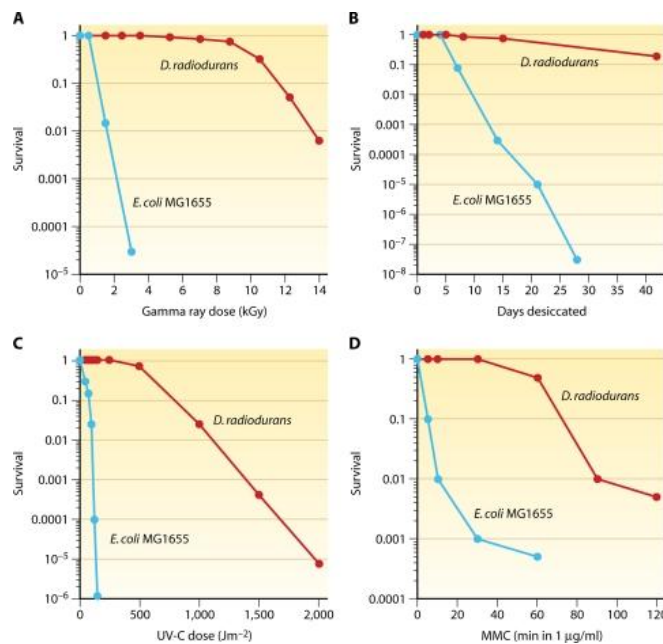


**Figure 1-3: Survival curves of *D. radiodurans* following DNA damage.**

Comparison of the sensitivity to DNA damage between *D. radiodurans* and *E. coli* cultures exposed to: (A) Gamma radiation (B) Desiccation (C) UV-C radiation (D) MMC. Figure is adapted from Slade, 2011 (9).

In 1999, the genome sequence of *D. radiodurans* was obtained and researchers began searching for gene products that may play a role in its resistance to ionizing radiation (12). A starting point was to search its genome for homologues of DNA repair enzymes known to exist in other bacteria such as *E. coli* (12-14). To date, various enzymatic pathways in *E. coli* that repair single base lesions have been identified in *D. radiodurans* (15). These pathways include base-excision repair (BER), nucleotide excision repair (NER) and mismatch repair (MMR). This suggests there is no novel pathway for repairing such damage in *D. radiodurans* (15).

However, some of the essential enzymes identified for HR in bacteria like *E. coli* are absent (**Table 1**) from the genome of *D. radiodurans*. As a result, the RecBCD and AddAB complexes do not exist in *D. radiodurans*; it lacks homologs of *recB*, *recC*, *addA* and *addB* (13, 14). The observation could suggest that HR is not a primary pathway for repair of DSB in *D. radiodurans* and some other novel pathway exists. This seems unlikely because *D. radiodurans* does contain a homolog of *recA* and cells with a defective RecA are sensitive to ionizing radiation, confirming that recombinational events are key to its resistance phenotype (16). Therefore, it must mean the initiation pathway for HR (generation of 3' ssDNA tails from DSBs) in *D. radiodurans* occurs through a different mechanism than the RecBCD/AddAB pathways responsible for this in most other bacteria (5, 14, 17).

**Table 1: Comparison of enzymes involved in Homologous Recombination (HR) in *D. radiodurans* (DR) and *E. coli*.**

<b>Process In HR</b>	<b>Protein</b>	<b>Gene in DR</b>	<b>Protein function <i>E. coli</i></b>	<b>Same function in DR?</b>	<b>References</b>
<i>Strand Invasion</i>	RecA	DR_2340	DNA strand exchange and recombination	Yes; different mechanism	(16, 18-23)
	SSB	DR_0099	Binds ssDNA	Yes	(24)
<i>Initiation (RecBCD)</i>	RecB		3'-5' helicase; exo/endonuclease	-	-
	RecC		Inactivated helicase/nuclease; Recognizes Chi	-	-
	RecD	DR_1902	5'-3' helicase	No	(25-27)
<i>Initiation (RecFOR)</i>	RecF	DR_1089	Binds junctions; facilitates RecA loading (w/ RecOR)	Yes	(28, 29)
	RecO	DR_0819	Binds junctions; facilitates RecA loading (w/ RecFR)	Yes	(28, 29)
	RecR	DR_0198	Binds junctions; facilitates RecA loading (w/ RecFO)	Yes	(28, 29)
	RecJ	DR_1126	5'-3' exonuclease	Yes; differences exist	(28, 30)
	RecN	DR_1477	ATP Binding	Unknown	
	RecQ	DR_1289	3'-5' helicase	No; UvrD (DR_1775) might	(29, 31)
<i>Branch Migration</i>	RuvA	DR_1274	Binds junctions; helicase (w/RuvB)	Assumed to be	-
	RuvB	DR_0596	Binds junctions; 5'-3' helicase (w/RuvA)	Similar	(32)
<i>Resolution</i>	RuvC	DR_0440	Junction endonuclease	Assumed to be	-

## 1.2 Homologous Recombination in *D. radiodurans*

In *E. coli*, the RecFOR pathway is responsible for the repair of ssDNA gaps (SSG) and initiation of HR when the RecBCD pathway is inactivated (33). The major enzymes in this pathway are the RecQ helicase with 3'-5' polarity, the 5'-3' RecJ exonuclease and the RecFOR protein complex. To initiate RecA loading, RecQ and RecJ unwind and degrade the end of a DSB to generate a 3' ssDNA tail. This ssDNA tail is bound by single-strand binding protein (SSB). It is believed that RecF (possibly RecFR complex) interacts with SSB and binds the ssDNA-dsDNA junction produced by RecQ and RecJ. Then the RecOR complex (possibly just RecO) binds to the RecF site resulting in a destabilization of SSB with the ssDNA. The RecFOR complex then facilitates the loading of RecA on the newly exposed ssDNA tail (17).

*D. radiodurans* contains homologs of all of the genes which code for these enzymes: *recQ* (DR\_1289), *recJ* (DR\_1126), *recF* (DR\_1089), *recO* (DR\_0819) and *recR* (DR\_0198). Additionally, there is experimental evidence to suggest this pathway not only exists in *D. radiodurans*, but is the primary pathway for RecA-dependent HR (28, 29). Strains devoid of *recA*, *recF*, *recO* and *recR* all display similar growth defects and sensitivity to ionizing radiation compared to wild-type strains (28). Additionally, two separate studies, including one performed in our own lab, concluded that RecJ was an essential enzyme in *D. radiodurans* and heterozygous mutant strains experienced growth defects and sensitivity to ionizing radiation relative to wild-type strains (28, 30). These genetic analyses indicate that these proteins are vital to proper initiation of HR following exposure to ionizing radiation.



Interestingly though, deletion of *recQ* only results in a slight (~5-10 fold) decrease in sensitivity to ionizing radiation relative to wild-type strains; not what you would expect from a critical helicase in the RecFOR pathway (28, 31). Strains devoid of RecQ were found to be sensitive to MMC (introduces intrastrand cross-links), H<sub>2</sub>O<sub>2</sub> and UV radiation so though it appears it may have a role in DNA repair, it doesn't appear to be the primary helicase in the RecFOR pathway (31). Similar results were obtained for *D. radiodurans* strains devoid of the RecD helicase further complicating the question of what helicase was acting as the primary helicase in the RecFOR pathway (26, 28).

To date, the best evidence suggests it is the UvrD helicase (28), typically known for its role in NER and MMR in *E. coli* (34). Cells where *uvrD* has been deleted are sensitive to ionizing radiation (~1000 fold), display a delay in repair kinetics and experience a large delay in DNA synthesis and DNA fragment reassembly post-radiation relative to wild-type strains (28). However, the fact that the *uvrD* mutant was not as sensitive to ionizing radiation as a *recA* deficient strain suggests the existence of a backup helicase(s) that somewhat compensates for the lack of UvrD. It is unlikely that these helicases could be RecD or RecQ because when *recD* or *recQ* are deleted in *uvrD* deficient strains, these strains were still not as sensitive as *recA* mutant strains to ionizing radiation (28). The HelIV (HelD) helicase in *E. coli* has been associated with RecJ in the RecFOR pathway in *E. coli* (17), but inactivation of this gene in *D. radiodurans* resulted in the same radioresistance as wild-type (35).

Despite this uncertainty, a model (**Figure 1-4**) for how the RecFOR pathway proceeds in *D. radiodurans* was put forth by Slade and Radman whereby UvrD and

RecJ work together to unwind and resect the ends of DSBs generating 3' ssDNA tails which are subsequently coated by SSB (9). Following this, RecF associates with the ssDNA-dsDNA junction and through an interaction with RecR, which is complexed with RecO, promotes the formation of the RecFOR complex. RecRO then displaces SSB proteins and initiates the loading of RecA onto the 3' ssDNA tails (9). This model describes the typical RecFOR HR pathway characterized in most bacteria. However, it fails to properly address the finding that after exposure to ionizing radiation there is a massive amount of DNA synthesis (more than during normal replication) and chromosomes are repaired in what appears to be a RecA-independent manner (36).

To account for this finding, a new model of HR has been put forth referred to as 'extended synthesis dependent strand annealing' (ESDSA). This model proposes repair takes place in two stages in *D. radiodurans* where the first occurs through ESDSA and the second as RecA-dependent HR (**Figure 1-5**). The ESDSA model is a modification to a previous model known as synthesis dependent strand annealing (SDSA). The basic idea of ESDSA is that following massive DSBs, the ESDSA pathway turns the many fragmented pieces of the genome into just a few, essentially making fewer substrates for the eventual RecA-dependent HR pathway that must occur to remake circular chromosomes. The pathway is suggested to proceed in a similar fashion as previously described for the RecFOR pathway, whereby RecJ and probably UvrD generate 3' ssDNA tails which through RecA or probably RadA-mediated strand invasion, prime synthesis on the overlapping fragments of the D-loop. Massive DNA synthesis is carried out likely by DNA polymerase III with DNA

polymerase I filling in gaps. These newly synthesized single strands then dissociate from the template and anneal with other complementary single strands just synthesized. These form long dsDNA intermediates with 3' ssDNA flaps which could be removed by the SbcCD complex or some other nuclease complex. The corresponding nicks are sealed, possibly by DNA polymerase I and these long dsDNA intermediates are then used in RecA-dependent HR to generate full circular chromosomes (9). The precise molecular components of this pathway have yet to be revealed and given the current experimental evidence it seems likely there exists additional nucleases or helicases which could either be the primary components or backups to this two-step HR pathway in *D. radiodurans*.

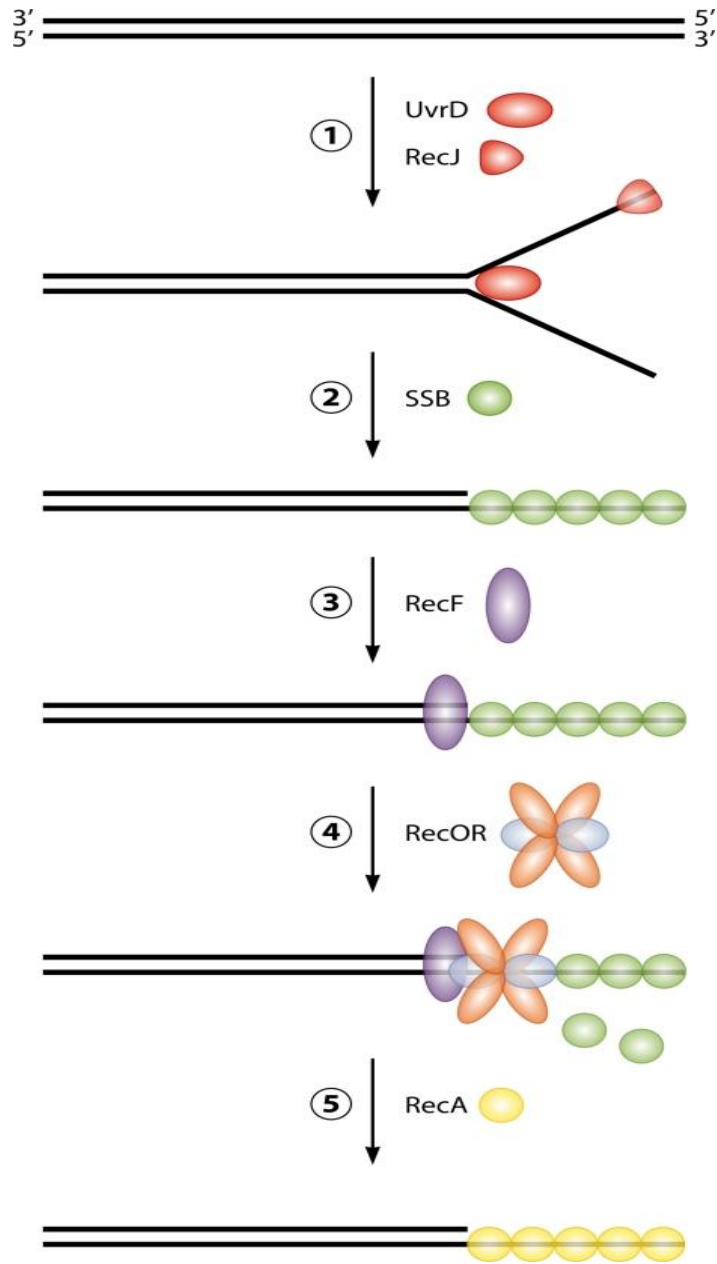


**Figure 1-4: Initiation of HR in *D. radiodurans* by RecFOR pathway.**

(1) The ends of a DSB is processed by the UvrD helicase and RecJ (5'-3') exonuclease to generate a 3' ssDNA tail. (2) SSB binds the 3' ssDNA tail. (3) RecF binds the ssDNA-dsDNA junction. (4) RecF facilitates the assembly of the RecOR complex onto the ssDNA-dsDNA junction. (5) RecOR loads RecA onto 3' ssDNA after displacing SSB proteins. Figure adapted from Slade 2011 (9).

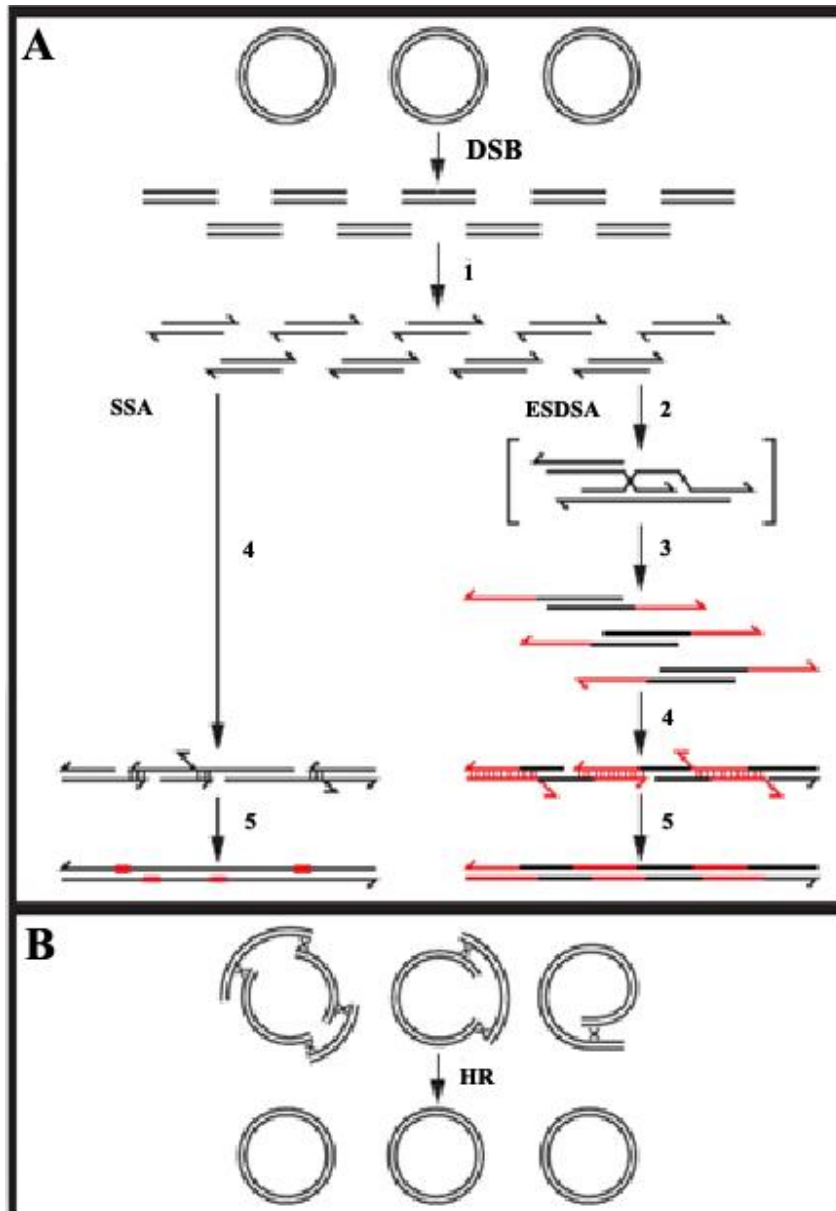


**Figure 1-5: The repair of DSB through the SSA and ESDSA models in *D. radiodurans*.** (A) DSBs occur in several genome copies and (1) their ends processed, likely through the RecFOR pathway, to generate linear dsDNA molecules with 3' ssDNA tails. In SSA, (4) DNA fragments are rejoined through annealing of complementary regions on the 3' ssDNA tails. (5) Gaps that form are repaired via synthesis and excess DNA is degraded by nucleases resulting in long linear pieces of dsDNA. In ESDSA, (2) through RecA/RadA mediated strand invasion, the 3' ssDNA tails are used to prime synthesis on homologous regions of partially overlapping fragments. (3) Synthesis continues, extending the 3' ssDNA tails until the end of the template is reached leading to much longer 3' ssDNA tails (red). This process can occur again, further extending the length of these tails. From this point, the generation of long, linear dsDNA molecules occurs just as it does in steps (4) and (5) in SSA. (B) Circular chromosomes are regenerated through RecA mediated HR. Figure adapted from Zahradka et al, 2006 (36)

### 1.3 The Role of NurA and HerA in Archaea

Archaea and eukaryotes have a shared evolutionary relationship when it comes to the proteins and complexes each utilize for the processes of DNA translation, transcription, replication and recombination (37-39). In eukaryotes, the MRX complex (Mre11, Rad50, Xrs2) acts together with several other proteins to prime the ends of DSBs for Rad51-dependent recombination (40). Mre11 is a 3'-5' ssDNA exonuclease that also contains an endonuclease activity, Rad50 is a member of the SMC (structural maintenance of chromosomes) and Xrs2 is a protein which mediates the interaction of the MRX complex with other DNA repair proteins (41). The MRX complex alone does not have the proper enzymatic activities to properly generate the necessary 3' ssDNA tails for Rad51 loading and thus there is a requirement for additional proteins (Sgs-Exo1/Dna2).

In all archaeal genomes there are Mre11, Rad50 and Rad51 orthologs, but other helicases and nucleases which are critical to the proper development of 3' ssDNA tails needed for recombination have not been identified (42). In thermophilic archaea the genes for *mre11* and *rad50* are found in a conserved operon with two other genes encoding a DNA nuclease and DNA helicase, *nurA* and *herA* respectively (42).

*In vitro*, NurA has been shown to have a 5'-3' exonuclease activity on both ssDNA and dsDNA as well as having a ssDNA endonuclease activity (43). The crystal structures of NurA (**Figure 1-6**) have been solved in *Sulfolobus solfataricus* (*S. solfataricus*) and *Pyrococcus furiosus* (*P. furiosus*) (44, 45). These structures reveal that NurA forms a dimer with an RNAase-H like domain and each subunit contains a catalytic site capable of nuclease activity. The central cavity of the NurA

dimeric nuclease complex was found to be too narrow ( $< 20 \text{ \AA}$  in diameter) to accommodate B form DNA, but was wide enough to accommodate two separated single strands of DNA, such as that unwound by a helicase.

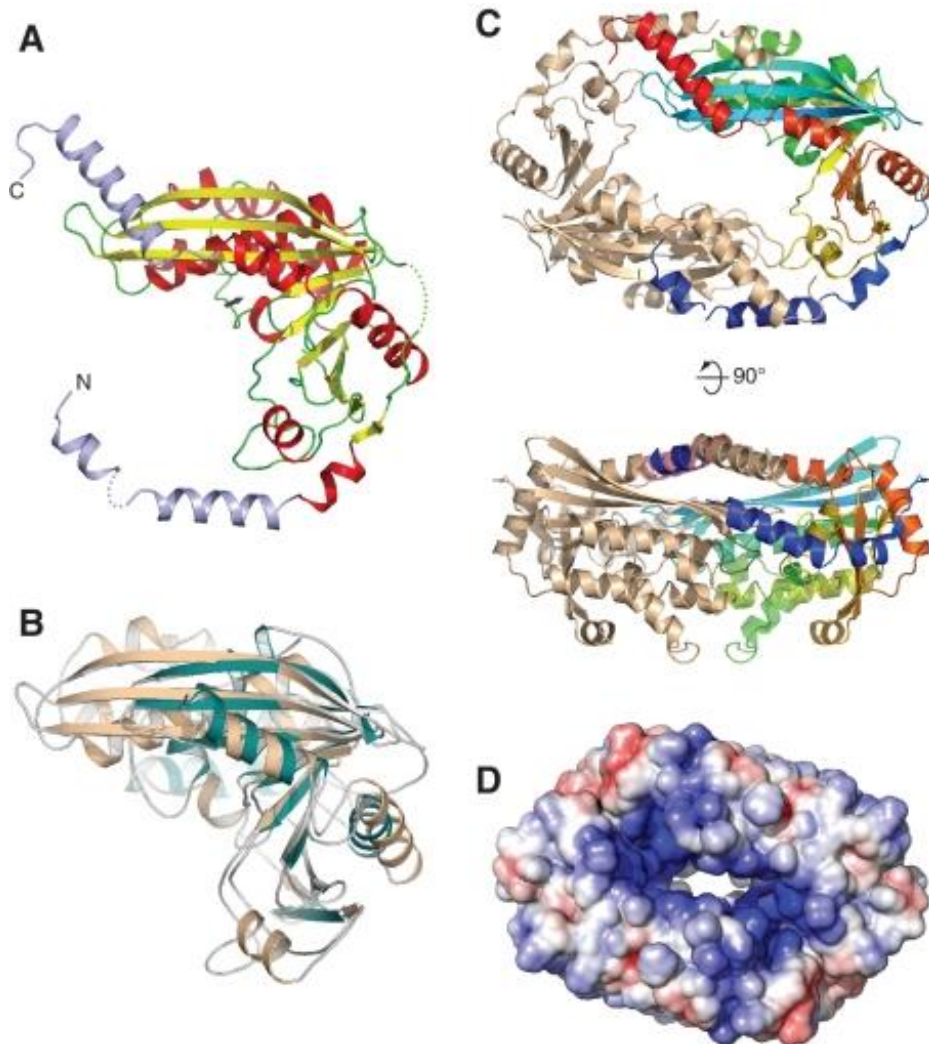


**Figure 1-6: The crystal structure of NurA from *Sulfolobus solfataricus*.**

(A) The structure of the NurA nuclease is shown as a ribbon with alpha helices colored as red and beta sheets yellow. The blue regions are the N- and C-terminal extensions which are not part of the RNAaseH fold. (B) The NurA structure (light brown) superimposed on its closest, functionally characterized, structural relative endonuclease V (green) from *Thermotoga maritima*. (C) The dimeric arrangement of the NurA nuclease. One protomer is colored brown while the other is colored from its N-(blue) to C-terminus (red). View below is a  $90^\circ$  rotation of the view above. (D) The electrostatic potential is mapped across the solvent-accessible surface of the NurA dimeric structure at contouring levels of  $\pm 5 \text{ kT}$  (blue/red) (44).

The archaeal HerA is a hexameric, ATP dependent bipolar DNA helicase with a range of substrates it can unwind *in vitro*. It's been reported to unwind DNA from 3' or 5' ssDNA ends, unwind Holiday junctions and splayed-arm DNA (44, 46-48). A phylogenetic analysis of the HerA proteins has revealed that they are a major clade of the FtsK/HerA superfamily of P-loop ATPases predicted to utilize the hydrolysis of ATP to process DNA substrates (42). This family includes TrwB proteins that are implicated in DNA conjugation, VirD4 proteins which are believed to be involved in DNA translocation from bacteria to plants and FtsK which is known to be involved in DNA pumping during cell division as well as assisting in the resolution of chromosome dimers and catenated chromosomes (42).

In both *S. solfataricus* and *P. furiosus* NurA and HerA have been demonstrated to functionally interact with a stoichiometry of 2:6 (44, 47). Each of the enzymes depends on the presence of the other for their activities in *S. solfataricus* and *P. furiosus* (44, 47), but in *Sulfolobus. acidocaldarius* and *Sulfolobus todokaii* the opposite was found to be true and rather their activities were only stimulated by the presence of one another (46, 48). In *S. solfataricus* the NurA-HerA complex did not degrade supercoiled or relaxed circular plasmid DNA, but when the DNA was linearized, regardless of the type of ends, the complex was capable of unwinding and degrading the DNA (44).

An interesting result was found in *S. solfataricus* when HerA was combined with a nuclease deficient NurA (the catalytic aspartic acid residue at position 58 was mutated to an alanine residue) in that this nuclease deficient complex could unwind substrates with 3' or 5' overhangs, but not blunt end DNA.



The finding suggested the *in vitro* activity of the NurA-HerA complex may depend on the nature of the DNA ends. To further test this idea the nuclease deficient complex was given an artificial Holliday junction substrate, where all but one of the four DNA ends were capped by hairpins such that loading could only occur on the free end. When this free end was blunt, the major product was the double stranded product which was consistent with branch migration of the Holliday junction, but when the free end contained a 5' overhang, a single stranded product was obtained which demonstrated a preference to unwind the ssDNA (44). The result demonstrated the complex could either translocate duplex DNA or unwind duplex DNA depending on the nature of the DNA ends it was loaded on.

No crystal structure for HerA exists, but one for the TrwB protein from the conjugative plasmid R388 does and this structure was utilized to estimate what the NurA-HerA complex may look like by using a homology model calculated in Modeller and the solved hexameric structure of TrwB (44). This structural model (**Figure 1-7**), combined with the *in vitro* data described above, has led to a proposed mechanism for how HerA and NurA might process the ends of dsDNA.

For blunt or small overhangs (< 5 bases), the NurA-HerA complex could degrade both strands of DNA through a process where the HerA helices unwind and feed the two strands into the two catalytic nuclease domains of the NurA dimer bound to the HerA ATP Synthase (HAS)-barrel domain of HerA. If another protein partner exists which could inactivate the nuclease domain of NurA it is also possible the complex could instead translocate this DNA, possibly facilitating branch migration of a Holliday junction. If the overhangs were larger (>10 bases) then DNA degradation

would only occur on one strand and because NurA contains a 5'-3' exonuclease activity this would generate a 3' ssDNA tail which is the desired substrate for recombinase loading in HR (44).

This dual mode of action proposed for the NurA-HerA complex in archaea is similar to the activity observed for the RecBCD and AddAB complexes in bacteria, although no equivalent situation like the Chi-site mechanism has been proposed for this complex which could switch the modes. Instead, it has been proposed that double strand digestion mode could be a defense mechanism against foreign DNA. The single strand mode, it is speculated, could be regulated by the Mre11/Rad50 complex, which could prime the DNA ends sufficiently for loading of the NurA/HerA complex which would then generate 3' ssDNA tails. These tails could be utilized for recombinase loading, which in archaea is RadA. In such a model, NurA and HerA would essentially be doing what Sgs-Exo1/Dna2 do in eukaryotes with Mre11 and Rad50. However, there is no evidence at this time to precisely say how NurA/HerA work with Mre11/Rad50 to generate the 3' ssDNA tails for RadA loading or if such an activity exists *in vivo*. There is *in vitro* evidence though that NurA, HerA, Mre11, and Rad50 from *P. furiosus* can, along with RadA, catalyze the formation of a joint molecule (47).

There is compelling evidence from the *in vitro* studies characterizing the activities of the archaeal NurA and HerA enzymes that suggests in archaea they have a role in the resection of DNA ends to help facilitate HR, similar to RecBCD/AddAB in bacteria (40). There have only been two attempts to delete these genes from archaea and both of these attempts failed leading to the opinion that these are

essential DNA repair genes (49, 50). However, as said before there is very limited *in vivo* evidence to confirm that the activities observed in the test tube translates to what is going on inside the cell. It could be their essentiality is due to a role in HR, but that would be unique as many of the other important enzymes which are critical to proper initiation of HR are not essential, such as RecBCD in *E. coli* (51) .

In *S. acidocaldarius*, HerA has been demonstrated to physically interact with Mre11 and Rad50 during normal exponential growth, but no interaction with NurA was detected, though the authors noted it could be due to the nature of how the antibodies used for their immunoprecipitation assays were developed (against peptides instead of whole proteins (52). When cultures of *S. acidocaldarius* were irradiated with gamma rays at a sub-lethal dose, but enough to introduce many DSBs into its genome, it was observed that Mre11 and Rad50 are recruited to DNA following the treatment, but NurA and HerA were not immediately recruited. After 7 hours though, HerA did begin to associate with the damaged DNA. However, a peculiar result was that the DNA bound fraction of HerA increased as the culture grew in both irradiated and non-irradiated cultures (52).

When this result was taken into context of other studies like one that examined gene expression in *S. acidocaldarius* and saw that *herA* expression was induced in S phase and again at the S/G2 transition (53), it led to the suggestion that HerA may also have a role in chromosome segregation (42, 52). Furthermore, as stated before, HerA is part of the FtsK-HerA superfamily of ATPases and given the fact there is no FtsK homolog found in archaea it seems plausible the HerA could be the FtsK analog

in archaea (42). Thus maybe the essentiality of NurA and HerA in archaea is a combined role in the initiation of HR and a role in chromosome segregation.

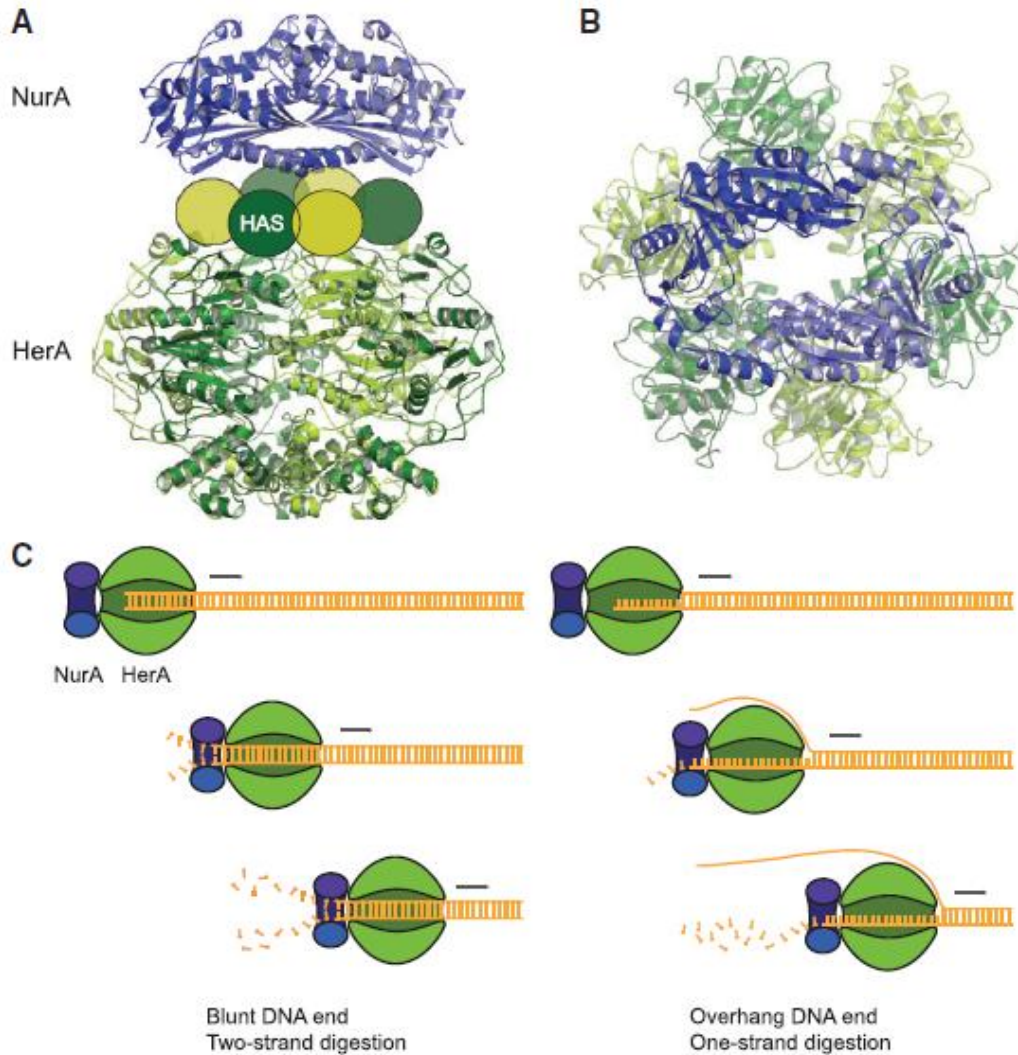


**Figure 1-7: The HerA-NurA complex and models of DNA end resection.**

(A) The HerA structure (alternating hues of green) was generated using a homology model calculated in Modeller based on the hexameric structure of the conjugation protein TrwB (PBD ID: 1E9R) and modeled with the known NurA dimeric structure (blue and lightblue). The HAS barrel ring of each HerA unit is shown as an oval and serves as the interaction site between HerA and NurA. (B) A top down view of the proposed HerA-NurA DNA end resection complex showing the continuous channel formed by the arrangement. (C) Two modes of DNA end resection are shown for the HerA-NurA complex. On the left, the complex binds a blunt or short (<5 bases) DNA overhang and degrades both strands. On the right, in the presence of larger (>10 bases) DNA overhangs, the HerA-NurA complex degrades only one strand leading to the formation of 3' ssDNA tails (44).

#### 1.4 The Role of NurA and HerA in *D. radiodurans*

Helicases and nucleases play a critical role in repair of damaged DNA (1, 54). Any of the proposed models for repair of DSBs in *D. radiodurans* will require the assistance of helicases, nucleases and at least two genome copies (32, 33). The genetic analyses described in **Section 1.2** used to characterize the pathways for the initiation of HR in *D. radiodurans* suggests a role for additional nucleases and/or helicases (other than those already identified) in this process. The NurA nuclease and HerA helicase from archaea represent two potential enzymes capable of participating in the repair of DSBs by working together to generate 3' ssDNA tails to initiate HR (46, 47, 55). The most compelling evidence for this suggestion has come from their ability to help catalyze a strand exchange reaction when combined with Mre11, Rad50 and RadA from *P. furiosus* (47). Homologs of these genes have been reported to be present in some bacterial genomes, yet to date nobody has attempted to study what the role of these genes in bacteria are (42). It seems possible they could be utilized in bacteria as they are in archaea.

As mentioned before, the genes for HerA and FtsK are distant homologs. In 2004, a detailed computational analysis (42) of HerA and FtsK proteins was performed. In this analysis they performed PSI-BLAST (E-value threshold  $10^{-4}$ - $10^{-7}$ ) searches of the non-redundant (NR) database of protein sequences (NCBI, NIH, Bethesda, MD) with PSSMs designed for orthologs of FtsK and HerA in order to explore the evolutionary history of these two enzymes as well as identify new members related to these proteins. Multiple alignments of these members were made using T\_Coffee or PCMA programs and corrected using PSI-BLAST results. These

alignments were used as input to predict protein secondary structures using the PHD program. This all led to the identification and classification of the FtsK/HerA superfamily of P-loop ATPases based on the identification of conserved residues and motifs which made this superfamily distinct from other P-loop ATPases. A similar approach was performed to identify the highly divergent NurA superfamily of nucleases.

In this study, the authors identified two genes in *D. radiodurans* that appear to be homologs of the genes which code for the NurA and HerA enzymes studied in archaea. The multiple alignment showing the HerA ATP synthase (HAS) domain, an essential motif to HerA proteins, is shown in **Figure 1-8** and includes the predicted HerA protein (labeled as DR0837) in *D. radiodurans*. A similar alignment is shown in **Figure 1-9** for the NurA superfamily and it includes the putative NurA protein (labeled DR0836) in *D. radiodurans*, which is shown to contain the predicted active site containing 6 charged/polar residues (Two Asp at end of strands 1 and 5; Two Glu in helix 1; a basic and acidic residue after strand 8; a polar residue in C-term helix).

The apparent homologs of *nurA* and *herA* in *D. radiodurans* have been shown to be expressed and translated as they have both been detected in transcriptomic and proteomic experiments (56, 57). If the *in vitro* characterizations of NurA and HerA in archaea properly describe their activities *in vivo*, then it seems *D. radiodurans* is expressing homologs which could participate in the generation of 3' ssDNA tails during the initiation of HR. With this possibility in mind, we set out to characterize the biological role of these two putative DNA metabolizing enzymes (NurA-HerA) in *D. radiodurans*.

Secondary Structure	Str1	Str2	Strand-3	Strand-4	Str5	Str6						
PH0932_Ph_14590784	9	IGIVRGESSF-INYEFSVNP	2	N.SFGQFVVTKNR	1	G2WVIGVVSVM	1	EENEVAVTV	RILGKVDG	100	HAS fused to HerA	
AF1030_Aful_11498635	4	VGLVMCKSSI-TDFSFVNP	2	IPKFGYVTAINR	1	GEEVIGVREISN	1	KNDVIVATA	TVIGVVKD	95		
MJECL08_Mj_10954499	9	VGTVWASKNV-NEFEFVIEH	4	KIKRKGFEVITKNT	1	GDYLLSKITKIVS	1	NSSKFLASA	RILGVINN	104		
FacI0361_Pac_22405468	11	IGYIIGENTS-GRQFVISED	2	NKKWYEVVLIKIK		NEIVIGRIEIEIKS		NDFVNICIS	TILGLKLD	96		
aq_aa31_Aae_10957065	31	IKEEYSSEFGDOLLGFTVNP	14	DIGLHSYVEVKLQ		EGIVLGRKITSIFA		DDEWKAAI	16	DVIGILKD	155	
PAE2903_Pae_18313675	3	IGYVAASTP-FEPIATLDP	2	PISLYDYVAVDHW	1	YDFSRGELTNVRL	1	IIEVQIAKV	KVLGVVGG	97		
Cate1457_Cth_23021377	5	IGKLGINTGPNNDLKTALEN	2	SAKRGEFVAKHR	6	DTYVLRIVSISR	6	TGETLFPTI	ELVGYRDN	99		
MJ1565_Mj_15669760	7	IGYIIGETRI-DELTFLAKE		APKVGQYVVIHYD		DSELLQWVESTIQ		SSYYILGKI	KVLGDIRD	91		
APE0137_Ape_14600455	13	IGVIGESSYSYSCTILLERD	3	KVIVGSHVVTNLN		GRCVLQIVESTIRS		VESTRVHVA	2	RWVSYLET	106	
MTH307_Mth_15678335	4	VGRCYGETSP-NWVSFVRSR		MPGVGEYVMEYD		GRRILQWVESLLR		GRQVVRGTV	RILGVLET	88		
HerA_Sac_37665381	3	IGYIIGSATI-NEATALEQ		KTRAGYVIVLEID		GDKILGLITNWT		P-FFIKARI	KILCKLDG	89		
t112095_The1_22299638	6	LGIIVQGSLLT-QGLEVRLSG	5	ELRVGQFLVWQGR		RSRPFCLLTDVTL		GTFATLSVA	3	MILDDEQE	101	
s110294_Syn_16331876	6	LGSVYQGSLS-KGLEVRLHA	5	EMRVGRFLVIQGR		RSRPFCLLTDVSL		GTYGTLELA	37	VQAMNAD	135	
qlr4405_Glivi_37523974	18	IGTVYQGSLS-EGLEVRLSP	5	EMRVGRFCVYVGR		RTRFFCLLTDVTL		STFGTVOLT	5	ETVNGQSE	115	
Tery4431_Tery_23043894	7	LGSVYQGSLS-QGLEVRLHP	5	DMRVGRFLVWQGV		RAHFFCLLTDVLL		STYGTLELA	38	AQSSSQIK	137	
Npun6235_Npun_23129935	7	LGSVYQGSLLT-EGLEVRLHP	5	DMRVGRFLVWQGM		RSRPFCLLTDVAL		GTYGTINLA	35	PQTSTTME	134	
MTH542_Mth_15678570	5	AGQIIGGETA--AVLRQKA	2	PEELGDLVAEGE		GTYLLQVQLRY		YGREVELLE	11	RPILQVET	96	
SSQ2200_Sac_15898975	9	IGIVLQKSEA-NEMQGLIRA	2	EISVQQLLVD--		DSEKLSLRVENY		EILDMNTII	KATLHLIK	94		
APE0090_Ape_14600433	39	MGEVGRVTRYSPTVTSPPGS	15	GVRIGDYLCITVDP	2	LHIILGVSTTKR	2	TSPELSLTS	5	RLLLEADP	144	
SSQ2295_Sac_15899052	25	LGDLVQKVSRYIPMKEDEN	17	LKIGFLGALDI	2	LYFVLRVIGYER	2	SLIYNWTLR	1	EMLTKVDF	132	
DR0837_Dr_15805863	15	IGMVLGTEDVTPVVEAVS	3	SVGLDILVVETIR	5	PVRYGLVDNWRK	5	LPAQVYAA	RVLWTRVD	103		
aq_1692_Aae_15606779	3	VGIVLGTKPS-NPLEFVWG-		-VEKGRFLQDDV	3	NSKIDGNEEIKF	3	GVPANLAY	2	RVSVTRIE	92	
TM1257_Tma_15644013	6	IGVVTGIFQS-SPYEFVVM	1	AEKPGEAYKVAQ	14	TVVYGMVDIQN	14	IYIAKVVVT	3	LKEGNKLL	109	
t1r0250_The1_22297794	11	VGIVRGPGDS-GSEYVFITA	3	PVRIGEFVYIELS	6	SKSPAGAVHVLG	6	LIGPTCEPA	7	VIGEFHR	116	
PAE2998_Pyae_18313750	4	IGVVIKSPSI-HYIIFRFP	2	ELDVGARVIAEVD		GVRVSRVTAIRH		VLYYTEAKA	VVLGARRG	97		
SMc01432_Smc1_15965868	28	LGRVACNGS-RACIAVAE	8	LWSVGLVSIISVG		TNRVVALVSMQT		NKPFRIVE	-LMGEVHV	105		
Atu2038_Atu_17935924	28	LGRVIACNGA-HACIAAETE	8	LWSVGRILSIEMG		TSRVVALVSMRT		PNRLLDVE	-LVGEVYR	105		
mlr1445_Mlc_13471466	28	LGNVQCDGA-RACISAYAD	8	LWTVGKMISINLG		TTRVVALVYGIGK		QNALEVSLE	-LIGEVRD	105		
FNV2193_Fnu_34762304	6	IGRVISVDSF-KIMIELDN	14	VAKVNSYIVVPIG		SKKIVALITRVKT		GIRFSKSKR	4	TMLGTITE	96	
EF2348_Efae_29376849	10	VALVVEVNGI-RCKAITFD	14	NLSVNSFVVIKQN		FIKIIGRINSESI		TKRILDIQ	-IIGYISE	103		
aq_1852_Aae_15606891	148	VGYAVSSRSP-KEAEVILE		DLKEQYLGIQ--		-GEEFFLCRLSNV		ALFAHLER	8	EILGEYER	239	
Cnl00592_Cau_22970556	10	IGEVIESSTI-HEVAATYEL	2	SPPFGLVRAATT	2	GLHNYGLIYDIHT	2	DLNVVQTE	3	LIVGYTLH	109	solo HAS
s111318_Syn_16329340	18	IAEVIFSTT-GFLAQCLEP	7	MPAFGSWVATDE	2	GNTIFAVVSVATT	2	QTFAMLTE	3	ATVGFQSR	115	
t1r0637_The1_22298179	11	FAEIIQTATD-HCAQCHEP	7	VPALGSWVIEPG	1	-RVYGVVAIVVT	1	HIFAMKTE	3	AIAGFQER	106	
Cwat2305701_Cwat_45526704	18	IAEVIFSTT-OFLAQCLEP	7	MPPFGLWKSLESD	2	GNKIIAVVYVATT	2	QIFAMKTE	3	TIVGFESY	115	
Flii_Hp_15646029	16	LSPRYGSVKKIMPHIVYADG	1	NPSVGVVVKLEKS	1	GSECVKVVVAEK	1	EQFGFTFPN	5	RAGDKVLF	85	HAS fused to F0F1
l0CWA_Bota_1827809	24	DLEETGRVLSIGDGIARVHG	1	RNVQABEMVEFS-		-SGLKGMSLNEP		DNVGVVVP	5	KEGDIVKR	90	ATfaaes
1SKY_Thth_114531	24	QVSDVGTVIQVGGDIARAHG	2	NVMSGEAVEFA--		-NAVMEALNLEE		NNVGVILG	5	KEGDVRR	90	
FIATP_Car0_11466328	45	QPVLLGEVERVKDGVAEVTR	2	NVRFSELVGFIFA	13	NLIVEGMVVGIEQ	13	DYISVIFG	5	KVGDVRVP	127	
IMAB_Rno_6729934	24	DLEETGRVLSIGDGIARVHG	2	NVQABEMVEFS-		-SGLKGMSLNEP		DNVGVVVP	5	KEGDIVKR	90	
AtpA_Bacs_114531	24	QVSDVGTVIQVGGDIARAHG	2	NVMSGEAVEFA--		-NAVMEALNLEE		NNVGVILG	5	KEGDVRR	90	
AtpA_Spol_114527	25	KVVNTGTWLQVGGDIARVHG	2	EVNAGELVEFE--		-ZGTIGIALNLES		NNVGVVLMG	5	QEGSVKA	91	
AtpA_Ec_15804334	24	EAHNEGTVSVSDGVIIRVHG	2	DCMCGEMISLPE--		-GNRYIAIALNLER		DSVGVVVMG	5	AEGMKVKC	90	
AtpB_Af_11498767	2	KMKLYKTIITVAGAPLV-VEK	2	PVAYGELVITLTP	1	GSTRKQVLDISK	1	DVVVVQVE	5	DTSSIVRF	72	
VATP_Tvo_13540884	2	PKLTYSKVSIEISGELLEVEN	2	NAAYNEMVDIELD	1	GETRQQVLDIRK	1	GLAIVQIFG	6	TEGTRVKE	73	
Vma2p_Sc_6319603	24	PRLNNTVSGVNGPLVILEK	2	FPRYNEIVNLTP	1	GTVROGVLEIRG	1	DRAIVQVE	6	VKKTIVVF	95	
Consensus/80%		.s.h.h.s.....h.hp.		...sph.h...		....hubl...h...		.....		...s....		

**Figure 1-8: Multiple Alignment of HAS-barrel domain of the HerA Superfamily.** Proteins are shown as their gene names, species abbreviations and GI numbers. The putative HerA from *D. radiodurans* is outlined in red. Residues are colored according to the nature of their side chains and conservation in the multiple alignment. 80% consensus is seen as the coloring and also shown at the bottom of the alignment. The predicted secondary structures at the top are based off the TrwB crystal structure and secondary structure prediction programs. A helix is denoted by H and a strand by E. The method for abbreviations and coloring is as follows: h, hydrophobic (ACFILMVWY) and shaded yellow; s, small residues (AGSVCDN) and u, tiny residues (GAS) and colored green; o, residues containing -OH functional group (ST) and colored blue; p, polar residues (STEDKRNQHC) -, acidic residues (DE) and +, basic residues (HRK) are colored purple. Conserved secondary structure elements across the ASCE fold are numbered as integers. Additionally, big residues (LYIERFQKMW) are shaded gray. Figure was adapted from Iyer 2004 (42).



Multiple alignment of Nura Superfamily proteins. The table shows protein sequences from various species (e.g., PF1168, PA8083, MJC1097) aligned across 84 columns. Consensus sequences are shown at the bottom. The Nura protein (PF1168) is highlighted in red in the original image.

**Figure 1-9: Multiple Alignment of Nura Superfamily.**  
Proteins are shown as their gene names, species abbreviations and GI numbers. The putative Nura from *D. radiodurans* is outlined in red. Residues are colored according to the nature of the side chains and conservation in the multiple alignment. 80% consensus is seen as the coloring and also shown at the bottom of the alignment. The predicted secondary structures at the top are based off the secondary structure prediction programs. The coloring, consensus abbreviations and secondary structure representations are the same as in Figure 1-8. The figure was adapted from Iyer 2004 (42).



### 1.5 Specific Aims

The original goal of this project was to facilitate a better understanding of how DNA repair occurs in *D. radiodurans* through genetic, molecular biology and biochemical investigations. In the bacterium *Deinococcus radiodurans* (*D. radiodurans*), no homologs of *recB*, *recC*, *addA* or *addB* exist and one might expect this bacterium to be highly sensitive to DSB. However, despite lacking the primary initiation components for repair of DSB in most bacteria, *D. radiodurans* is one of the most efficient bacteria known at repairing DSB (9). This study attempts to explore the possibility that two homologs of a possible archaeal DNA repair complex (NurA-HerA) contribute to its extreme efficiency at repairing DSB. There were two specific aims included in this project.

#### 1.5.1 Specific Aim 1: Biological Characterization of NurA from *D. radiodurans*

*D. radiodurans* locus DR\_0836 encodes a hypothetical protein which is annotated by the NCBI Conserved Domain Database (CDD) to be a member of the NurA nuclease superfamily, but its function has yet to be revealed in *D. radiodurans* or any other bacteria. The gene for the *D. radiodurans* NurA is found together in an operon with gene for the HerA helicase which is typical of these genes in archaea. There is evidence from archaea that suggests NurA is a nuclease involved in DNA repair of DSBs. The specific aim is to obtain evidence for a possible role in DNA repair for the putative NurA nuclease in *D. radiodurans* by generating a *nurA* deletion strain and characterizing the effect of this deletion in regards to DNA repair relative to wild-type strains.

1.5.2 Specific Aim 2: Biological Characterization of HerA from *D. radiodurans*

*D. radiodurans* contains an apparent homolog of the archaeal HerA helicase (DR\_0837) and as reported for other *herA* genes it is found together with the *nurA* gene in an operon. The NCBI CCD has annotated this gene as part of the HerA helicase superfamily, but there is no knowledge about its role in *D. radiodurans* or any other bacteria. There is existing evidence from archaea that suggests HerA is likely involved in the DNA repair of DSBs. The specific aim is to obtain evidence for a possible role in DNA repair for the putative HerA helicase in *D. radiodurans* by generating a *herA* deletion strain and characterizing the effect of this deletion on DNA repair relative to wild-type strains.

## Chapter 2: ASSESSMENT OF DNA REPAIR PHENOTYPES OF NURA AND HERA MUTANT STRAINS

### 2.1 INTRODUCTION

*Deinococcus radiodurans* cells are naturally competent and mutant strains are rather easily constructed via gene replacement (9, 26, 29). The most pressing issue in generating mutants via gene replacement is the fact *D. radiodurans* can contain up to 10 copies of its genome in a cell and thus total replacement typically requires several passes with antibiotic pressure. Many gene deletion strains have been made targeting suspected DNA repair enzymes such as nucleases and helicases (9). In order to assess if the targeted genes contribute to the DNA repair capacity of *D. radiodurans*, these mutant strains are compared to wild-type strains for their sensitivity to a wide variety of DNA damaging agents including ionizing radiation, UV-C radiation, MMC, methylmethane sulfonate (MMS) and H<sub>2</sub>O<sub>2</sub> (9).

As discussed in **Chapter 1**, *D. radiodurans* lacks the genetic precursors to repair DSBs using the RecBCD or AddAB pathways and appears instead to utilize the RecFOR pathway. However, mutant strains deficient in the nuclease (RecJ) and helicase (UvrD) implicated in this pathway do not show the same radiation sensitive phenotypes that *recA* deficient strains show (29, 30). This indicates that in the absence of these enzymes, RecA-dependent HR is still somehow able to occur, albeit less efficiently. The only way this pathway can occur is if some complex with a 5'-3' exonuclease activity and helicase activity is able to generate 3' ssDNA tails from an end of a DSB.

Experiments with the NurA nuclease and HerA helicase from archaea have demonstrated they are capable of generating the necessary 3' ssDNA tails from a DSB *in vitro* (44, 47). *D. radiodurans* contains apparent homologs of the *nurA* and *herA* genes found in archaea and they are expressed (56) indicating they have some function inside the cell. It seems possible that the putative NurA and HerA in *D. radiodurans* could assist in recovering from DSBs by priming the ends of a DSB for RecA loading.

In the present study, *nurA* ( $\Delta$ *nurA*) and *herA* ( $\Delta$ *herA*) mutant strains were generated via replacement of the respective target gene with a streptomycin resistance cassette (*aadA*) through HR. The resulting strains were evaluated for changes in their resistance to DNA damage induced by UV-C, phleomycin, MMC and H<sub>2</sub>O<sub>2</sub> relative to wild-type strains. Deletion of the *nurA* gene did not result in any significant difference in DNA damage sensitivity relative to wild-type for any of the agents tested. The loss of *herA* resulted in the same sensitivity as wild-type when both were treated with UV-C, MMC and H<sub>2</sub>O<sub>2</sub>. A mild increase in sensitivity to phleomycin was observed relative to wild-type. These results suggest no major role for the putative NurA and HerA enzymes from *D. radiodurans* in DNA repair.

Additionally, the putative protein product of HerA from *D. radiodurans* was expressed and purified from the *E. coli* Lemo21 (DE3) expression strain. Its biochemical characterization was only partially initiated so nothing can be confidently reported about its *in vitro* capabilities.

## 2.2 MATERIALS AND METHODS

### 2.2.1 Bacterial Strains, Plasmids and Culturing

The wild-type *D. radiodurans* R1 strain used in this study was purchased from the American Type Culture Collection (ATCC), Manassas, Va. Cultures of *D. radiodurans* were grown at 30°C in 2x TGY medium (1% tryptone, 0.6% yeast extract and 0.2% dextrose) or on 1x TGY agar plates (0.5% tryptone, 0.3% yeast extract and 0.1% dextrose, 1.5% agar). Liquid cultures were grown in either 15 mL conical tubes, 50 mL conical tubes or 125 mL Erlenmeyer flasks (ratio of container to culture volume was at least 5:1) and shaken at 250 rpm in the dark. Culture densities were estimated by OD<sub>600</sub> readings using a Cary 50 Bio UV/Vis spectrophotometer (Varian) with a 1 cm cuvette. When needed, streptomycin (Sigma-Aldrich) was added to cultures and plates at a concentration of 5 µg/mL.

The pCRII-Blunt-TOPO (Life Technologies), referred to herein as pCRTPOPO, was used to clone the  $\Delta$ *nurA* overlap fragment (see **Section 2.2.6**) and the Top10 *E. coli* (Life Technologies) strain was used to amplify this plasmid for subsequent sequencing of the overlap fragment.

The Zero Blunt cloning vector (Life Technologies), referred to herein as pCRBlunt, was used to clone the  $\Delta$ *herA* overlap fragment (see **Section 2.2.8**) and the Top10 *E. coli* strain was used to amplify this plasmid for subsequent sequencing of the overlap fragment.

The pTNK103 plasmid used to amplify the *aadA* gene was obtained as a kind gift from Dr. John Battista at Louisiana State University. The pET15b expression

plasmid (Novagen) was used to express the putative *herA* gene for subsequent purification.

*E. coli* strains were grown in Luria-Bertani (LB) medium (1% tryptone, 0.5% yeast extract, 1.0% NaCl) at 37°C and shaken at 250 rpm in the dark. Kanamycin (Sigma-Aldrich) was used at a concentration of 50 µg/mL for selection in strains containing the pCRTPOPO or pCRBlunt vectors. Ampicillin (Sigma-Aldrich) was used at a concentration of 100 µg/mL for selection in strains containing the pET15b plasmid. The *E. coli* expression strain, *Lemo21 (DE3)* was obtained as a kind gift from Dr. Hutcheson. *D. radiodurans* is known for its use of rare codons (9) and the *Lemo21 (DE3)* strain is capable of providing tRNA for rare codons.

#### 2.2.2 Isolation of Genomic DNA

*D. radiodurans* genomic DNA (gDNA) was isolated as described before (58) and used for genotyping mutant strains via PCR. A 5 mL culture was started from a single colony in 3 mL 2x TGY in a 15 mL conical tube and grown at 30°C while being shaken at 250 rpm overnight. The stationary phase culture was then utilized for gDNA isolation. The culture was spun down at 10,000 x g for 1 minute and the supernatant removed via decanting followed by pipetting. The resulting pellet was resuspended in 1 mL 95% (v/v) ethanol and incubated at room temperature (23°C) for 10 minutes to break down the outer membrane. This suspension was then spun down at 5,000 x g for 3 minutes and the supernatant discarded as described before. The resulting cell pellet was white and was resuspended in 1 mL resuspension buffer (10 mM Tris-HCl, 0.1 mM EDTA, pH 7.5) and lysozyme added (Sigma-Aldrich) to a

concentration of 0.25 mg/mL. This was incubated at 37°C in a water bath for 30 minutes.

This cell lysate was then supplemented with 9 µL 10% SDS and 1 µL proteinase K (20 mg/mL; Thermo Scientific) and incubated at 55°C for 3 hours. This was then split into two microcentrifuge tubes (~500 µL per tube) and each aliquot extracted 3x times with 500 µL phenol:chloroform:isoamyl alcohol (25:24:1; Sigma Aldrich). To perform the extraction, the organic solvent was added to the cell lysate and this was inverted several times. The solution was then spun at 10,000 x g for 5 minutes and the upper aqueous layer removed and added to a new microcentrifuge tube. This process was repeated until all three extractions had been performed and two tubes containing the aqueous layers were obtained. These tubes were then combined into a single tube.

To precipitate gDNA, 1 volume of 99% (v/v) isopropyl alcohol and 1/10 volume of 3M sodium acetate (pH 5.2) was added and this was subsequently incubated at -20°C for a minimum of 30 minutes (on occasion, due to timing issues, extractions were left overnight at -20°C). Following this incubation, the solution was spun at 10,000 x g for 30 minutes at room temperature and supernatant decanted as described before. The resulting pellet was washed 3x times with 1 mL ice-cold 70% ethanol to remove any remaining salt. Each wash step included a 1 minute spin down at 10,000 x g and a subsequent removal of the supernatant. After the final wash, the pellet was air dried and resuspended in 100 µL resuspension buffer or ultra-pure water. The concentration of extracted gDNA was determined by taking absorbance readings at 260 nm using a UV spectrophotometer (Varian).

### 2.2.3 Transformation of *D. radiodurans*

DNA transformations into *D. radiodurans* were performed as described previously (26). A 5 mL wild-type culture was started from a single colony in 2x TGY in a 50 mL conical tube and shaken at 250 rpm at 30°C overnight. The following day, the overnight culture was diluted to an OD<sub>600</sub> of 0.1 in 5 mL 2x TGY in a 50 mL conical tube. This was shaken at 250 rpm and 30°C until the OD<sub>600</sub> reached 0.5, indicating the culture was in the early stages of exponential growth. Once the desired OD<sub>600</sub> had been achieved, 1 mL of the culture was spun down at 5,000 x g for 1 minute and the supernatant removed. This was repeated two more times so that a final 3 mL pellet was obtained. This pellet was resuspended in 25 µL of sterile 0.1 M CaCl<sub>2</sub> and 75 µL 2x TGY medium. This was subsequently supplemented with transforming DNA and placed on ice for 10 minutes. Following this, the transformation mixture was then shaken at 250 rpm at 30°C for 1 hour. This mixture was then supplemented with 1 mL 2x TGY medium, transferred to a 15 mL conical tube and shaken overnight at 250 rpm at 30 °C. The following day 100 µL of this transformation mixture was spread on 1x TGY plates containing the appropriate selection antibiotic (streptomycin; 5 µg/mL). Plates were incubated about 48 hours at 30°C to allow colonies to form.

### 2.2.4 Restriction Digestions, Ligations and Transformations in *E. coli*

Restriction digestions were performed according to manufacturer's protocols. Briefly, all digestion reactions were carried out in a volume of 20 µL in 1x of the suggested buffer for the particular restriction enzyme being used. Reactions which required double digestion were performed in the recommended buffer suggested by



NEBs Double Digest Finder (<https://www.neb.com/tools-and-resources/interactive-tools/double-digest-finder>). Following the digestion reactions, the products of these reactions were visualized by gel electrophoresis on a 0.7% 1x TAE (40mM Tris, 20mM acetic acid, 1mM EDTA, pH 8) agarose gel pre-stained with ethidium bromide (1µg/mL; BioRad). If digested products needed to be isolated they were cut out of the gel with a razor blade and subsequently purified using the Illustra GFX PCR DNA and Gel Band Purification Kit (GE Healthcare) according to manufacturer's protocols.

When target DNA was to be ligated into a corresponding plasmid which could replicate in *E. coli* a 10:1 molar ratio of the insert to vector was used. Once the vector and plasmid were mixed in the appropriate molar ratios, the ligation reaction was set up in 1x T4 DNA ligase buffer (New England Biolabs; NEB) with 1 µL of T4 DNA ligase (NEB) in a 20 µL reaction volume. The reaction was diluted as need with ultra-pure water. This reaction was allowed to react at room temperature (23°C) for 30 minutes. *E. coli* Top 10 competent cells were transformed directly with this ligation mixture using the heat shock method (59). All 20 µL of the reaction mixture was added to 100 µL Top 10 competent cells which had been thawed from -80°C for 10 minutes on ice. This mixture was left on ice for 30 minutes and then heat shocked at 42°C for 90 seconds in a water bath before being placed back on ice for 1 minute.

Following this the cell suspension was diluted with 900 µL SOC media (2% tryptone, 0.5% yeast extract, 10 mM NaCl, 2.5 mM KCl, 10 mM MgSO<sub>4</sub>, 10 mM MgCl<sub>2</sub>, 20 mM dextrose, pH 7.5) and transferred to a 15 mL conical tube. This was grown at 37°C for 1 hour while being shaken at 250 rpm before 50-100 µL was plated

on LB agar plates containing 50 µg/mL kanamycin (pCRTPO) or 100 µg/mL (pET15b) ampicillin depending on the vector being used.

### 2.2.5 Polymerase Chain Reactions

PCR reactions were carried out using the Phusion DNA polymerase (NEB). Reactions were carried out for either genotyping or amplification of desired DNA fragments. PCR reactions were performed in 200 µL PCR tubes in 50 µL reaction mixtures containing 0.5 µM of both forward and reverse primers, 200 µM deoxynucleotide triphosphates (dNTPs), 5% (v/v) dimethyl sulfoxide (DMSO), 1.7 mM MgCl<sub>2</sub>, 1x Phusion GC Buffer, 1 unit of Phusion DNA polymerase and 200 ng of gDNA or 1 ng of plasmid DNA as a template. Ultra-pure water was used to dilute reaction mixtures to desired concentrations.

When multiple reactions were being performed with the same primer pairs, but with different DNA templates, master mixes were made which contained all the necessary components of the reaction except the template. Master mixes were made in excess of the number of samples needed such that if 8 reactions were being performed, the master mix was made for 9. DNA templates were added to individual PCR tubes and then the master mix added. 15 µL of mineral oil was added to each sample following completion of the 50 µL reaction mixture to reduce the chances of buffer concentration changes in the reaction mixture which could occur if the reaction mixture evaporated. All reactions were carried out on a MasterCycler (Eppendorf) thermocycler.

The thermocycler conditions started with an initial denaturation step at 98°C for 30 seconds. This was followed by an additional denaturation step at 98°C for 10

seconds, an annealing step which was 3°C above the T<sub>m</sub> for the lower T<sub>m</sub> primer (typically between 50-65°C depending on primer pair) for 30 seconds and an extension step at 72°C for 20 seconds per kilobase (kb) of the desired target. These three steps were repeated 30-35 times and then a final extension at 72°C for 10 minutes was performed. Reactions were thermoquenched by holding them at 4°C until they could be removed from thermocycler for evaluation.

PCR reactions were analyzed by electrophoresis as described above. Images of the gels were taken using a Canon Cool Pix 8 MP camera and analyzed using Image J software (version 1.48o; National Institutes of Health, <http://imagej.nih.gov/ij>). Bands of the predicted size were excised and extracted as described above. All primers used in PCR reactions can be found in **Table 2** and **Table 3**.

#### 2.2.6 Cloning and Sequencing of *nurA* and $\Delta$ *nurAKO* Fragment

The *nurA* gene was amplified from wild-type *D. radiodurans* gDNA using primers FrwNurA and RevNurA as described above. The resulting blunt-end fragment was ligated into the pCRTOPO vector (Invitrogen) and subsequently transformed into *E. coli* Top 10 strain (Invitrogen). The complete sequence for the 1057 base pair (bp) *nurA* gene was determined at the DNA sequencing facility in the Center for Biosystems Research, University of Maryland. The entire sequence was able to be read using the M13Rev and M13 (-21) universal sequencing primers provided by the DNA sequencing facility.

The *nurA* gene was cut out of pCRTOPO\_*nurA* with the restriction enzymes BamHI and NdeI and subsequently ligated into the pET15b expression plasmid cut with the same enzymes. The new plasmid, pET15b\_*nurA* was sequenced as well and

found to be correct. This plasmid was never used to express the NurA protein in *E. coli* due to time restrictions in this study, but is available for future studies.

The  $\Delta nurA$  KO fragment was constructed as described below and subsequently ligated into the pCRTOPO vector. This was transformed into the *E. coli* Top 10 strain as described above. The complete sequence of the 2849 bp product was determined using 4 primers: M13Rev, M13 (-21), MJ5 and MJ6. The primers MJ5 and MJ6 are the forward and reverse primers used to amplify the *aadA* gene. Using all four primers a complete read was achieved.

**Table 2 DNA oligonucleotides used for  $\Delta$ nurA strain**

<i>Usage</i>	<i>Sequence (5'-3')</i>
<b>nurA gene replacement</b>	
<b>nurA upstream DNA amplification:</b>	
FNur1	gAACgCgggATCCggTAggC
RNur2	gAACC <u>ggATCC</u> ggCTg <u>AATTC</u> gCgggggAggATTgTACggCAGC BamHI EcoRI
<b>nurA downstream DNA amplification:</b>	
FNur2	CCAgg <u>CATAT</u> ggggCg <u>AATTC</u> gCCCggggAATgACgTgCAAgg NdeI EcoRI
RNur1	gCgTCggAAAACACgTAggg
<b>aadA gene amplification:</b>	
MJ5	CgCg <u>AATTC</u> AgCC <u>ggATCC</u> ggTTCgCgAgggCCTgAgggCCATg EcoRI BamHI
MJ6	ggCg <u>AATTC</u> gCCC <u>AAgCTT</u> CCTggTCgAAAgTTTAAACTTATTTgCCgACTACCTTggTg EcoRI HindIII
<b>Genotyping</b>	
RTNurF	gCTgAgCAGCCTgAAATg
RNur1	gCgTCggAAAACACgTAggg
aadAFrw	gCgAgATTCTCCgCgCTgTA
RTNurF	gCTgAgCAGCCTgAAATg
FrwNurA	<u>CATAT</u> gCgTATTCgTCTggACCCC-3 NdeI
RevNurA	<u>ggATCC</u> TTCCCCgTCACgCCACCAC- BamHI
<b>Cloning</b>	
FrwNurA	<u>CATAT</u> gCgTATTCgTCTggACCCC NdeI
RevNurA	<u>ggATCC</u> TTCCCCgTCACgCCACCAC BamHI

### 2.2.7 Generation of $\Delta nurA::strep$ ( $\Delta nurA$ )

A fragment ( $\Delta nurAKO$ ) containing the *aadA* gene flanked by the upstream and downstream regions of the *nurA* gene was made using overlap PCR (58, 60). The upstream region (U) and downstream (D) regions of the *nurA* gene were amplified (using primers FNur1/RNur2 and FNur2/RNur1 respectively) from wild-type *D. radiodurans* gDNA by PCR. The *aadA* gene was amplified from the plasmid pTNK103 using PCR. Bands of the predicted size (0.800 kb upstream, 1.161 kb *aadA*, 0.929 kb downstream) were visualized from electrophoresis (**Figure 2-1,A**) and purified as described above.

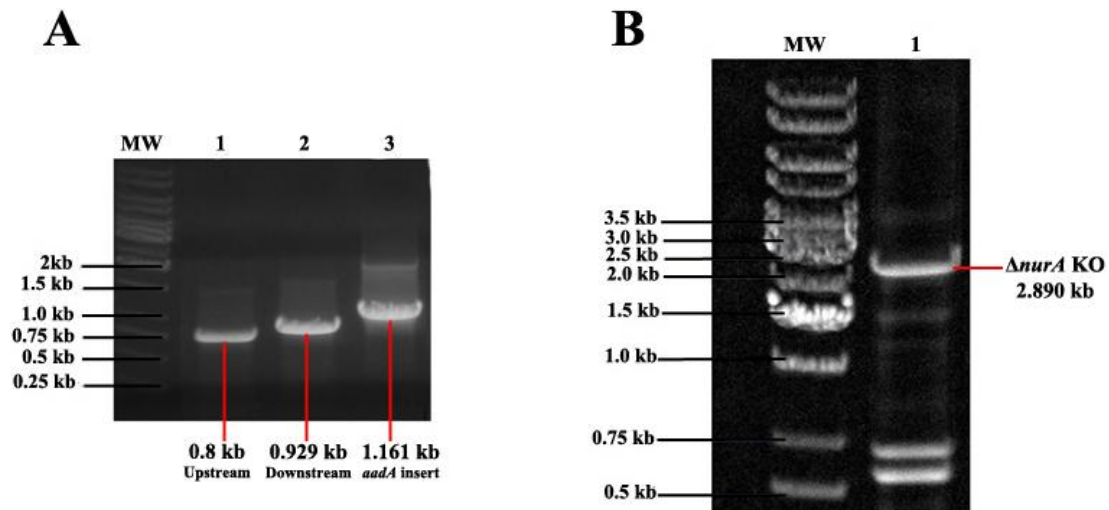


**Figure 2-1: Making pCRBlunt\_  $\Delta nurA$ .**

(A) An agarose gel image of the amplified DNA fragments used to make the  $\Delta nurA$  overlap fragment. Molecular weight marker is denoted by lane labeled MW. Lane 1 is DNA region upstream of *nurA* amplified from gDNA with primers FNur1/RNur2 (0.800 kb). Lane 2 is DNA region downstream of *nurA* amplified from gDNA with primers FNur2/RNur1 (0.929 kb). Lane 3 is *aadA* gene amplified from pTNK103 plasmid with primers MF5/MJ7 (1.161 kb). (B) An agarose gel image of the  $\Delta nurA$  overlap PCR reaction made using the upstream, downstream and *aadA* insert mixed in a 1:1:1 molar ratio as the DNA template with primers FNur1/RNur1. Molecular weight marker is denoted by lane labeled MW. Predicted product is 2.890 kb and is marked in Lane 1.

The  $\Delta nurA$  KO fragment was made by using an overlap extension PCR reaction (61). Briefly, the 5' end of the *aadA* gene overlapped with the 3' end of the *nurA* upstream fragment and the 3' end of the *addA* gene overlapped with the 5' end of the *nurA* downstream fragment. These three PCR generated fragments were used as template DNA in a reaction using the primers FNur1 and RNur1 and were mixed in a 1:1:1 molar ratio. The product of this reaction was a blunt end 2849 bp product (**Figure 2-1, B**). The  $\Delta nurA$  PCR product was purified from the reaction mixture as described above. The PCR-amplified fragment was ligated into pCRTOPO (pCRTOPO\_  $\Delta nurA$ ) and sequenced to verify the desired sequence with no mutations.

The  $\Delta nurA$  deletion strain was created by transforming wild-type cultures in the early-exponential phase of growth with the linear  $\Delta nurAKO$  fragment as described before (58, 60). The *aadA* gene codes for an enzyme which allows cells to grow in the presence of streptomycin. Transformations were carried out as described above. This procedure was repeated 3 times resulting in the isolation of 5  $\Delta nurA$  strains. Strains were stored at -80°C as glycerol stocks when they were not being studied. These stocks were made by mixing 700µL of an overnight culture with 300 µL of 50% glycerol that was filtered through a 0.2 µm filter using a syringe.

#### 2.2.8 Cloning and Sequencing of *herA* and $\Delta herAKO$ Fragment

The ORF of the *herA* gene was amplified using the Phusion Polymerase as described before using the FrwHerA and RevHerA primers (**Table 3**). The resulting PCR fragment was purified and ligated into pCRBlunt and transformed into Top10 competent cells. The *herA* gene fragment was excised from this plasmid (pCRBlunt\_ *herA*) by cleavage with BamHI and NdeI, purified, and ligated into the

pET15b (Invitrogen) expression plasmid (cut with BamHI and NdeI). The resulting plasmid (pET15b\_herA) was isolated and sequenced to ensure the plasmid contained the *herA* gene in the proper orientation with no mutations.

The  $\Delta$ *herAKO* fragment was constructed as described below using the pCRBlunt vector as a scaffold for its construction. This was transformed into *E. coli* Top10 strain. The complete sequence of the 2677 bp product was determined using 4 primers: M13Rev, M13 (-21), MJ5 and MJ8. The primers MJ5 and MJ8 are the primers forward and reverse primers used to amplify the *aadA* gene. Using all four a complete read was achieved.



**Table 3: DNA oligonucleotides used for  $\Delta herA$  strain**

<i>Usage</i>	<i>Sequence (5'-3')</i>
<b><i>herA</i> gene replacement</b>	
<b><i>herA</i> upstream DNA amplification:</b>	
FHer1_Over	ggCTg <u>AATTC</u> gCgCAgCCCACgCAACCCACAC EcoRI
RHer2_Over	gAACCGT <u>ggATCC</u> gCggCCACCACCCCCTgCgTC BamHI
<b><i>herA</i> downstream DNA amplification:</b>	
FHer2_over	CCAgg <u>AAgCTT</u> gggC <u>ggATCC</u> gCCgAgAAgCggACgATgCTgAgg HindIII BamHI
RHer1_Fin	CCAgg <u>TCTAgA</u> ggCgACgggCATTggCCggAC XbaI
<b><i>aadA</i> gene amplification:</b>	
MJ5	CgCg <u>AATTC</u> AgCC <u>ggATCC</u> ggTTCgCgAgggCCTgAgggCCATg EcoRI BamHI
MJ7	ggCg <u>AATTC</u> gCCCC <u>CATATg</u> CCTggTCgAAAgTTTAAACTTATTTgCCgACTACCTTggTg EcoRI NdeI
MJ8	ggCg <u>AATTC</u> gCCC <u>TCTAgA</u> CCTggTCgAAAgTTTAAACTTATTTgCCgACTACCTTggTg EcoRI XbaI
<b>Genotyping</b>	
RTHerF	gggTCAATCTCCAgACCTTC
RHer1	gACgggCATTggCCggAC
aadAFrw	gCgAgATTCTCCgCgCTgTA
RTNurF	gCTgAgCAgCCTgAAATg
RNur1	gCgTCggAAAACACgTAggg
FNur1	gCgAACgCgggATCCggTAggC
<b>Cloning</b>	
FrwHerA	<u>CATATg</u> ACggggAATgACgTgCAAg NdeI
RevHerA	<u>ggATCC</u> TTCTCTTCAGCgCAgCAgCCC BamHI

### 2.2.9 Generation of $\Delta herA::strep$ ( $\Delta herA$ )

There were many attempts to generate the  $\Delta herA$  KO fragment using overlap PCR, but all were unsuccessful. As a result, an alternative strategy was employed to

make this KO fragment. The strategy used the pCRBlunt cloning vector as a scaffold for ligating the three individual segments of the  $\Delta herAKO$  together. The details are described below and a schematic representation is shown in **Figure 2-2**.

As described before, the regions upstream (U; FHer1\_Over/RHer2\_Over), downstream (D; FHer2\_Fin/RHer1\_Fin) and the *aadA* (A; MJ5/MJ8) streptomycin resistant gene were amplified by PCR (**Figure 2-3,A**). Following this, ligation reactions were set up such that U and A were ligated with T4 DNA ligase in a 1:1 molar ratio (~40nm) of DNA ends. This ligation reaction was then used as a template (5 $\mu$ L) to amplify the UA insert using PCR (**Figure2-3, B**).

The ~1.8 kb amplified product was used in a ligation reaction with pCRBlunt after weeks of trying to ligate and amplify this fragment (via overlap PCR) with D. The ligation reaction used 700 ng UA with 1  $\mu$ L pCRBlunt stock (25 ng/ $\mu$ L; 1:20). This was transformed into Top10 *E.coli* competent cells and colonies that formed on LB-KAN (50 $\mu$ g/mL) were screened further. The blunt end ligation method meant that the UA insert could orient in two different directions such that the insert could be UA (5'-3') or AU (5'-3'). Several colonies were cultured and the potential pCRBlunt-UA plasmids isolated. These plasmids were subjected to restriction digestion analysis using the XbaI restriction enzyme. If the UA fragment was inserted correctly, digestion with XbaI will linearize the plasmid and if not it will excise UA.

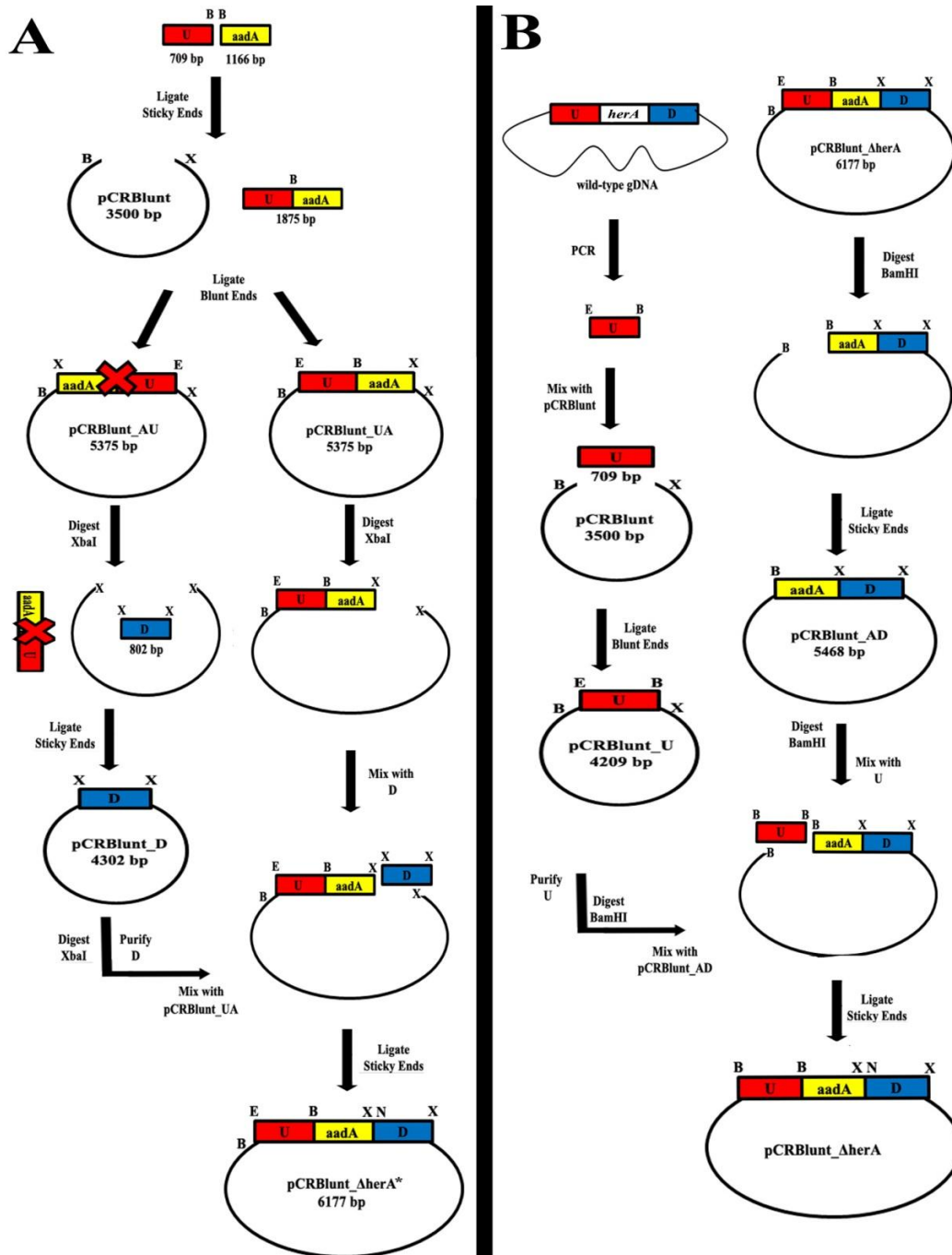


**Figure 2-2: Making pCRBlunt\_ΔherA\*.**

A schematic representation of the steps taken to generate the pCRBlunt\_ΔherA plasmid. **(A)** The progression of steps taken to generate the pCRBlunt\_ΔherA\* plasmid which contained mutations in the upstream region of the ΔherKO fragment. **(B)** The progression of steps taken to generate the pCRBlunt\_ΔherA plasmid which did not contain any mutations. U-709 bp region of DNA upstream of herA. D-802 bp region of DNA downstream of herA. E-EcoRI site. B-BamHI site. X-XbaI site, N-NdeI site. All molecular biology techniques shown in schematic were carried out as described in Methods.

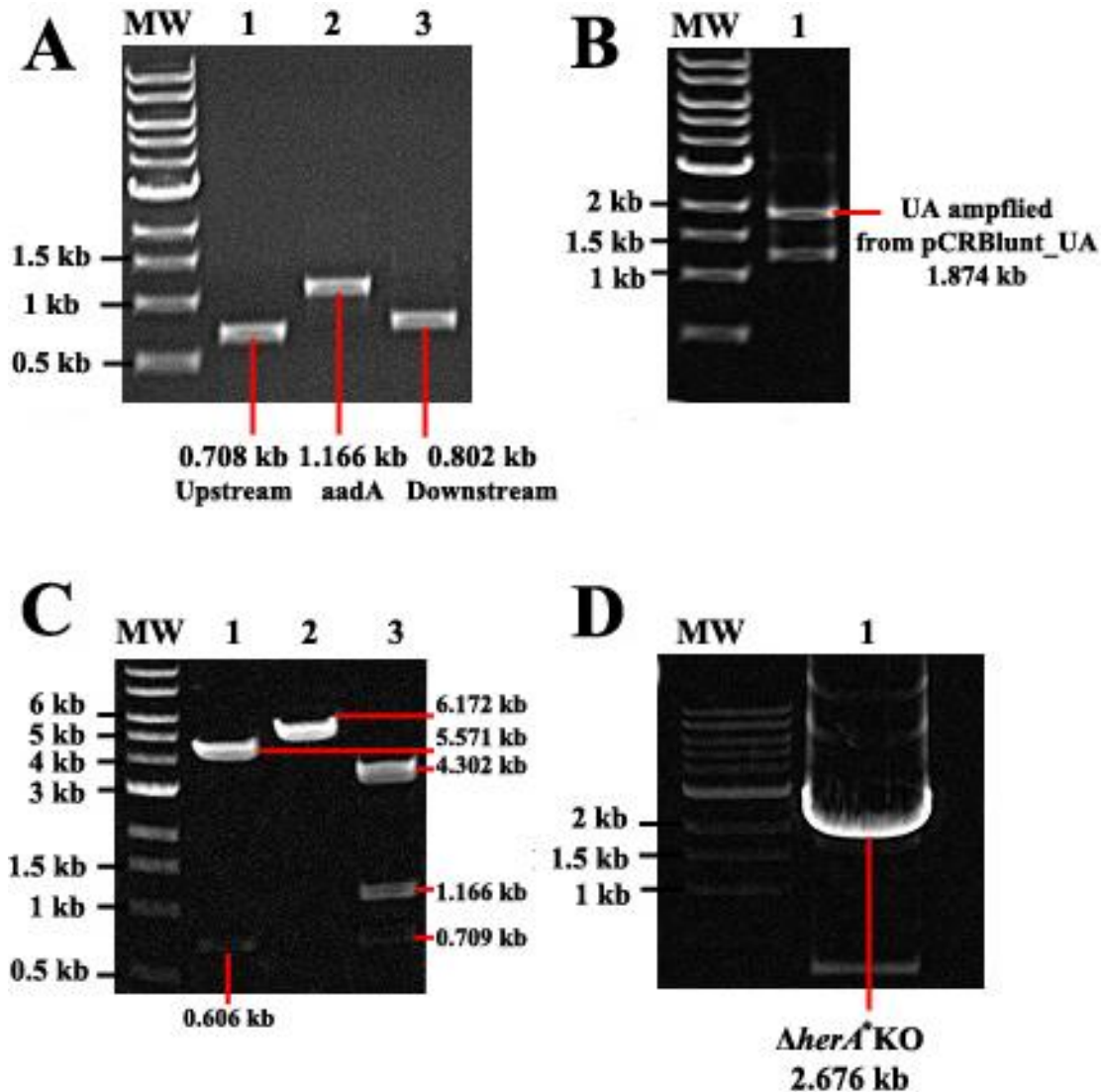


**Figure 2-3: Generation of pCRBlunt\_ΔherA\*.**

Images of agarose gel electrophoresis analysis of PCR reactions and restriction enzyme analysis performed during the construction of pCRBlunt\_ΔherA\*. Molecular weight markers are denoted above lanes with MW. (A) Phusion PCR products of the DNA fragment upstream from *herA* (Lane 1; 708 bp), the *aadA* gene (Lane 2; 1166 bp) and the DNA fragment downstream from *herA* (Lane 3; 802bp). (B) The upstream fragment was ligated to the *aadA* gene and inserted into pCRBlunt (pCRBlunt-UA). Image shows this UA (Lane 1; 1874 bp) fragment amplified by PCR from pCRBlunt-UA with Phusion polymerase. (C) pCRBlunt\_ΔherA\* was digested with HindIII (Lane 1) to give two linear fragments of 0.606 kb and 5.571 bp, with BamHI to give a linear pCRBlunt\_ΔherA\* plasmid (6.172 kb; Lane 2) and BamHI/NdeI to give three fragments of 4.302 kb, 1.161 kb and 0.709 kb (Lane 3). (D) The ΔherA\* KO (2.676 kb) fragment amplified from pCRBlunt\_ΔherA\* with Phusion polymerase.

The first several screens all had the UA insert in the wrong orientation. These improper pCRBlunt-UA plasmids (pCRBlunt-AU) were further utilized. The UA fragment was cut out of pCRBlunt-AU with XbaI and the resulting pCRBlunt plasmid containing XbaI sticky ends was purified. This plasmid was then used in a ligation reaction with D (also digested with XbaI) and then transformed into *E. coli* Top 10 to give pCRBlunt\_D, which allowed for easy isolation of D through digestion with XbaI.

The UA insert was ligated again with pCRBlunt and eventually pCRBlunt-UA in the proper orientation was made. Both pCRBlunt-UA and pCRBlunt\_D were digested with XbaI in separate reactions. The linear pCRBlunt-UA was purified as well as the D fragment. The pCRBlunt-UA plasmid was then ligated with D in a reaction with a 70:1 molar ratio of D to pCRBlunt-UA. The corresponding products of these ligation reactions became known as pCRBlunt\_ΔherA\*. The resulting plasmid gave the appropriate restriction digestion patterns when digested with BamHI/NdeI, NdeI, and HindIII, indicating that the ΔherA\* KO fragment had been successfully made (**Figure 2-3, C**). The BamHI/NdeI reaction gave 0.709 (U), 1.161 kb fragment (A) and 4.302 kb fragments (pCRBlunt\_D). The NdeI reaction gave a 6.172 kb band and the HindIII reaction gave a 5.571 (partial pCRBlunt\_ΔherA\*) and 0.6 kb bands (partial U).

This pCRBlunt\_ΔherA\* plasmid was used in a reaction with Phusion which gave the expected 2.677 kb band which was subsequently isolated (**Figure 2-3, D**). The plasmid this was amplified from was never subjected to sequence analysis prior to using the purified PCR product to transform wild-type *D. radiodurans*. Failure to

confirm the sequence resulted in the generation of several  $\Delta herA^*$  mutant strains which contained mutations in the *nurA* gene that must have been introduced into the upstream (U) fragment during the construction of the  $\Delta herA^*$  KO fragment. The results from the partial characterizations of these strains and other information regarding these strains are presented in **Appendix 1**.

As a result of the unintended mutations described above, the  $\Delta herA$  KO fragment was remade. To do this, the pCRBlunt\_ $\Delta herA^*$  plasmid containing the upstream (U) fragment with the *nurA* mutations was excised with BamHI in a restriction digestion reaction. The resulting pCRBlunt\_AD plasmid with BamHI sticky ends was isolated and then set up in a ligation reaction to circularize the plasmid via the XbaI sticky ends. This was transformed into *E. coli* Top 10 competent cells and subsequently purified as described before. The upstream (U) fragment was amplified again from wild-type gDNA by PCR and subsequently ligated into pCRBlunt (with blunt ends). This introduced a BamHI site upstream of the U fragment allowing the U fragment to be excised with a single digestion reaction with BamHI.

Both pCRBlunt\_AD and pCRBlunt\_U were digested with BamHI in separate reactions. The linear pCRBlunt\_AD was purified as well as the U fragment. The pCRBlunt\_AD plasmid was then ligated with U in a reaction with a 70:1 molar ratio of U to pCRBlunt\_AD. The corresponding products of these ligation reactions became known as pCRBlunt\_ $\Delta herA$ . This plasmid was sequenced as described in Methods and once the sequence was confirmed to be correct, the plasmid was digested with EcoRI and ApaI resulting in a linear  $\Delta herA$  KO fragment which was subsequently used to transform wild-type *D. radiodurans* as described before. This

was repeated 3 times and 3 strains isolated. All displayed similar growth properties, but only the original strain  $\Delta herAI$  ( $\Delta herA$ ) was fully characterized. Genomic DNA was isolated from colonies of the  $\Delta herA$  strains for genotyping by PCR using primers listed in **Table 3**. Strains were stored at  $-80^{\circ}\text{C}$  as glycerol stocks when they were not being studied.

#### 2.2.10 *In vivo* Survival Assays with Treatments of DNA Damaging Agents

In all biological survival assays, cultures of wild-type and mutant ( $\Delta nurA$  or  $\Delta herA$ ) strains were grown into stationary phase (~48 hrs growth) and then diluted into 2x TGY media to an  $\text{OD}_{600}$  between 0.01-0.1. When the  $\text{OD}_{600}$  was between 0.5-1.0, such that cells were in an exponential state of growth, aliquots were removed and tested against a specific DNA damaging agent as described below.

In all survival assays, plates spotted with cells (treated or untreated) were allowed to incubate for at least 48 hours to allow colonies to form and then the number of colony forming units per mL (CFU/mL) determined from colony counts by taking the average number of colonies from the replicate spotting, multiplying this value by the dilution factor and then dividing this product by the volume spotted in mL. Normalized CFU/mL calculations were compared to determine the various sensitivities to the agents.

##### 2.2.10.1 Treatment with $\text{H}_2\text{O}_2$

When wild-type and mutant exponential cultures had reached the desired  $\text{OD}_{600}$ , four 500  $\mu\text{L}$  aliquots from each culture were removed and pipetted into 1.5 mL microcentrifuge tubes. All the tubes had a tiny hole punctured in the top (21 gauge,

sterile needle) to allow O<sub>2</sub> that was formed during the reaction with H<sub>2</sub>O<sub>2</sub> to escape, essentially ensuring pressure didn't build inside the tube during treatment. 30% H<sub>2</sub>O<sub>2</sub> (less than 3 weeks old; stored sealed at 4°C) was added to 3 of these tubes such that the concentration of H<sub>2</sub>O<sub>2</sub> in each was 100, 150 and 200 mM respectively. One tube was left untreated as a control. Upon addition of H<sub>2</sub>O<sub>2</sub> the tubes were placed in a microcentrifuge rack secured upon a shaker with temperature control such that the samples were shaken at 250 rpm for 30 minutes at 30°C. Following this incubation period, cells were spun down for 2 minutes at 10,000 x g and the supernatant removed via pipetting. Cell pellets were resuspended in 500 µL 2x TGY and then serially diluted such that the final dilution was diluted 1 x 10<sup>5</sup> fold. Either three or four of these dilutions were spotted (10 µL) in triplicates onto 1x TGY plates. The number of CFU/mL from treated plates was normalized to the control plates which received no treatment with H<sub>2</sub>O<sub>2</sub>.

#### 2.2.10.2 Treatment with MMC

When wild-type and mutant exponential cultures had reached the desired OD<sub>600</sub>, a 500 µL aliquot from each culture was removed and pipetted into 1.5 mL microcentrifuge tube. This aliquot was serially diluted up to 1 x 10<sup>5</sup> fold and either three or four of these dilutions were spotted (10 µL) in triplicates onto 1x TGY plates and 1x TGY plates containing 100 ng/mL MMC.

#### 2.2.10.3 Treatment with UV-C

When wild-type and mutant exponential cultures had reached the desired OD<sub>600</sub>, a 500 µL aliquot from each culture was removed and pipetted into 1.5 mL



microcentrifuge tube. This aliquot was serially diluted up to  $1 \times 10^5$  fold and either three or four of these dilutions were spotted (10  $\mu$ L) in triplicates onto four 1x TGY plates. Three of these plates were exposed to different amounts of UV-C radiation generated by a 15 Watt germicidal lamp (FG15T8; Fisher) with a calibrated dose rate of  $1.6 \text{ J/m}^2 \cdot \text{s}$ ; measured using UVX Radiometer (UVP, Upland, CA). Once the desired dose was achieved, the plates were removed and left in the dark at 30 °C until colonies formed. The dose rate was checked before and after exposure to ensure a constant dose was delivered during the exposure time. Plates spotted with WT and mutant cultures were exposed simultaneously to UV radiation so that they received equivalent doses.

#### 2.2.10.4 Treatment with Phleomycin

When wild-type and mutant exponential cultures had reached the desired  $\text{OD}_{600}$ , a 500  $\mu$ L aliquot from each culture was removed and pipetted into 1.5 mL microcentrifuge tube. This aliquot was serially diluted up to  $1 \times 10^5$  fold and either three or four of these dilutions were spotted (10  $\mu$ L) in triplicates onto 1x TGY plates and 1x TGY plates containing 1, 2.5 and 5  $\mu\text{g/mL}$  phleomycin.

#### 2.2.11 Expression and Purification of Putative HerA Enzyme

To generate whole cell lysates, a single colony of the *E.coli* expression strain *Lemo21(DE3)* (kind gift from Dr. Hutcheson) transformed with our HerA expression plasmid (pET15b\_herA) was inoculated into LB media and allowed to grow into stationary phase (37°C;250 rpm shaking). This culture was subsequently diluted into

1L of LB media and allowed to grow until  $OD_{600}$  was 0.1 upon which the culture was induced with IPTG (Sigma-Aldrich) such that the final concentration was 1mM.

The induced culture was grown for 3 hours and then cell pellets collected by centrifugation at 10,000 x g for 1 hour at 4°C. Wet pellets were lysed with Bug Buster Master Mix (Novagen; 1mL/g wet cell paste) according to manufacturer's protocols to obtain the soluble fraction of the cell extract. The soluble fraction was loaded onto a 5 mL His-Trap column hooked up to an AKTA FPLC system. The column was equilibrated with binding buffer (20 mM  $H_2PO_4$ , pH 7.4; 0.5 M NaCl; 45 mM imidazole). Protein was eluted using a gradient consisting of wash buffer (20 mM  $H_2PO_4$ , pH 7.4; 0.5 M NaCl; 65 mM imidazole) and elution buffer (20 mM  $H_2PO_4$ , pH 7.4; 0.5 M NaCl; 500 mM imidazole) at a flow rate of 3 mL/min.

Fractions containing a protein approximately 67 kD were determined by SDS-PAGE and subsequent visualization via Coomassie blue and/or silver staining. These were combined and loaded into a SLYDE-a-Lyzer (Piercenet) and dialyzed overnight into HiTrap Q-F/F binding buffer (20 mM Tris-HCl, pH 8.0). Dialyzed samples were loaded onto 20 mL Hi-Trap Q-F/F column and eluted by a linear gradient consisting of binding buffer and elution buffer (20 mM Tris-HCl, pH 8.0; 1 M NaCl). Fractions that tested positive after SDS-PAGE and silver staining analysis for a ~67kD band were combined and concentrated using Amicon Ultra 2 Centrifugal Filter Devices according to manufacturers' protocol. Purified samples showed no signs of other proteins in silver stain. Protein concentration and ATPase activity was assessed as described below.

### 2.2.12 Micro-Bradford Assay

Total protein concentration was estimated using the Bradford method which is based on the equilibrium between three forms of the Coomassie Blue G dye. Under strongly acidic conditions the dye is most stable as the +1 ion (red), but when bound protein becomes more stable as -1 anion (blue). The change in protonation state can be observed by monitoring the absorbance at 595nm which is the  $\lambda_{\text{max}}$  for the dye and protein complex. BSA stocks (20 mg/mL; NEB) were serially diluted into ultra-pure water give a series of standards ranging from 100 to 10  $\mu\text{g/mL}$  of BSA. 800  $\mu\text{L}$  of protein samples were mixed with 200  $\mu\text{L}$  of 1x Coomassie Blue G solution (100  $\mu\text{g/mL}$  Coomassie Blue G, 10% methanol (v/v), 17% phosphoric acid (v/v), pH 1.1). Samples were mixed and the absorbance at 595 nm determined using our UV-Vis spectrophotometer. A plot of  $A_{595}$  vs. the concentration of BSA standards was made and subjected to linear regression analysis ( $y = 0.246x - 0.03$ ;  $r^2 = 0.98$ ). The slope from this standard curve was used to estimate the concentration of the HerA protein.

### 2.2.13 ATPase Activity Assay

ATPase assays were carried out in triplicates in 20  $\mu\text{L}$  reactions using 80 or 160 nM HerA enzyme in the ATPase reaction buffer (10 mM Tris-HCl, pH 7.5, 1 mM DTT, 1 mM ATP, 1 mM  $\text{MgCl}_2$ ). ATPase activity was determined as the amount of nmols of phosphate generated per monomer of HerA following incubation of HerA in ATPase buffer for 20 minutes at room temperature. Free phosphate was determined by spectrophotometry after incubation of the reaction mixture with 200  $\mu\text{L}$  of the reagent BIOMOL Green (Enzo Life Sciences) for 30 minutes. Analysis was performed according to the manufacture's protocol. When HerA enzyme was

incubated with DNA substrates, 10  $\mu$ M of total DNA molecules was the final concentration in these reactions.

## 2.3 RESULTS

### 2.3.1 Confirmation of *nurA* and *herA* deletion

The removal of the *nurA* and *herA* genes was confirmed by PCR (**Figure 2-4**). Four separate reactions were designed to probe the *nurAherA* operon. The replacement of *nurA* or *herA* with the *aadA* gene resulted in a distinct size change of the *nurAherA* operon in the gDNA of the wild-type (4.483 kb),  $\Delta$ *nurA* (4.554kb) and  $\Delta$ *herA* (3.747 kb) strains. The length of the *nurAherA* operon was checked using a forward primer (FNur1, see **Table 3**) upstream of *nurA* and reverse primer (RHer1) downstream of *herA*. As shown in **Figure 2-4, A**, the size of the bands amplified from gDNA extracted from wild-type,  $\Delta$ *nurA* and  $\Delta$ *herA* cells were found to be their predicted sizes. The three additional reactions were designed to specifically detect the *nurA*, *herA* or *aadA* genes. In these reactions, the forward primers were designed to bind internally to the *aadA* gene (*aadAFrw* primer), the *nurA* or the *herA* gene (RTNurF or RTHerF). The reverse primer was designed to bind to DNA downstream of the *nurA* or *herA* gene (RNur1 or RHer1). The reverse primer binding site should be present in both the wild-type and deletion strains, but each should have only one of the internal binding sites for the forward primers. The exception is the downstream reverse primer RNur1, which should not be present in the *herA* deletion strain because its annealing site is found within the *herA* gene.

The reactions for the internal check on the *aadA* gene (*aadAFrw*/RHer1; **Figure 2-4, B**) gave the expected product sizes from  $\Delta$ *nurA* (3.225 kb) and  $\Delta$ *herA* (1.368 kb)

gDNA. Reactions using wild-type gDNA did not give a major product band and only non-specific products were observed.

When the primers RTHerF and RHer1 were used, the gDNA from wild-type and  $\Delta nurA$  cells gave the predicted product size of 1.537 kb indicating the *herA* operon was intact. In contrast, the  $\Delta herA$  gDNA did not have the appropriate template to amplify this product and only non-specific bands were observed (**Figure 2-4, C**). This indicated that the RTHerF binding site was not present in the  $\Delta herA$  gDNA upstream of the RHer1 primer binding site, which was shown to be present in other reactions (**Figure 2-4, A**).

In the final reaction, an internal *nurA* primer binding site was checked for its position upstream of an internal *herA* primer binding site (RTNurF/RNur1). As expected, the wild-type gDNA gave the predicted 1.344 kb product band while the  $\Delta nurA$  and  $\Delta herA$  gDNA did not give this and only gave non-specific products (**Figure 2-4, D**). Such a result is consistent with the *nurA* and *herA* genes being absent from the gDNA of their respective mutant strains.

The reactions gave the product bands expected in mutant strains where all copies of the target gene were completely replaced by the *addA* antibiotic cassette. The results indicate that the  $\Delta nurA$  and  $\Delta herA$  mutant strains were knockout strains for their target genes.

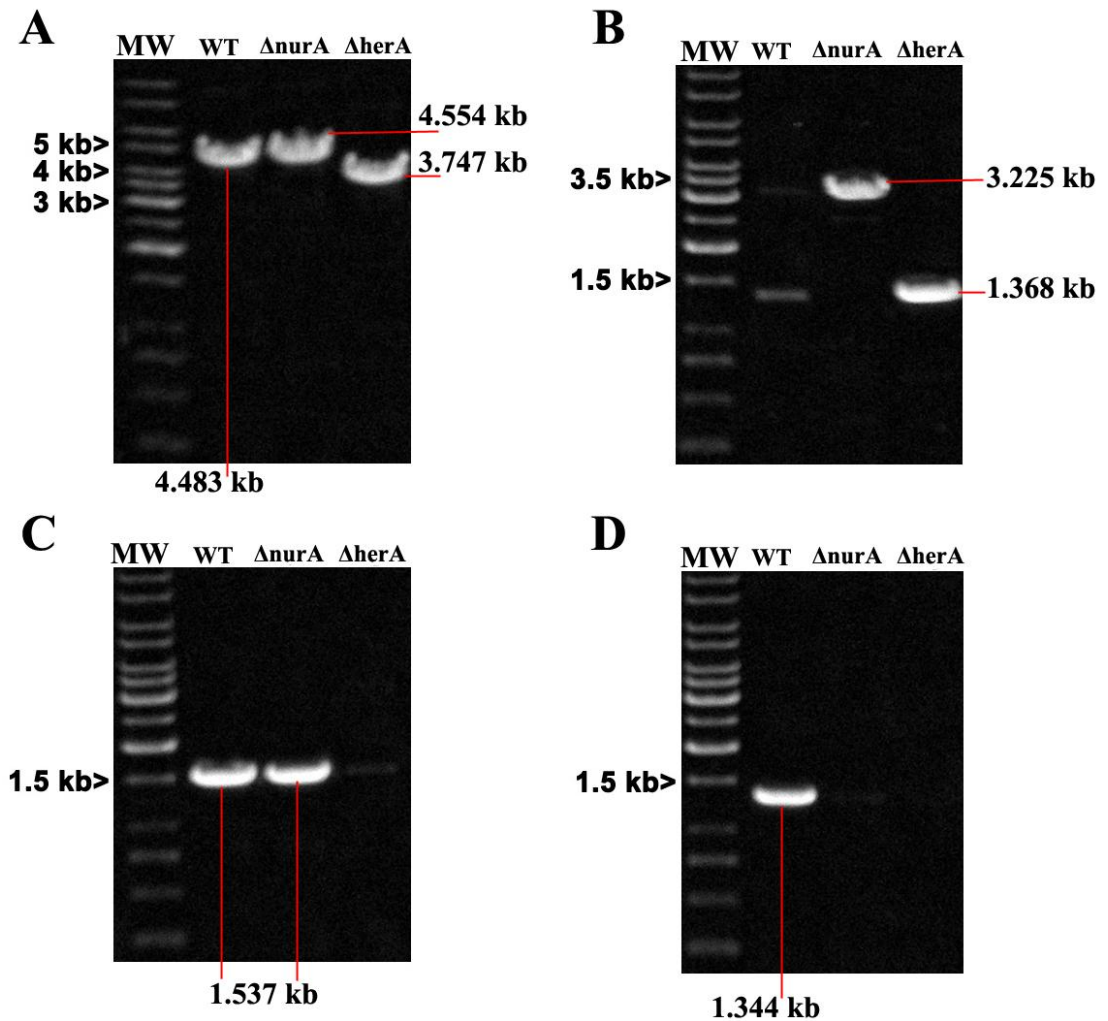


**Figure 2-4: Genotype PCR reactions for wild-type,  $\Delta nurA$  and  $\Delta herA$  strains.** Genomic DNA was isolated from a colony of wild-type *D. radiodurans* and from a streptomycin-resistant transformant colony. Lanes containing wild-type (WT),  $\Delta nurA$  gDNA and  $\Delta herA$  gDNA are labeled. Primer sequences are listed in **Table A1**. **(A)** The entire *nurAherA* operon was analyzed by PCR using a primer ~800 bp upstream of the *nurA* gene (FNur1) and a primer ~800 bp downstream of the *herA* gene (RHer1). The expected PCR product size from wild-type cells is 4.483 kb, from  $\Delta nurA$  cells is 4.554 kb and from  $\Delta herA$  cells is 3.747 kb. **(B)** PCR was done using a primer *aadA*Fw, which anneals within the *aadA* gene, and the RHer1 primer. A 3.225 kb PCR product is expected from  $\Delta nurA$  gDNA with the *aadA* gene replacing *nurA*. A 1.368 kb PCR product is expected from  $\Delta herA$  gDNA with the *aadA* gene replacing *herA*, while no product is expected from wild-type DNA. **(C)** The *herA* gene region was analyzed by PCR using a primer internal to the *herA* gene (RTherFw) and a downstream primer (RHer1). The expected PCR product size from wild-type cells is 1.537 kb. This fragment should be produced from DNA isolated from a  $\Delta nurA$  cell, but not from a  $\Delta herA$  cell. **(D)** The *nurA* gene region was analyzed by PCR using a primer internal to the *nurA* gene (RTnurFw) and a downstream primer (RNur1), which is also an additional internal primer for the *herA* gene. The expected PCR product size from wild-type cells is 1.344 kb. This fragment should not be produced from DNA isolated from a  $\Delta nurA$  or  $\Delta herA$  cell.

### 2.3.2 *In vivo* survival assay results for mutant strains

The  $\Delta nurA$  and  $\Delta herA$  strains were examined for differences in their sensitivity to treatment with various DNA damaging agents relative to wild-type. Cultures were treated with ionizing radiation in the form of UV-C, the ssDNA break inducing antibiotic phleomycin, the cross-linking agent MMC and the oxidizing agent  $H_2O_2$ , (Figure 2-5).

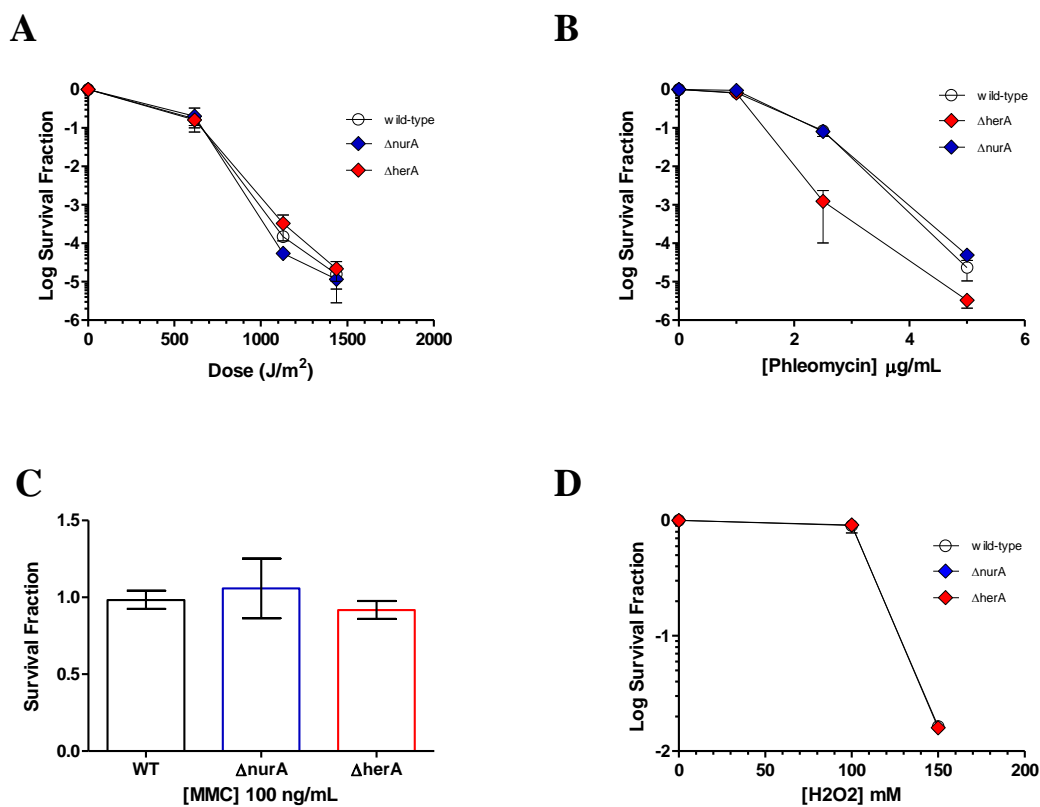


**Figure 2-5:** Effect of DNA damaging agents on viability of wild-type,  $\Delta nurA$  and  $\Delta herA$  cells.

In all assays, treated and untreated cultures were spread onto 1x TGY plates in triplicates without antibiotic and allowed to grow for 48 hours before colonies were counted. In all graphs, except D, Open circles, wild-type. Blue diamonds,  $\Delta nurA$ . Red diamonds,  $\Delta herA$ . (A) Exponential phase cultures were exposed to the indicated dose of UV light from a germicidal lamp. (B) Exponential phase cultures were spread in triplicate on TGY plates containing 0, 1, 2.5 and 5  $\mu$ g/mL phleomycin. (C) Exponential phase cultures were spread in triplicate on TGY plates containing 100 ng/mL MMC. (D) Exponential phase cultures were treated with 0, 100 and 150 mM  $H_2O_2$  for 1 hour.

### 2.3.3 *In vivo* survival assay results: UV-C

Exposure to UV-C radiation (100 to 295 nm) generates cyclobutane pyrimidine dimers (CPDs) and pyrimidine-(6-4) pyrimidone (6-4 PPs) photoproducts in DNA. If these lesions are not properly repaired they can lead to DSBs induced by replication fork collapse. They can also, indirectly, lead to DSB if lesions in close proximity (like on opposite strands) are simultaneously repaired through BER or NER (62).

If NurA or HerA are involved in the removal of CPDs/6-4PPs or are involved in repair of DSBs, then we would expect to see an increase in sensitivity relative to wild-type upon treatment with UV-C radiation in strains devoid of these putative enzymes. When both wild-type and mutant cultures were spotted on 1x TGY plates and simultaneously exposed to UV-C radiation they experienced similar sensitivities to this type of DNA damage, regardless of dose (**Figure 2-5, A**). The results suggest that NurA and HerA do not have a major role in repairing the types of DNA damage induced by exposure to UV-C radiation.

### 2.3.4 *In vivo* survival assay results: Phleomycin

Phleomycin is a copper-chelated glycopeptide which induces DNA strand breaks *in vivo* through a metal ion dependent, free radical mechanism that utilizes molecular oxygen (63, 64). Upon entering the cell, phleomycin is activated through its reduction by sulfhydryl compounds allowing it to interchelate with the negatively charged phosphodiester backbone of DNA leading to strand breakage. Acute treatment of *E. coli* cultures with phleomycin (30 µg/mL) results in many ssDNA breaks (~78 ssDNA breaks per cell) (63). When these ssDNA breaks occur in



clusters they can lead to DSBs. Therefore, the type of damage believed to occur *in vivo* is a combination of ssDNA breaks and DSBs, but no other type of base damage; it does not generate reactive oxygen species (ROS) as treatment with hydroxyl radical scavengers, like ethanol or hydroxyurea, does not inhibit DSBs caused by phleomycin.

If NurA or HerA are involved in the repair of ssDNA breaks or DSBs then we would expect to see the  $\Delta nurA$  and  $\Delta herA$  strains display an increased sensitivity to treatment with phleomycin relative to wild-type. When wild-type and  $\Delta nurA$  cultures were grown on 1x TGY plates containing 1, 2.5 and 5  $\mu\text{g/mL}$  phleomycin, there was no detectable difference in their sensitivities (**Figure 2-5, B**) The result suggests against a major role for NurA in the repair of ssDNA or dsDNA breaks in *D. radiodurans*.

In slight contrast to this, the  $\Delta herA$  mutant was found to be a little more sensitive than wild-type to phleomycin (**Figure 2-5, B**). The sensitivity appeared to be greatest at the concentration of 2.5  $\mu\text{g/mL}$  (~100-fold less viable cells compared to wild-type) and oddly this was less (~10-fold) at the higher concentration of 5  $\mu\text{g/mL}$ . There was no difference detected between wild-type and the  $\Delta herA$  strain at 1  $\mu\text{g/mL}$ . The result suggests there may be something unique about the type of damage that occurs within *D. radiodurans* cells when grown on agar plates containing 2.5  $\mu\text{g/mL}$  phleomycin compared to 5  $\mu\text{g/mL}$ . Regardless, the mild increase in sensitivity to phleomycin observed in the  $\Delta herA$  strain indicates HerA may have a minor role in some aspect associated with DNA repair, but it clearly is not a critical component in the repair of ssDNA or dsDNA breaks in *D. radiodurans*.

### 2.3.5 *In vivo* survival assay results: MMC

Mitomycin C is a cross-linking agent that is enzyme activated inside the cell and once activated reacts with the O6 or N2 atoms of guanine and the N6 atom of adenine (65). Once alkylated these adducts can form covalent bonds with atoms on the opposite strand resulting in a cross-link or they can simply remain as bulky adducts. The bulky adducts can act as an obstacle for replication, likely causing a stall, but the cross-links act as an absolute block regarding DNA replication and transcription (66). Collapse of replication forks can lead to DSBs and the main pathways for repair regarding treatment with MMC are HR and NER (9).

If the  $\Delta nurA$  or  $\Delta herA$  strain experiences an increase in sensitivity relative to wild-type when treated with MMC, then it would suggest loss of *nurA* or *herA* has impaired one of the pathways of repair. When wild-type,  $\Delta nurA$  and  $\Delta herA$  cultures were grown on 1xTGY plates containing 100 ng/mL MMC, they did not experience any loss in viability (**Figure 2-5, C**). This dose is lethal to *D. radiodurans* mutant strains which are severely impaired in their ability to repair DSB via HR (22). The results suggest that NurA and HerA do not have a major role in repairing the types of DNA damage induced by treatment with MMC.

### 2.3.6 *In vivo* survival assay results: H<sub>2</sub>O<sub>2</sub>

When cultures of *D. radiodurans* are treated with H<sub>2</sub>O<sub>2</sub> it triggers its antioxidant defenses and molecules of H<sub>2</sub>O<sub>2</sub> which cannot be properly reduced can undergo the Fenton reaction ( $H_2O_2 + Fe^{2+} \rightarrow Fe^{3+} + OH^{\bullet} + OH^-$ ) to produce hydroxyl radicals (9). These hydroxyl radicals are very unstable species and can easily react with biological molecules such as proteins (leading to oxidative protein damage) or DNA/RNA

(leading to base damage) (67). Reaction of hydroxyl radicals with DNA can lead to direct base damage, such as the formation of 8-oxo-guanine bases, or can produce ssDNA breaks when they react with the sugar backbones of nucleotides (68). When clusters of ssDNA breaks occur, this can lead to the formation of DSBs.

Additionally, during repair by pathways such as BER, which are needed to remove damaged bases like 8-oxo-guanine, if the resulting nicks are not sealed in time they will remain as ssDNA breaks and if such attempts to repair oxidized bases occur in clusters, these clustered nicks can result in DSBs (8). As the concentrations of H<sub>2</sub>O<sub>2</sub> are increased, the likelihood of generating DSBs increases.

Thus if the  $\Delta nurA$  and  $\Delta herA$  strains display an increased sensitivity to treatment with H<sub>2</sub>O<sub>2</sub>, then depending on the shape of the curve it could indicate that one of DNA repair pathways (such as BER or HR) has been compromised by the replacement of *nurA* or *herA* with the *aadA* gene. When both wild-type and mutant cultures were grown in the presence of different concentrations of H<sub>2</sub>O<sub>2</sub> they displayed essentially the same sensitivities to the oxidizing agent which can be seen in the shape of their survival curves (**Figure 2-6, D**). The results suggest that the putative NurA and HerA in *D. radiodurans* do not have a major role in repairing the types of oxidative DNA damage induced by treatment with H<sub>2</sub>O<sub>2</sub>.

### 2.3.7 Expression and purification of putative HerA enzyme from *E. coli*

The *herA* gene was cloned into the pET15b expression plasmid and subsequently transformed into the *E. coli* expression strain *Lemo21 (DE3)*. The *herA* gene from *D. radiodurans* is expected to code for a 67 kDa protein and based on sequence analysis it seems likely that this protein will be capable of hydrolyzing ATP and possibly

acting as a helicase or translocase (42). When *Lemo21 (DE3)* strains harboring the pET15b\_*herA* plasmid were induced with IPTG the HerA protein was expressed as a soluble protein (**Figure 2-6**). The soluble fraction from an induced culture was loaded onto a nickel column to purify the HerA protein through affinity chromatography. The HerA protein was subsequently isolated and purified again through an anion exchange column. Following this two-step purification process, the HerA enzyme appeared as a single band when subjected to silver-stain analysis.

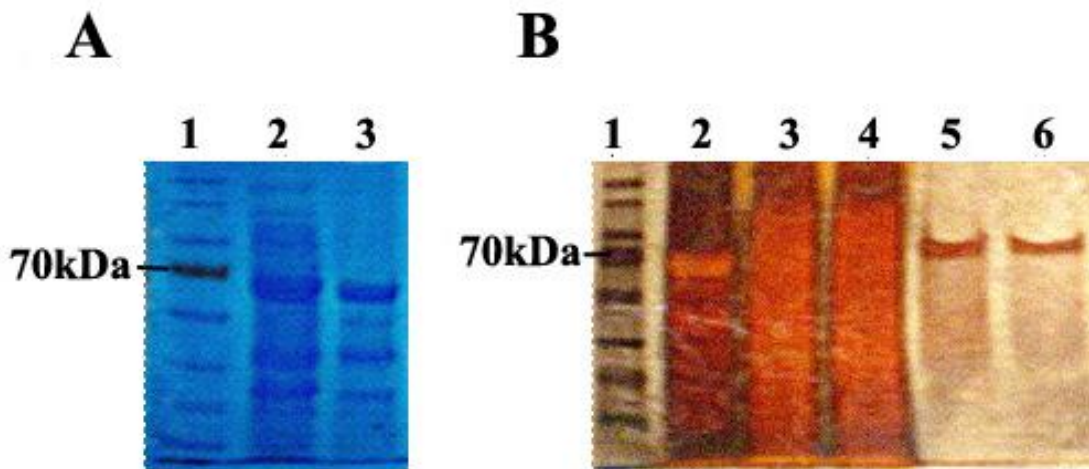


**Figure 2-6: Expression and Purification of Putative HerA Enzyme.** (A) Coomassie brilliant blue stain of whole cell lysates. Lane 1 is standardized protein ladder. Lane 2 is soluble fraction. Lane 3 is insoluble fraction. (B) Silver stain showing various stages of protein purification. Lane 1 is standardized protein ladder. Lane 2 is soluble fraction from whole cell lysate. Lane 3 is insoluble fraction from whole cell lysate. Lane 4 is flow through prior to elution from His-Trap purification step. Lane 5 is His-Trap purified product. Lane 6 is HiTrap Q-F/F purified product.

### 2.3.8 Initial ATPase activity measurements on putative HerA enzyme

The concentration of the HerA protein was determined using a micro Bradford assay using BSA as a standard as described in Methods. The concentration of the

HerA stock was found to be 1.54 $\mu$ M. This stock was used to test for intrinsic ATPase activity using the BIOMOL green reagent as described in Methods.

When 80 nM of HerA was incubated with 250  $\mu$ M ATP at room temperature for approximately 20 minutes, ~1pmol of  $\text{PO}_4^{3-}$  was released. When the concentration of HerA was doubled, the amount of  $\text{PO}_4^{3-}$  released appeared to as well (~2.4 pmol; **Figure 2-7, A**). It was clear that the ATPase activity of the HerA protein was low, suggesting that something went wrong with the isolation procedure resulting in retention of enzyme, but loss of activity or it could be that its activity is only stimulated in the presence of a DNA substrate or binding partner like NurA.

We investigated the possibility that a DNA substrate could stimulate the ATPase activity of our purified HerA by incubating 160nM of HerA with 10  $\mu$ M of 5 different DNA substrates in our 1x ATPase buffer. The DNA substrates were a linear, blunt dsDNA molecule (pCRBlunt\_ $\Delta$ herA cut with SmaI), a short ssDNA oligonucleotide (MJ8 primer), circular plasmid DNA (pCRBlunt\_ $\Delta$ herA, uncut), a shorter piece of linear dsDNA (UPstream herA fragment) and gDNA from *D. radiodurans* wild-type strain. We did not detect any increase in the amount of  $\text{PO}_4^{3-}$  released when HerA was incubated with any of these DNA substrates in 1x ATPase buffer (**Figure 2-7, B**).

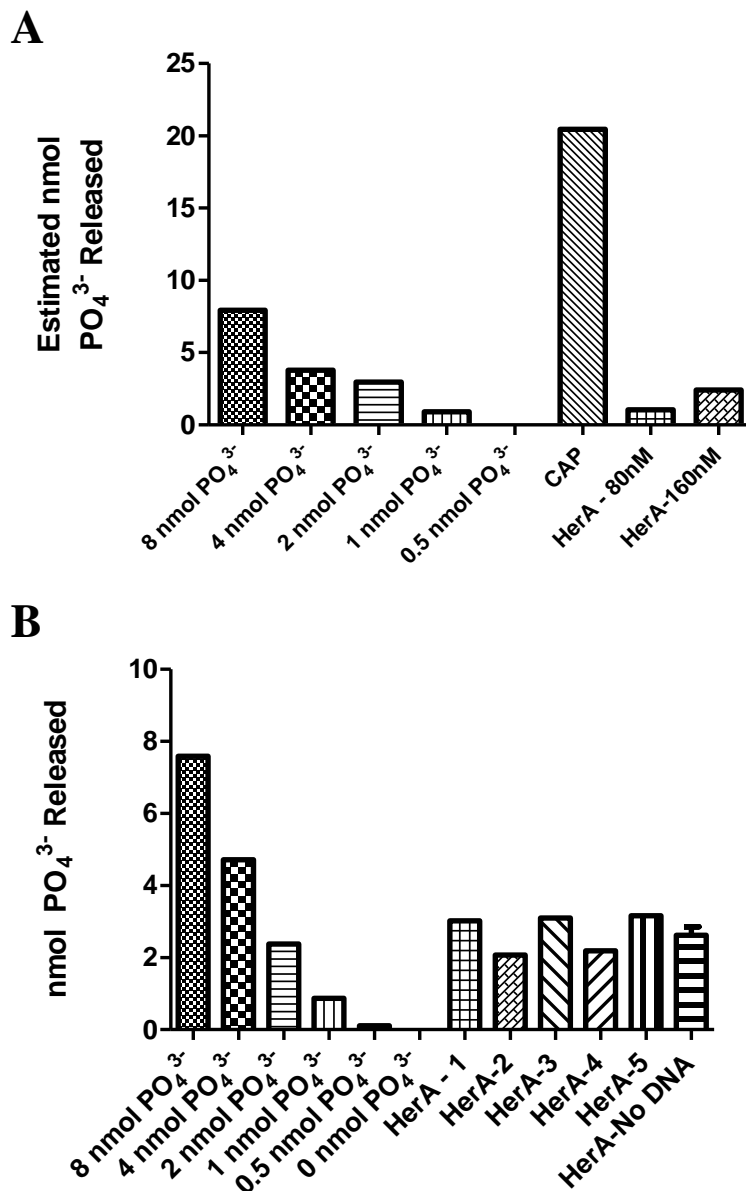


**Figure 2-7: ATPase assays with HerA enzyme from *D. radiodurans*.**

ATPase assays were performed with the purified HerA enzyme as described in Methods. **(A)** Bar graph showing the estimated nmol  $PO_4^{3-}$  present in the sample tested. The  $PO_4^{3-}$  standards are shown first, followed by a positive control of ATPase activity using calf-alkaline phosphatase and finally the results from HerA at 80 and 160 nM concentrations. **(B)** Same as A, except HerA (80 nM) incubated with 10  $\mu$ M of: linear plasmid DNA (pCRBlunt\_ΔherA; HerA-1), single strand oligonucleotide (MJ8 primer; HerA-2), linear blunt end DNA (UPstream fragment from ΔherAKO; HerA-3), circular plasmid DNA (pCRBlunt\_ΔherA; HerA-4) and wild-type *D. radiodurans* gDNA (HerA-5)

## 2.4 DISCUSSION

Deletion of *nurA* from *D. radiodurans* genome did not result in any difference in this mutant strain's ability to recover from the DNA damaging effects of MMC, H<sub>2</sub>O<sub>2</sub>, UV-C radiation and phleomycin relative to wild-type. The same was true when *herA* was deleted from *D. radiodurans*, except for when  $\Delta herA$  cultures were grown on TGY agar plates containing 2.5-5  $\mu\text{g/mL}$  phleomycin. Under these conditions the  $\Delta herA$  strain experienced a mild decrease (~100 fold) in viability relative to wild-type. The results indicate that neither the putative NurA or HerA are primary components of the DNA repair pathways required to recover from the types of damage induced in these experiments.

### 2.4.1 *In vivo* Survival Analysis

As described in **Chapter 1**, nucleases and helicases play an important role in the repair of damaged bases or in the repair of DNA stand breaks (1). The most deadly type of damage is a DSB and the major pathway for repair of DSB is HR, which in bacteria requires a nuclease and helicase to generate the necessary 3' ssDNA tails that can be subsequently bound by the recombinase RecA. The NurA nuclease and HerA helicase in archaea have been demonstrated *in vitro* to display the necessary biochemical properties for the initiation of HR; the ability to unwind and degrade linear DNA generating 3' ssDNA tails. This finding was one of the main reasons these genes were chosen to be investigated in *D. radiodurans*.

The  $\Delta nurA$  and  $\Delta herA$  strains were compared to wild-type for their sensitivity to DNA damaged induced by MMS, MMC, H<sub>2</sub>O<sub>2</sub>, UV-C radiation and phleomycin. Each of these can create different types of damage inducing different repair systems.

However, regardless of the method for generating DNA damage, the  $\Delta nurA$  strain displayed no difference in its sensitivity to these agents compared to wild-type. NurA is believed to be an essential enzyme in DNA repair in archaea based off what it has been shown to do *in vitro* (43, 44) (47) and the fact the two attempts to knock it out in two different archaea failed (49, 50). It seems odd that an apparent essential enzyme for DNA repair in archaea could be present in *D. radiodurans*, but not be somewhat important for recovery from DNA damage. It may be that NurA does have a role in DNA repair in *D. radiodurans*, but that this role is easily compensated for by other nucleases encoded in *D. radiodurans* genome, like RecJ.

It was also surprising to see that the  $\Delta herA$  strain did not display any difference in sensitivity to the DNA damage induced by UV-C, MMC or H<sub>2</sub>O<sub>2</sub>. Like NurA, in archaea, HerA is believed to be an essential helicase required for DNA repair (49, 50). There was a mild difference (~100-fold) in sensitivity relative to wild-type when the  $\Delta herA$  strain was grown on TGY-agar plates containing 2.5  $\mu\text{g}/\text{mL}$  of phleomycin. On plates with higher doses (5 $\mu\text{g}/\text{mL}$ ) this difference diminished (~10-fold). It is unclear why the mutant would be less sensitive to the higher dose of phleomycin. At the higher doses it is believed more cells die because more DSBs occur than would at lower doses. It may be that HerA is involved in a type of ssDNA repair pathway, like the ssDNA gap (SSG) pathway in *E. coli*. Given that phleomycin generates dsDNA breaks by generating ssDNA breaks in close proximity on opposite strands, it seems likely that many ssDNA gaps are also be generated. Thus it may be that  $\Delta herA$  is important for the repair of ssDNA gaps, presumably



which are most prominent at 2.5 µg/mL phleomycin, but less important for repair of dsDNA breaks which are more abundant at the higher dose.

In *E. coli*, the RecFOR pathway is responsible for the repair of SSG (17, 21). This pathway exists in *D. radiodurans* and is believed to be the primary pathway for the initiation of HR (28, 29). It seems likely this pathway could also operate to repair SSG in *D. radiodurans*. Therefore, if HerA has a role in ssDNA gap repair in *D. radiodurans* it suggests an alternative pathway for ssDNA gap repair exists or that HerA is somehow involved in the RecFOR pathway during repair of ssDNA gaps, but not during repair of dsDNA breaks. Additionally, the fact that the *nurA* deletion strain did not show any increased sensitivity to phleomycin suggests that if HerA is involved in the repair of damage induced by phleomycin, NurA is not involved. This is interesting because it is believed that NurA and HerA function together as a complex to repair DNA damage in archaea, but these results suggest this is not the case in *D. radiodurans*.

Counter to the argument that HerA could have a role in SSG repair is that the  $\Delta herA$  strain is no more sensitive to damage caused by UV-C radiation than the wild-type. In *E. coli*, deletion strains deficient in SSG repair (*recF*, *O*, or *R* mutants) are more sensitive to UV radiation than wild-type strains (69). This is because the repair of damage induced by UV radiation is repaired by the NER repair system which introduces ssDNA gaps following removal of the bulky damaged bases (69, 70). However, without truly knowing the extent and type of damage caused in *D. radiodurans* cells growing on plates containing concentrations of phleomycin  $\geq 2.5$  µg/mL, the suggestion of a role for HerA in the repair of SSG is only speculative.

It is worth noting that in *B. subtilis*, mutant strains devoid of *sftA* are more sensitive to the effects of MMC than wild-type (71). This treatment introduces interstrand cross-links into DNA leading to transient cell cycle arrest so that DNA repair can occur (SOS response). SftA is a member of the FtsK/HerA superfamily of P-loop ATPases and has been demonstrated to have a role in chromosome segregation in *B. subtilis* (71-73). The increased sensitivity of *sftA* mutant strains apparently highlighted the importance of proper chromosome segregation following damage-induced cell cycle arrest in order for cells to remain viable. Therefore, it is believed that SftA is not involved in the DNA repair process, but following repair, its role in chromosome segregation becomes increasingly important.

As mentioned in **Chapter 1**, there is some evidence to suggest HerA in archaea is actually an FtsK analog (42, 44, 52, 53) and has a role in chromosome segregation alternatively or in addition to its possible role in DNA repair. If this is true, then it seems entirely possible that HerA in *D. radiodurans* has a role in chromosome segregation similar to that observed for SftA in *B. subtilis*. This could mean that the phenotype observed upon treatment of the  $\Delta herA$  strain with phleomycin is emphasizing a role in chromosome segregation for HerA. Given the fact that in *S. solfataricus* HerA was demonstrated to act as a DNA translocase (44), an activity associated with FtsK in bacteria (74), when bound with a nuclease deficient NurA and the fact that the *nurA* deletion apparently had no effect on *D. radiodurans*' ability to recover from DNA damage, it may be that the NurA in *D. radiodurans* is nuclease deficient and complexes with HerA to help facilitate its DNA translocase activity. If this were true, then it would mean that the tertiary structure of NurA or quaternary

structure creates a situation which structurally silences its nuclease activity because it appears to have the conserved residues of the NurA active site (42). However, if this were the case, then it could explain the unexpected finding that these genes were not important for the recovery of DNA damage in *D. radiodurans*.

#### 2.4.2 *In vivo* Survival Analysis: Future Work

Additional work likely needs to be done in order to entirely rule out a role in DNA repair. As said before, it could be these enzymes are involved in backup repair pathways and function more similar to the NurA and HerA studied in *S. acidocaldarius* and *S. todokaii* where the activities each demonstrated *in vitro* were independent of each other. This may explain why the  $\Delta herA$  strain showed a mild DNA damage phenotype to phleomycin but the  $\Delta nurA$  strain did not. In order to truly rule out a role in DNA repair for NurA and HerA in *D. radiodurans*, double or even triple mutant strains, where other, known DNA repair enzymes are knocked out in combination with *nurA* and *herA* need to be made and tested. Knocking out the genes for other helicases like *uvrD* (28), *recQ* (31) or *recD*(26) that have been shown to sensitize *D. radiodurans* cells to DNA damage in a *herA* null background could implicate HerA in DNA repair if these double knockout strains are more sensitive than either of the respective single mutant strains.

Similar studies could be carried out with the *nurA* deletion strain except that the candidates of other 5'-3' exonucleases is rather limited for *D. radiodurans*. The only two known enzymes with 5'-3' exonuclease activity in *D. radiodurans* are RecJ and DNA polymerase I (9). Attempts to completely knock out *recJ* have proven unsuccessful, but it would be interesting to see if you could delete *nurA* in the *recJ*

heterozygous mutant strain and observe how sensitive this double mutant strain was DNA damage.

#### 2.4.3 Concluding Remarks about NurA and HerA in DNA repair in *D. radiodurans*

Unfortunately, no biochemical analysis on the purified *D. radiodurans* putative NurA protein was able to be carried out because the process of expressing and purifying the enzyme was never done due to an emphasis on other elements of this project (namely the *herA* work). We did express and purify the putative HerA protein and were able to show that this protein was soluble and was approximately the predicted size of 67 kDa. Initial attempts to assess the purified HerA for an intrinsic ATPase activity indicated it could hydrolyze ATP, but the rate qualitatively appeared to be quite low. This could be due to several factors: 1) The purification process resulted in loss of enzymatic activity; HerA not in its native form 2) The N-terminal His-Tag, which was not removed, inhibited HerA's ability to hydrolyze or bind ATP 3) HerA's ATPase activity is only stimulated in the presence of additional binding partners such as NurA 4) The ATPase activity of HerA is stimulated by the presence of DNA. We did test the fourth possibility by incubating the purified HerA with high concentrations of various DNA substrates, but in each case saw no increase in the amount of ATP being hydrolyzed.

It would have been helpful to have characterized the purified NurA and HerA in manners similar to how they have been characterized in archaea (43, 44, 46, 48). Such information could have at least provided information regarding a potential activity inside the cell or any similarities/differences to the *in vitro* properties

observed for HerA and NurA in archaea. However, one simple fact does remain and that is that both *nurA* and *herA* were able to be completely replaced by the *aadA* gene in *D. radiodurans* and such attempts in archaea failed. This result in and of itself demonstrates that the priority given to NurA and HerA in archaea regarding their roles in the cell is much different than for *D. radiodurans*.

Although it appears our initial hypothesis that the NurA and HerA in *D. radiodurans* were involved in the initiation steps of DNA repair of DSB by HR was wrong, the negative results obtained are still significant given the fact this is the first report of the potential role of these genes in bacteria and what is expected of these genes in archaea. Furthermore, because we were able to generate these deletion strains, it provided us an additional opportunity to explore the other potential role for the putative NurA and HerA in *D. radiodurans* that has been proposed for these enzymes in archaea which was a role in chromosome segregation.

## Chapter 3: ASSESSMENT OF GROWTH PHENOTYPES OF NURA AND HERA MUTANT STRAINS

### 3.1 INTRODUCTION

Despite evidence that suggests *nurA* and *herA* code for enzymes important for recombinational repair in archaea, there is no knowledge about what the role of these genes in bacteria may be. Our original hypothesis that the putative NurA and HerA from *D. radiodurans* would be important for DNA repair was based off *in vitro* evidence (40, 44, 48) obtained studying archaeal NurA and HerA enzymes. These experiments led us to predict the homologs of the archaeal *nurA* and *herA* found in *D. radiodurans* would be important for recovery from DSBs. The results we obtained argue against this and a major role in DNA repair for these putative enzymes in *D. radiodurans* seems unlikely. However, as mentioned in **Chapter 1**, there exists additional evidence (42, 52, 53) in archaea that suggests these enzymes may have a role in chromosome segregation or some other DNA processing role, in addition to/alternatively to their proposed role in DNA repair.

HerA proteins are a major clade of the FtsK-HerA superfamily of P-loop ATPases that are predicted to utilize the hydrolysis of ATP to process DNA substrates (42). FtsK from *E. coli* is a DNA translocase that actively participates in chromosome segregation of newly replicated chromosomes and is essential for proper orientation of the division septa (74). It has multiple roles in the cell cycle through different activities associated with its N- and C-terminal domains (74). The N-terminal trans-membrane domain (**Figure 3-1**) localizes FtsK to the cell division septum through interactions with the cell membrane and divisome (75-78). The C-

terminal domain is responsible for its ability to translocate along DNA in an ATP-dependent fashion as a hexameric complex. Its translocase activity is necessary for segregation of the terminus region of the chromosome and for the resolution of chromosome dimers and catenated chromosomes that can result during DNA replication (79-86).

The *ftsK* gene is not found in archaea, and bacteria which lack *ftsK* normally have a copy of the *herA* gene (42). It has been proposed that the last common ancestor of *ftsK* and *herA* coded for a DNA pumping enzyme which evolved to fulfill different biological roles in bacteria and archaea (42). Recent work in *Sulfolobus solfataricus* utilizing a triplex displacement assay has shown that HerA complexed with a nuclease deficient NurA can translocate along dsDNA (44), an activity associated with FtsK from *E. coli* (74). It has been suggested that HerA in archaea could perform similar roles as FtsK in bacteria, but through fundamentally different mechanisms (42, 52). Therefore it's possible that horizontal transfer of *herA* into a bacterium allowed *herA* to be utilized more like *ftsK* in bacteria rather than *herA* in archaea.

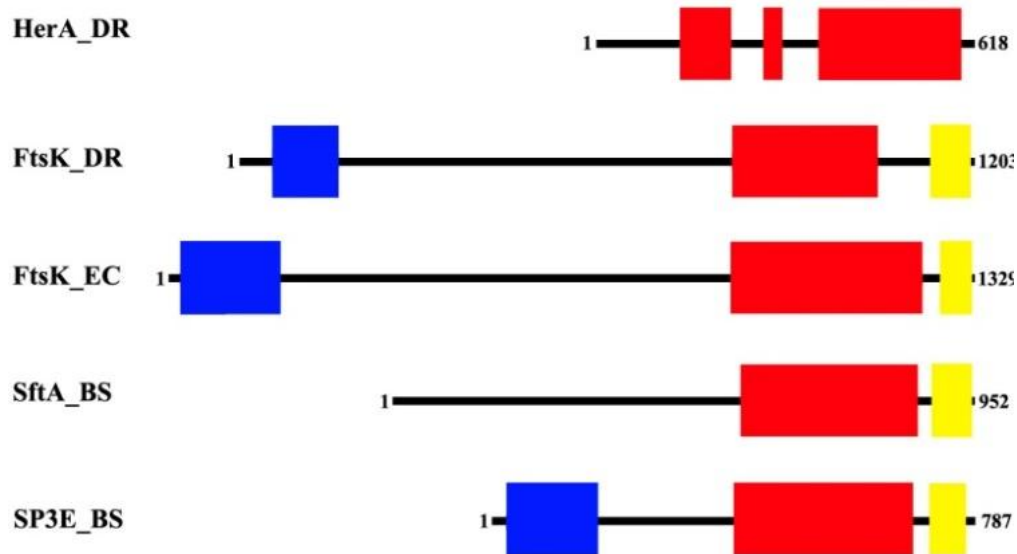


**Figure 3-1: Domain architecture of selected FtsK-like proteins.**

Conserved domain architectures from protein sequences for *D. radiodurans R-1* HerA (Uniprot primary accession no. Q9RW32), *D. radiodurans R-1* FtsK (Q9RXB5/Q9RXB4), *E. coli K-12* FtsK (P46889), *B. subtilis strain 168* SftA (C0SP86), and *B. subtilis strain 168* SpoIIIE (P21458). Black bars and numbers indicate the length in amino acids of the protein sequence. Conserved domains are shown as colored boxes and were determined from Interpro annotations (<http://www.ebi.ac.uk/interpro>). Blue = Predicted N-terminal transmembrane helices (Interpro domain no. IPR025199); Red = P-loop NTPase (IPR027417); Yellow = FtsK\_gamma (IPR018541). FtsK\_DR is the result of merged sequences of the *D. radiodurans* genes DR\_0400 and DR\_0401 (see Discussion). The Red regions contain all three defining motifs of the FtsK/HerA superfamily: A conserved histidine before the Walker A motif, Walker B motif, and a conserved polar residue (often glutamine) at the C-terminus followed by a conserved arginine (42).

*D. radiodurans* contains apparent homologs of the archaeal *nurA* and *herA*, which like other *nurA/herA* genes are found together in an operon (42). In addition, *D. radiodurans* contains an apparent homolog of *ftsK*<sup>1</sup>. The mRNA and proteins

<sup>1</sup> The annotated *D. radiodurans* FtsK protein sequence found in the NCBI database (locus DR\_0400, Uniprot primary accession no. Q9RXB5) does not include an N-terminal region containing predicted trans-membrane helices. However, the gene directly upstream of *ftsK* (locus DR\_0401, Uniprot primary accession no. Q9RXB4) is predicted to encode a small (223 amino acids) protein that aligns in a BLAST search to the N-terminus of annotated FtsK proteins from other *Deinococci*. According to the Conserved Domain Database (<http://www.ncbi.nlm.nih.gov/Structure/cdd>), this predicted protein contains a domain (DUF4117) that is commonly found in the N-terminal transmembrane domain of FtsK proteins. It seems likely that the *ftsK* gene in the *D. radiodurans* genome is misannotated due to a sequencing error and that loci DR\_0400 and DR\_0401 represent the full length *ftsK* gene. Such



encoded by these genes in *D. radiodurans* have been detected in transcriptomic and proteomic experiments (56, 57). It is possible that HerA could have a role in chromosome segregation, as observed for FtsK in *E. coli*. If so, *D. radiodurans* might have two DNA translocases – i.e., HerA and FtsK.

The involvement of two translocases in DNA segregation is not unprecedented in bacteria. In *Bacillus subtilis*, there are two proteins which share sequence identity with the C-terminal domain of FtsK from *E. coli* known as SpoIIIE and SftA (71, 72). When cells have divided and trapped chromosomal DNA in the membrane, SpoIIIE is responsible for rescuing this trapped DNA and completing the chromosome segregation process post-septationally in an ATP dependent manner (72). SftA on the other hand is a soluble ATP-dependent DNA translocase that localizes to the division septum during the formation of the divisome, but prior to septum closure, helping to segregate sister chromosomes before septation. Apart from their believed role in clearing sister chromosomes from the division septum during vegetative growth, they also have been demonstrated to work synergistically to facilitate the resolution of chromosome dimers which occur in about 20% of *B. subtilis* wild-type cells per cycle (73).

It may be that FtsK and HerA perform similar functions in *D. radiodurans*. If this is true, it is not obvious how or if NurA would assist HerA in its role in chromosome segregation. However, given the fact these enzymes are known to

---

annotation errors are not uncommon in the *D. radiodurans* genome 35. **Cao Z, Julin DA.** 2009. Characterization in vitro and in vivo of the DNA helicase encoded by *Deinococcus radiodurans* locus DR1572. *DNA Repair (Amst)* **8**:612-619, 87. **Eggington JM, Haruta N, Wood EA, Cox MM.** 2004. The single-stranded DNA-binding protein of *Deinococcus radiodurans*. *BMC Microbiol* **4**:2, 88. **Mennezier S, Coste G, Servant P, Bailone A, Sommer S.** 2004. Mismatch repair ensures fidelity of replication and recombination in the radioresistant organism *Deinococcus radiodurans*. *Mol Genet Genomics* **272**:460-469..

physically interact in archaea (47), and together, when the nuclease activity of NurA is silenced, can form a complex capable of translocating DNA *in vitro* (44), it seems possible they could work together in facilitating chromosome segregation in *D. radiodurans*.

Based on the above criteria, we explored the possibility that the homologs of the archaeal *nurA* and *herA* genes found in *D. radiodurans* code for putative enzymes involved in some aspect of DNA processing during growth, such as chromosome segregation. We hypothesized if they did then strains devoid of these genes would experience a growth defect and/or a change in their cellular/nuclear morphologies, similar to what has been observed for other bacteria impaired in chromosome segregation (71, 72, 84, 89).

We evaluated the  $\Delta nurA$  and  $\Delta herA$  strains (see **Chapter 2**) for their growth properties and cellular/nucleoid morphology relative to wild-type. We found that deletion of *nurA* did not result in any growth phenotype and cellular/nuclear morphology appeared identically to that of our corresponding wild-type strain. In contrast, we detected a subtle growth defect in the  $\Delta herA$  strain that was accompanied by an increase in the average/median cell size. Additionally, we detected a unique population (~2%) of abnormal cells in the  $\Delta herA$  strain which appeared to be deficient in their ability to properly segregate their chromosomes leading us to speculate the putative HerA has a role in chromosome segregation in *D. radiodurans*.

## 3.2 MATERIALS AND METHODS

### 3.2.1 Bacterial Strains and Culturing

The same *D. radiodurans* strains and culturing conditions were used as described in **Chapter 2**.

### 3.2.2 Growth and Morphology Assessment

Wild-type,  $\Delta nurA$  and  $\Delta herA$  stationary phase cultures, which were started from single colonies in 5 mL 2x TGY in 50 mL conical tubes ( $\Delta nurA$  and  $\Delta herA$  cultures contained 5  $\mu\text{g/mL}$  streptomycin), were diluted into 125 mL Erylenmeyer flasks containing 25 mL 2x TGY with no antibiotics to an  $\text{OD}_{600}=0.01-0.1$ . The diluted cultures were shaken at 30°C and 250 rpm. The optical density was monitored by taking  $\text{OD}_{600}$  readings every hour using our UV/Vis spectrophotometer. Growth rate constants were obtained from  $\text{OD}_{600}$  vs. time plots by fitting the data to the integrated version of the Verhulst-Pearl logistic growth equation (90):

$$Y(t) = \frac{P}{\{1 + \left(\left[\frac{P - Y_0}{Y_0}\right] \times e^{-kt}\right)\}} \quad \text{Equation 1}$$

where  $Y$  is the  $\text{OD}_{600}$ ,  $Y_0$  is the initial  $\text{OD}_{600}$  of the diluted stationary phase cultures,  $P$  is the maximum  $\text{OD}_{600}$  the culture reached,  $k$  is the growth rate constant and  $t$  is time in minutes. The generation doubling times,  $G$ , were determined from  $G = \ln(2)/k$ .

DNA was isolated from cultures after the final reading was taken and used to confirm genotypes of assayed strains using PCR as described in **Chapter 2**.

### 3.2.3 Growth Assay: Cell Concentration Determination

Cell concentrations (cells/mL culture) of wild-type,  $\Delta nurA$  and  $\Delta herA$  cultures were determined using 1 mL aliquots from exponential phase cultures. These were serially diluted as needed (~100 fold) and 500  $\mu$ L used to determine OD<sub>600</sub>. Dilutions were spotted onto a hemacytometer (Qiujing, Improved Neubauer 0.1  $\mu$ L) and images were taken using a light microscope (Amscope, Epi-Fluorescent Microscope FK-EPI-2) with a 10x objective (0.25 NA), 10 megapixel camera and dark-field condenser lens (0.7-0.8 NA). Each dilution was imaged at least three times. Images were processed using ImageJ software. Over 100 cells were counted for each hemacytometer spotting and cell concentrations were determined by dividing the number of cells in a counted area of an image by the volume of that area according to the hemacytometer dimensions and multiplying this by the dilution factor.

### 3.2.4 Growth Assay: Culture Density and Cell Mass Determination

Culture mass densities (grams cells per mL culture) of wild-type,  $\Delta nurA$  and  $\Delta herA$  were determined using aliquots from exponential phase cultures. Aliquots (4 mL) were removed in triplicate, applied to pre-weighed glass fiber filters with 1  $\mu$ m retention (GF/B 24 mm, Whatman) via vacuum filtration, and allowed to dry overnight at room temperature. An additional 500  $\mu$ L aliquot was removed for simultaneous determination of OD<sub>600</sub>. The difference in mass of dried and preweighed filter papers was used to determine the dry cell mass of each aliquot. Culture densities were determined by dividing these masses by the volume of the aliquots and reported as grams of cells per mL culture (g / mL).

### 3.2.5 Phase Contrast and Low Resolution Fluorescence Microscopy

Aliquots (500  $\mu\text{L}$ ) of wild-type,  $\Delta\text{nurA}$  and  $\Delta\text{herA}$  cells from the various phases of growth (determined by  $\text{OD}_{600}$  growth curves) were removed and diluted in ultra-pure water as needed (up to 100 fold). 10  $\mu\text{L}$  of the diluted cultures were spotted onto 1% agarose pads formed in the depressions of concave microscope slides (1 mm thickness). A 0.8 mm coverslip was then placed on top of the pads and the slide placed on the stage to be imaged using a 10 megapixel camera run using TopView software (Amscope). The microscope was fixed with either a 40x (0.65 NA) or 100x (1.25 NA, Oil) phase-contrast objective and a corresponding phase condenser lens (NA 1.25). Cell areas ( $\mu\text{m}^2$ ) were determined using ImageJ software after pixel values were calibrated to a known distance in  $\mu\text{m}$  (40x = 16.9 pixel/ $\mu\text{m}$ ; 100x = 40 pixel/ $\mu\text{m}$ ) using a stage micrometer with 1  $\mu\text{m}$  intervals. To calculate cell areas, binary images were created and this process is demonstrated in **Figure 3-2**.

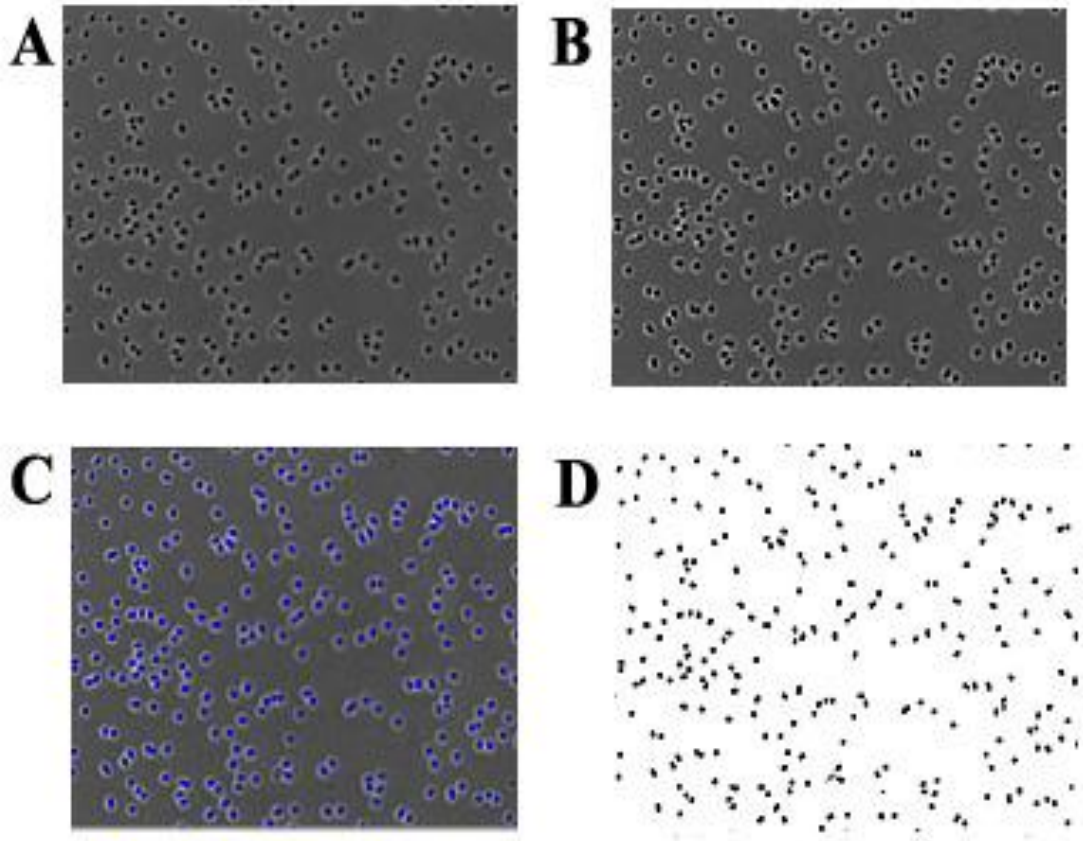


**Figure 3-2: The process of generating binary images to count cell areas.**

Cells from wild-type or a mutant strain were imaged at 400x magnification with phase contrast filters as described in methods. The process of going from these original images to ones which could be used to calculate cell areas is shown above (A) Original 400x 8-bit image of wild-type cells. (B) Unsharp mask tool of image J (10 pixel radius; 0.6 threshold) applied. (C) Threshold tool application to isolate only those areas in image which had pixel gray values of a particular threshold. (D) The resulting binary image when the threshold setting was applied. These binary images could be used to calculate cell areas.

The cell nucleoids were visualized by staining with DAPI (Excitation 358<sub>nm</sub> / Emission 461<sub>nm</sub>; Sigma-Aldrich) to a final concentration of 2 µg/mL and incubating for 15 min at room temperature in the dark before stained cells were applied to agarose pads. Cells were excited using a 100W HBO ultra hi-voltage spherical mercury lamp and imaged using a 100x fluorescence objective (1.25 NA, Oil) with

the appropriate UV filters (EX490; BA530). Over 100 cells were imaged from each slide using either phase-contrast or fluorescence microscopy.

### 3.2.6 High Resolution Fluorescence Microscopy

Access to the microscope used to obtain high resolution fluorescence images was provided most graciously by Dr. Wolniak of the Cell Biology and Molecular Genetics Department at the University of Maryland in College Park. Three wild-type,  $\Delta nura$  (data not shown) and  $\Delta herA$  cultures from exponential growth (determined by  $OD_{600}$  growth curves) had aliquots (500  $\mu$ L) removed and diluted in ultra-pure water as needed (up to 100-fold). Cells were stained simultaneously with DAPI (final concentration 2  $\mu$ g/mL) and the membrane stain FM1-43FX (Excitation 505<sub>nm</sub> / Emission 626<sub>nm</sub>; Final concentration 50 ng/ $\mu$ L) which was provided as a gift by Dr. Stein of the Molecular and Cell Biology Department at the University of Maryland in College Park. Upon addition of the stains, the cells were left to incubate for 15 minutes in the dark. 10  $\mu$ L of the diluted, stained cultures were spotted onto 1% agarose pads formed in the depressions of concave microscope slides (1 mm thickness). A 0.8 mm coverslip was then placed on top of the pads and the slide then placed on the stage to be imaged using a Zeiss AxioShop upright microscope equipped with a SPOT FLEX camera (SPOT Imaging Solutions). The microscope was fixed with 100x Achromplan fluorescence objectives (Ph 3, N.A. 1.25). Cells were excited using a mercury lamp and depending on which stain was being visualized either a Rhodamine B filter set (FM1-43FX) or UV filter (DAPI) was used. In all cases, images were brought into focus first using the FM1-43FX stain and an image taken. The filter was then carefully switched and the cell nucleoids, which were

almost always in focus after focusing with the FM1-43FX stain, were focused and imaged. This allowed for the generation of image overlays (**Figure 3-3**). Images were processed first in Adobe Photoshop CS5. The only thing done to these images in this case was that the background fluorescence was removed/diminished by using the auto-levels tool which essentially removed all intensities that were not as intense as the nucleoids themselves. This was only done so that image overlays could be created in a way that minimized the loss of information. Aside from this one-time correction of the background levels, the only other changes to images were minor adjustments in the brightness and contrast of each image. Cell areas ( $\mu\text{m}^2$ ) were determined using ImageJ software with the FM-143FX stained images after pixel values were calibrated to a known distance in  $\mu\text{m}$  ( $100\times = 54.2 \text{ pixel}/\mu\text{m}$ ) using a stage micrometer with 1  $\mu\text{m}$  intervals. The process in this case was identical to the case described above for the 40x Phase contrast images. Image overlays were created in Adobe Photoshop by overlaying the DAPI stained images onto the FM1-43FX images. In most cases little to no adjustments had to be made.

From these image overlays, the various cell types observed in the wild-type and mutant strains, characterized by the appearance of their shape and septa/ nucleoid morphology, were determined and categorized as ‘growth states’. The details for how the growth states were determined are described in **Figure 3-11**.



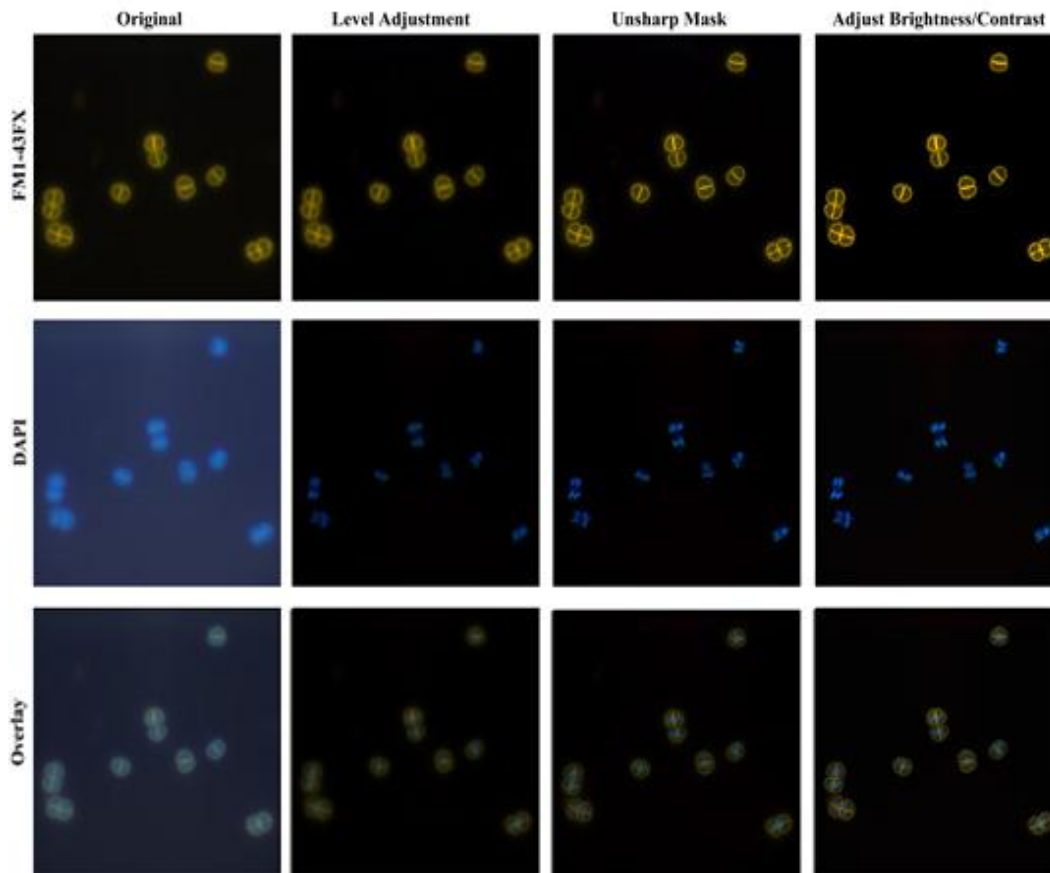


**Figure 3-3: The process of generating overlay images.**

Original images were opened in Adobe Photoshop CS5.1 and background levels adjusted using the Levels tool. The unsharp mask tool, which sharpens the image, was then applied. Adjustments to the images brightness and/or contrast were occasionally made. Corrected DAPI images were then overlaid onto corrected FM1-43FX images. The entire process for a particular wild-type image is shown above.

### 3.2.7 Flow Cytometry

Cell morphology and total DNA content were assessed by flow cytometry using viable stationary-phase wild-type,  $\Delta nraA$  and  $\Delta herA$  cultures with the kind assistance of Kenneth Class at the MPRI Flow Cytometry and Cell Sorting Facility at the University of Maryland in College Park. Cultures in either exponential growth ( $OD_{600}=0.5-1.0$ ) or stationary phase ( $OD_{600} \geq 2$ ) had 500  $\mu$ L aliquots removed and placed into microcentrifuge tubes. These were diluted into 1.5 mL 1x PBS in sterile

polystyrene culture tubes (16x125 mm; Fisher Scientific) such that the final cell concentrations were approximately  $1 \times 10^6$  cells/mL to ensure a proper flow rate could be achieved. Cells were stained with SYTO9 nucleic acid stain (Life Technologies; Excitation  $485_{\text{nm}}$  / Emission  $498_{\text{nm}}$ ) such that the final concentration was  $5 \mu\text{M}$  and allowed to sit in the dark for 15 minutes. SYTO9 is a nucleic acid stain that can penetrate the cell walls of viable cells allowing for fluorescence intensity measurements. Flow cytometry (FACSCanto II, B-D Biosciences) was used to determine the area of the forward scatter (FSC-A) and the SYTO9 emission (FITC-A) signal. A minimum of 30,000 events were recorded at a flow rate between 1000-2000 events per second for each sample. Blank controls (no SYTO9) were performed to ensure the nucleic acid stain was not altering FSC-A signal significantly. Non-cellular events were excluded from analysis by gating the events using 2D-scatter plots of their FSC-A and FITC-A signals. Histograms and 2-D scatter plots made to analyze and report the data were made using FlowJo or Cyflogic software.

### 3.2.8 $^3\text{H}$ -Thymidine Incorporation Assay

The DNA synthesis rates for wild-type and  $\Delta herA$  cultures were measured during exponential growth ( $\text{OD}_{600} = 0.7-1.7$ ) using a pulse label method (91). For a given experiment, WT or  $\Delta herA$  cultures were started by inoculating a single colony into a 50 mL conical tube containing 10 mL 2xTGY media. These cultures were grown to stationary phase to ensure that each strain to be tested is in the same stage of growth when diluted. Cultures in the stationary phase were diluted ( $\text{OD}_{600} = 0.01-0.1$ ) into 125 mL Erlenmeyer flasks containing 25 mL 2x TGY without antibiotics. These cultures were grown as described above until they reached the mid-late exponential

growth phase. Once cultures reached the desired OD<sub>600</sub>, two 500 µL aliquots were removed and placed into two different 1.5 mL microcentrifuge tubes. 250 µL from “tube 1” was added to another 1.5 mL microcentrifuge tube to be used for pulse labeling with <sup>3</sup>H-Thymidine while the remaining 250 µL was to be used for determination of cell concentration (via hemacytometer). The other 500 µL aliquot was allowed to shake for an additional 15 minutes with the pulse labeled sample to obtain an estimate as to how much the OD<sub>600</sub> changed during the incubation period.

The aliquot to be pulse labeled was mixed with 50 µL of prewarmed 2x TGY containing <sup>3</sup>H-Thymidine (84.4 Ci/mmol, 7.5 µCi/mL, Perkin Elmer) at a concentration of 0.045 µCi / mL. A timer was started as soon as the 1<sup>st</sup> aliquot of the <sup>3</sup>H-Thymidine media was added to the first sample and this sample was the first to be quenched after 15 minutes. This meant the other sample would be quenched after the 15 minute period but because they started late, net incubation time was essentially equal for all samples (+/- 10 second difference). Tubes were quenched by adding 1 mL ice cold 10% TCA to them. Samples were then chilled on ice for a minimum of 30 minutes (some longer due to filtration times) before being filtered through Whatman 21 mm GC/F Filter papers (pre-wetted with 10% TCA). 1 mL of 10% TCA was added to the now empty microcentrifuge tube to make sure all cells were obtained and subsequently loaded onto filter paper. This was repeated 2 more times, but using 95% ice cold ethanol. Filter papers were then dried under a heat lamp for 5 minutes.

Dried filter papers were placed in scintillation vials with 4 mL scintillation fluid. Blanks and hot controls were added directly to vials as fluids. The raw DPM counts

obtained were converted to pmol of  $^3\text{H}$ -Thymidine and the average DNA synthesis rates during the 15 minute time interval during mid-exponential growth (4 for each aliquot) were reported as pmol / min. This was normalized to the number of cells in solution by dividing this value by the number of cells estimated to be in those aliquots as determined by hemacytometer counts. Cell densities were estimated from  $\text{OD}_{600}$  curves and used to estimate the amount of  $^3\text{H}$ -thymidine incorporated per gram of dried cells. DNA synthesis rates were determined from the total amount of  $^3\text{H}$ -thymidine incorporated per cell per minute (pmol  $^3\text{H}$ -Thy / (cell•min)) and from the total amount of  $^3\text{H}$ -thymidine incorporated per gram of dried cells per minute (pmol  $^3\text{H}$ -Thy / (g •min)). DNA synthesis rates are reported as the average of all the instantaneous rates determined during mid-to-late exponential growth.

### 3.3 RESULTS

#### 3.3.1 Growth analysis of $\Delta nurA$ and $\Delta herA$ strains

The results from the DNA damage analysis indicated that the putative NurA and HerA did not have a major role in DNA repair in *D. radiodurans*, in contrast to their proposed role in archaea (40). A closer examination of the evidence for the role of NurA and HerA in archaea suggests these enzymes could be involved in some other DNA metabolizing process such as chromosome segregation (42, 52) . Therefore it may be that in *D. radiodurans*, the putative NurA and HerA have a role in some element of DNA processing which occurs during the cell cycle.

To test this hypothesis, we evaluated the growth of the  $\Delta nurA$  and  $\Delta herA$  strains and compared them to that of wild-type by monitoring the  $\text{OD}_{600}$  of exponentially

growing cultures. The  $\Delta nurA$  strain did not display any noticeable difference in its growth rate (**Figure 3-4, A**) relative to wild-type indicating that replacement of the *nurA* gene with *aadA* did not cause a change in its growth properties. It was confirmed that the OD<sub>600</sub> curves accurately reflected the accumulation of cells (**Figure 3-4, B**) and cell mass (**Figure 3-4, C**) with time. Thus the growth rates calculated from OD<sub>600</sub> curves accurately reflect the cell number and cell mass doubling times for the  $\Delta nurA$  and wild-type strains and are summarized in **Table 4**.

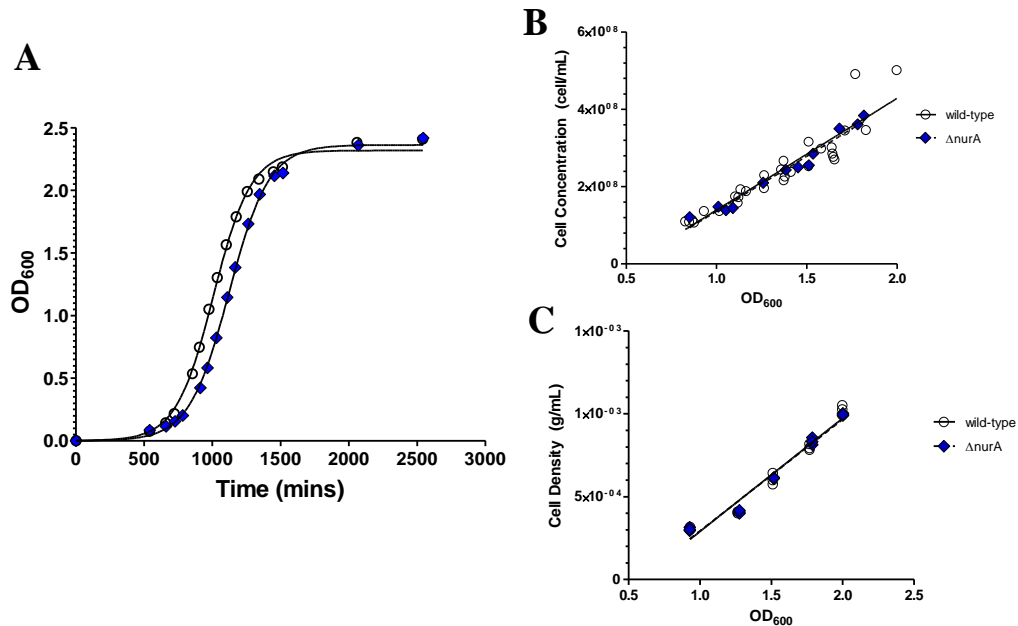


**Figure 3-4: Growth of wild-type and  $\Delta nurA$  cells.**

Stationary-phase cultures were diluted into 2x TGY to an initial OD<sub>600</sub> < 0.1 and shaken at 250 rpm and 30 °C. **(A)** Aliquots were removed and the optical density at 600 nm was recorded. Open circles, wild-type. Blue diamonds,  $\Delta nurA$ . The solid line is the fit to equation 1 (see Methods), with  $k = 0.0073 \text{ min}^{-1}$ ,  $P = 2.32$ , and  $Y_0 = 0.0015$  (wild-type), and  $k = 0.0068 \text{ min}^{-1}$ ,  $P = 2.36$ , and  $Y_0 = 0.001$  ( $\Delta nurA$ ). **(B)** Aliquots were removed and the optical density at 600 nm was measured. Aliquots were also diluted 20-100 fold, and the number of cells in 1 mL was counted using a hemacytometer. Open circles and solid line, wild-type. Blue diamonds and dashed line,  $\Delta nurA$ . Lines are linear regressions. **(C)** Aliquots were removed and the optical density at 600 nm was measured. 1 mL aliquots were also removed and cell mass determined as described in methods. Open circles and solid line, wild-type. Blue diamonds and dashed line,  $\Delta nurA$ . Lines are linear regressions.

**Table 4: Growth properties of wild-type, *ΔnurA* and *ΔherA* strains.**

Strain	Growth rate constant k (min <sup>-1</sup> )	G (min / generation)	N <sup>a</sup>	P (t-test)
wild-type	$6.9 (\pm 0.6) \times 10^{-3}$	101 ± 9	24	****
<i>ΔnurA</i>	$7.1 (\pm 0.7) \times 10^{-3}$	98 ± 6	6	0.6
<i>ΔherA</i>	$6.0 (\pm 0.7) \times 10^{-3}$	116 ± 12	17	0.0002

<sup>a</sup>Number of determinations.

The original *ΔherA* transformants took longer to form colonies than did wild-type cells, suggesting a growth defect due to the *ΔherA* mutation. We quantified this initial observation by monitoring the change in optical density (OD<sub>600</sub>) of wild-type and *ΔherA* cultures (**Figure 3-5, A**). The growth rate constants determined from the growth curves show that the *ΔherA* cultures double their mass ~15% more slowly than the wild-type (**Table 4**). The results indicate a growth defect in the *ΔherA* strain compared to the wild-type. We confirmed that the OD<sub>600</sub> curves accurately reflect the accumulation of cell mass with time by measuring the culture density directly as described in Methods (**Figure 3-5, C**). The density of a culture at an OD<sub>600</sub> of 1.0 is  $3.8 (\pm 0.9) \times 10^{-4}$  g/mL for wild-type and  $3.6 (\pm 0.7) \times 10^{-4}$  g/mL for *ΔherA*.

In contrast to the congruity of OD<sub>600</sub> with cell mass, the cell concentration for the wild-type strain was higher than that of the *ΔherA* strain at all OD<sub>600</sub> (~11% more cells per mL culture; **Figure 3-5, B**). This finding that equal culture densities resulted in an unequal cell concentration can only be explained if the *ΔherA* strain contained a population of cells which were larger/heavier than the wild-type strain.

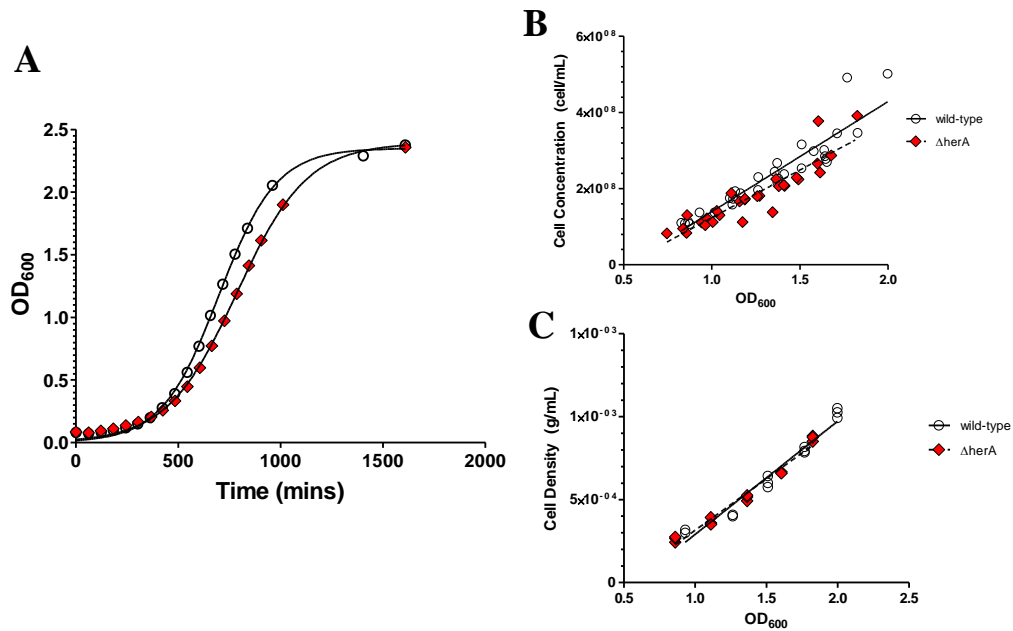


**Figure 3-5: Growth of wild-type and  $\Delta herA$  cells.**

Stationary-phase cultures were diluted into 2x TGY to an initial  $OD_{600} < 0.1$  and shaken at 250 rpm and 30 °C. (A) Aliquots were removed and the optical density at 600 nm was recorded. Open circles, wild-type. Red diamonds,  $\Delta herA$ . The solid line is the fit to equation 1 (see Methods), with  $k = 0.0071 \text{ min}^{-1}$ ,  $P = 2.35$ , and  $Y_o = 0.016$  (wild-type), and  $k = 0.0058 \text{ min}^{-1}$ ,  $P = 2.39$ , and  $Y_o = 0.024$  ( $\Delta herA$ ). (B) Aliquots were removed and the optical density at 600 nm was measured. Aliquots were also diluted 20-100 fold, and the number of cells in 1 mL was counted using a hemacytometer. Open circles and solid line, wild-type. Open red diamonds and red dashed line,  $\Delta herA$ . Lines are linear regressions (C) Aliquots were removed and the optical density at 600 nm was measured. 1 mL aliquots were also removed and cell mass determined as described in methods. Open circles and solid line, wild-type. Open red diamonds and red-dashed line,  $\Delta herA$ . Lines are linear regressions.

### 3.3.2 Morphology analysis: Phase contrast and low resolution fluorescence microscopy

The results from the growth assessment of the  $\Delta herA$  strain indicated that something was causing the strain to accumulate mass at a reduced rate and this likely was also leading to an increase in the average cell size. To help elucidate the nature of the growth defect and determine if the  $\Delta herA$  cells were indeed larger we examined the  $\Delta herA$  strain for differences in cellular morphology and size relative to wild-type using phase-contrast microscopy and fluorescence microscopy as described in Chapter 2. We also analyzed the  $\Delta nurA$  strain in the same way.

Depictions of the various cell types found in wild-type,  $\Delta nurA$  and  $\Delta herA$  cultures using phase contrast and low resolution fluorescence microscopy are shown in **Figure 3-6**. The distributions of cell sizes were estimated by determining the distribution of cell areas in a culture and the average and median cell areas from these distributions are reported in **Table 5**. The results indicate that the  $\Delta nurA$  and  $\Delta herA$  strains contained the same range of cell sizes that were found in the wild-type strain during both exponential and stationary growth (**Figure 3-7**). We did not detect the presence of any morphologies using phase contrast microscopy other than those shown in **Figure 3-6**, regardless of which strain was analyzed. However, there was an obvious shift in the population distribution of cell areas to one which favored larger cell types in the  $\Delta herA$  strain.



**Table 5: Summary of morphology data in wild-type,  $\Delta nurA$  and  $\Delta herA$  strains**

	<b>Avg. Area (<math>\mu\text{m}^2</math>)</b>	<b>P (t-test)</b>	<b>Median Area (<math>\mu\text{m}^2</math>)</b>	<b>P<sup>a</sup> (M-W)</b>	<b># cells</b>
<b>Exponential</b>					
wild-type	6. ( $\pm 2.$ ) <sup>b</sup>	****	5.9	****	801
$\Delta nurA$	6. ( $\pm 2.$ ) <sup>b</sup>	0.31	6.2	0.13	483
$\Delta herA$	8. ( $\pm 3.$ ) <sup>b</sup>	<0.0001	7.2	<0.0001	1591
<b>Stationary</b>					
wild-type	8. ( $\pm 2.$ ) <sup>b</sup>	****	7.7	****	309
$\Delta nurA$	8. ( $\pm 2.$ ) <sup>b</sup>	0.42	7.8	0.60	179
$\Delta herA$	9. ( $\pm 3.$ ) <sup>b</sup>	<0.0001	8.3	<0.0001	707

<sup>a</sup>P-value for Mann-Whitney nonparametric test. <sup>b</sup>Standard deviation of mean

We analyzed the nucleic acid content of wild-type,  $\Delta nurA$  and  $\Delta herA$  cells at 1600x magnification using low resolution (40 pixel/ $\mu\text{m}$ ) fluorescence microscopy. For fluorescence microscopy the nucleic acid stain DAPI was used to visualize the nucleoids. The resolution was sufficient for detection of anucleate cells (**Figure 3-6, B**). There was no significant increase in the fraction of anucleate cells between wild-type (0.85% anucleate cells; 3 of 355 cells counted),  $\Delta nurA$  (0.78%; 1 out of 129 cells) and  $\Delta herA$  (0.38%; 2 of 525 cells) strains. The resolution did not allow us to report on differences in nucleoid morphology or localization between the wild-type and mutant strains.

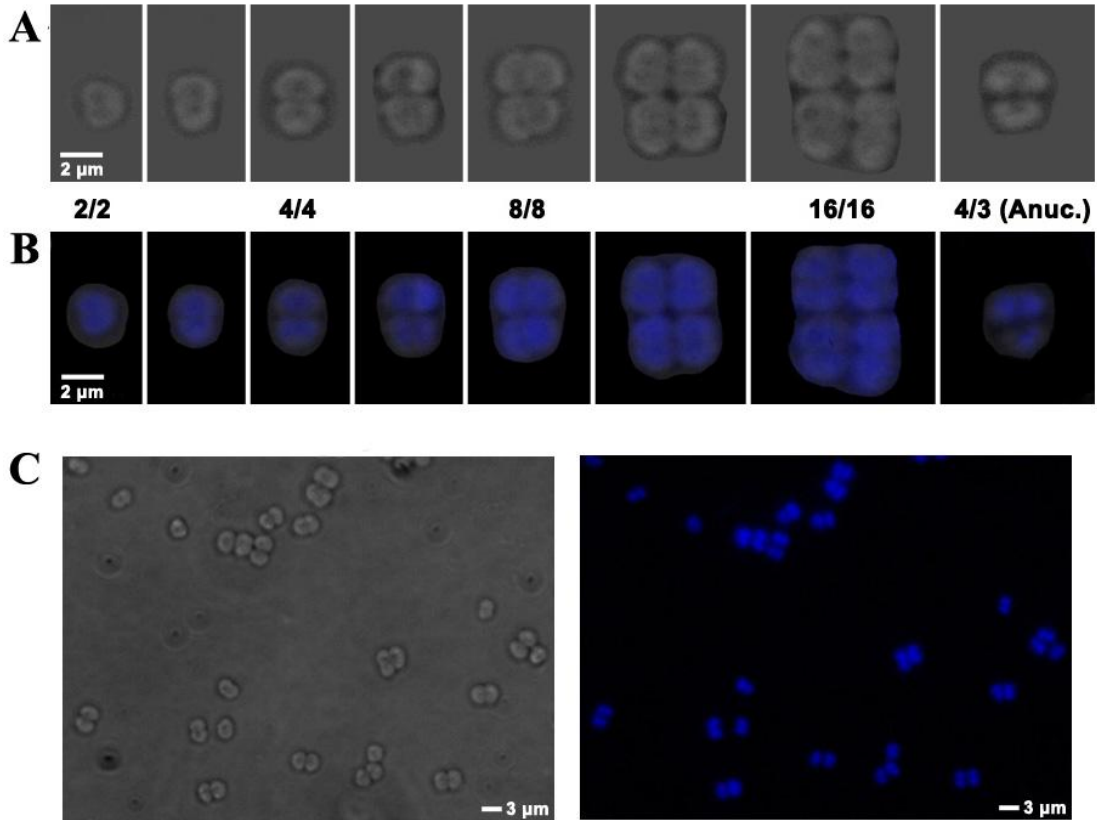


**Figure 3-6: Images of wild-type during late exponential phase of growth.**

All images are at 1600x magnification. **(A,B)** The various sizes and shapes (morphologies) of wild-type and  $\Delta herA$  cells seen during exponential and stationary growth. **(A)** Images show the different cell types from a diad (2/2) to four attached tetrads (16/16). **(B)** Same as **(A)** except showing the DAPI (Blue) staining. The fractions between panels **(A)** and **(B)** represent the estimated number of individual septa (top number) and individual nucleoids (bottom number). A representative image of a wild-type anucleate cell is shown labeled (4/3). **(C)** (Left) Phase contrast images of wild-type (Right) Fluorescent images of wild-type stained with DAPI. Images A and B are composite images made in Adobe Photoshop CS5.1. Wild-type cells which showed the desired morphology were cropped from images like those seen in **(C)** and **(D)**, rotated from their original imaged position to that shown and overlaid on gray **(A)** or black **(B)** backgrounds. These were then aligned to show the spectrum of cell sizes observed in a culture of *D. radiodurans* grown under the culture conditions described in Methods.

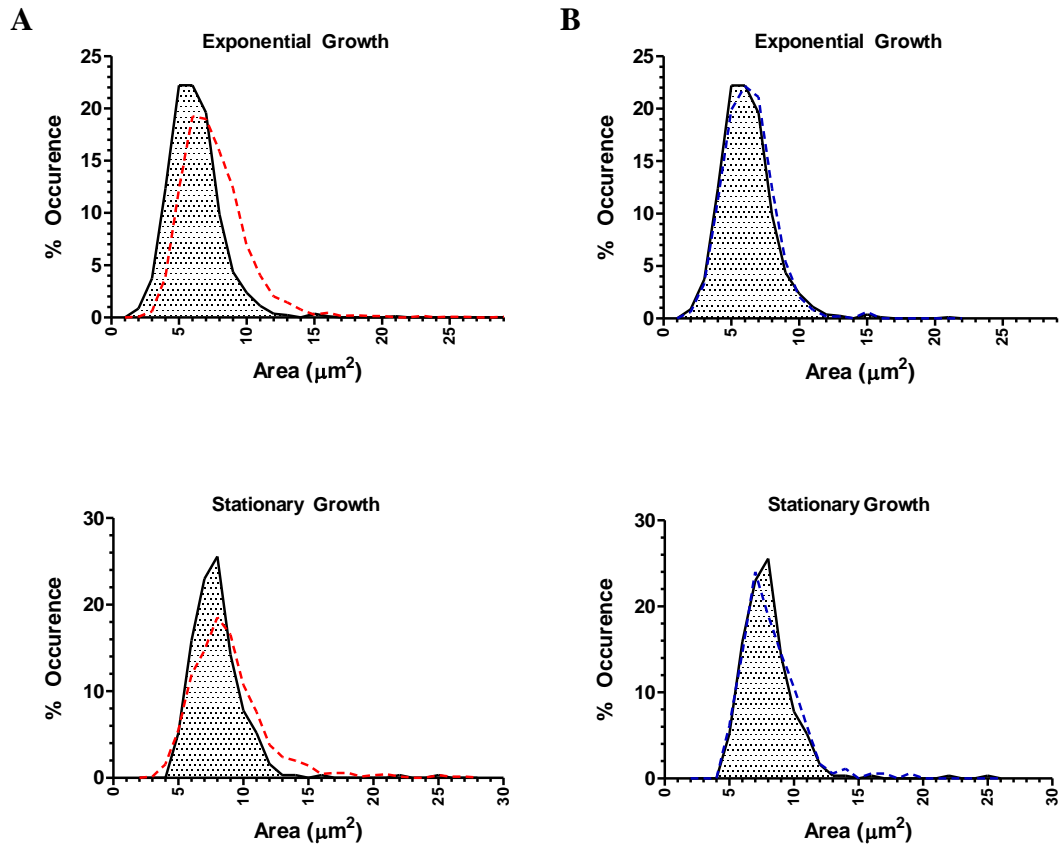


**Figure 3-7: Size Distributions of wild-type,  $\Delta herA$  and  $\Delta nurA$  cells.**

Cells were imaged at 400x magnification. Histograms show the percentage of cells with the indicated area in either exponential or stationary phase cultures. Bin sizes are  $1 \mu\text{m}^2$ . Black trace, wild-type. (A) Dashed red trace,  $\Delta herA$ . (B) Dashed blue trace,  $\Delta nurA$ .

### 3.3.3 Morphology assessment: Flow cytometry

The results from microscopy indicated that there is a difference in the cell size distribution between wild-type and  $\Delta herA$  cultures regardless of the growth state, but there was no difference with respect to the  $\Delta nurA$  strain. We used flow cytometry to measure the relative distribution of various cell sizes and nucleic acid content per cell in the wild-type,  $\Delta nurA$  and  $\Delta herA$  strains in exponential and stationary phase.

Two-dimensional scatter plots were made using the FSC-A signal, a measure of the cell size, and the FITC-A signal, which is indicative of nucleic acid content in the cells (**Figure 3-8** and **Figure 3-9**). These 2D-scatter plots allow for the detection of subpopulations of cells with unusual DNA content per cell, such as anucleate cells (low FITC; normal FSC) or cells that contain unusual amounts of DNA given their relative size (high or low FITC; normal FSC). Histograms of the FSC-A and FITC-A were also examined (**Figure 3-10** and **Figure 3-11**).

Consistent with the results in microscopy, the 2-D scatter plots (**Figure 3-8**) did not reveal a unique subpopulation of cells in the  $\Delta nurA$  strain and no difference in the cell size distribution was observed relative to wild-type. As expected, the histograms (**Figure 3-10**) revealed the same thing; that wild-type and  $\Delta nurA$  strains had essentially the same types of cells and same proportions of these cell types, regardless of the stage of growth

The 2-D scatter plots of the  $\Delta herA$  strain compared to the wild-type strain indicated that the  $\Delta herA$  strain had a higher population of the larger cells compared to wild-type (**Figure 3-9**). The DNA content (FITC-A signal) of the large  $\Delta herA$  cells (large FSC-A signal) is similar in magnitude to that for wild-type cells of the same size. The histograms for these strains (**Figure 3-10**) confirmed this observation showing a shift in the cell size population distribution for the  $\Delta herA$  strain to one with larger cells relative to wild-type. The data also suggest there is not a significant population of anucleate cells or cells with abnormal DNA content that exists in the mutant strain but not in the wild-type strain. These results are consistent with the microscopy results which indicated the  $\Delta herA$  strain experienced an increase in the

average cell size without an increase in the number of anucleate cells relative to wild-type.

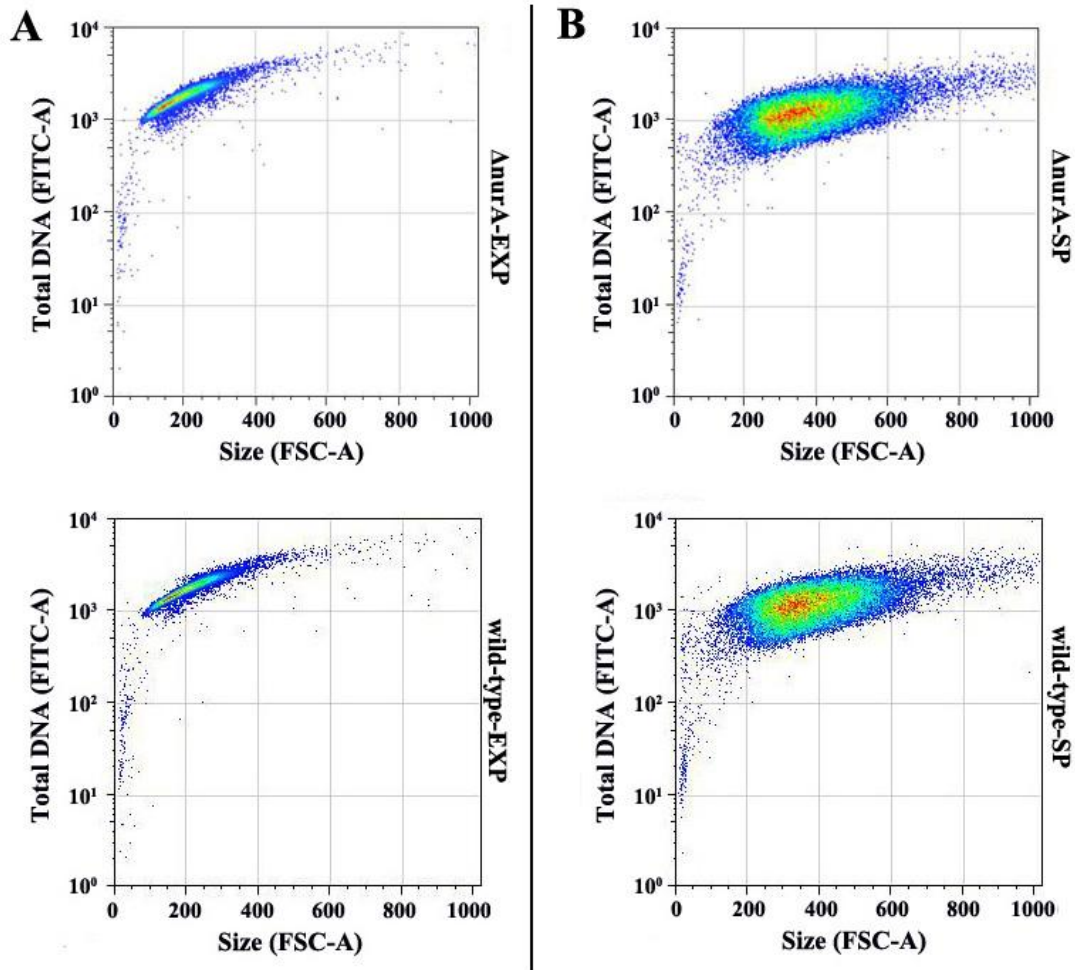


**Figure 3-8: 2-D scatter plots of FSC-A and FITC-A signals from flow cytometry of wild-type and  $\Delta nurA$  strains.**

Representative 2-D Scatter plots of SYTO9 fluorescence signal (FITC-A; DNA content) vs. forward-scatter signal (FSC-A; size) from wild-type and  $\Delta nurA$  cells (>30,000) in exponential and stationary (>48 hours old) phase of growth. (A) Wild-type (bottom) and  $\Delta nurA$  cells (top) in exponential phase. (B) Wild-type (bottom) and  $\Delta nurA$  cells (top) in stationary phase. Cells are larger and contain more DNA from left-to-right, and bottom-to-top, respectively, on the graphs. Scatter plots are shown as density plots where lower concentrations of cells are shown in blue and higher in red.

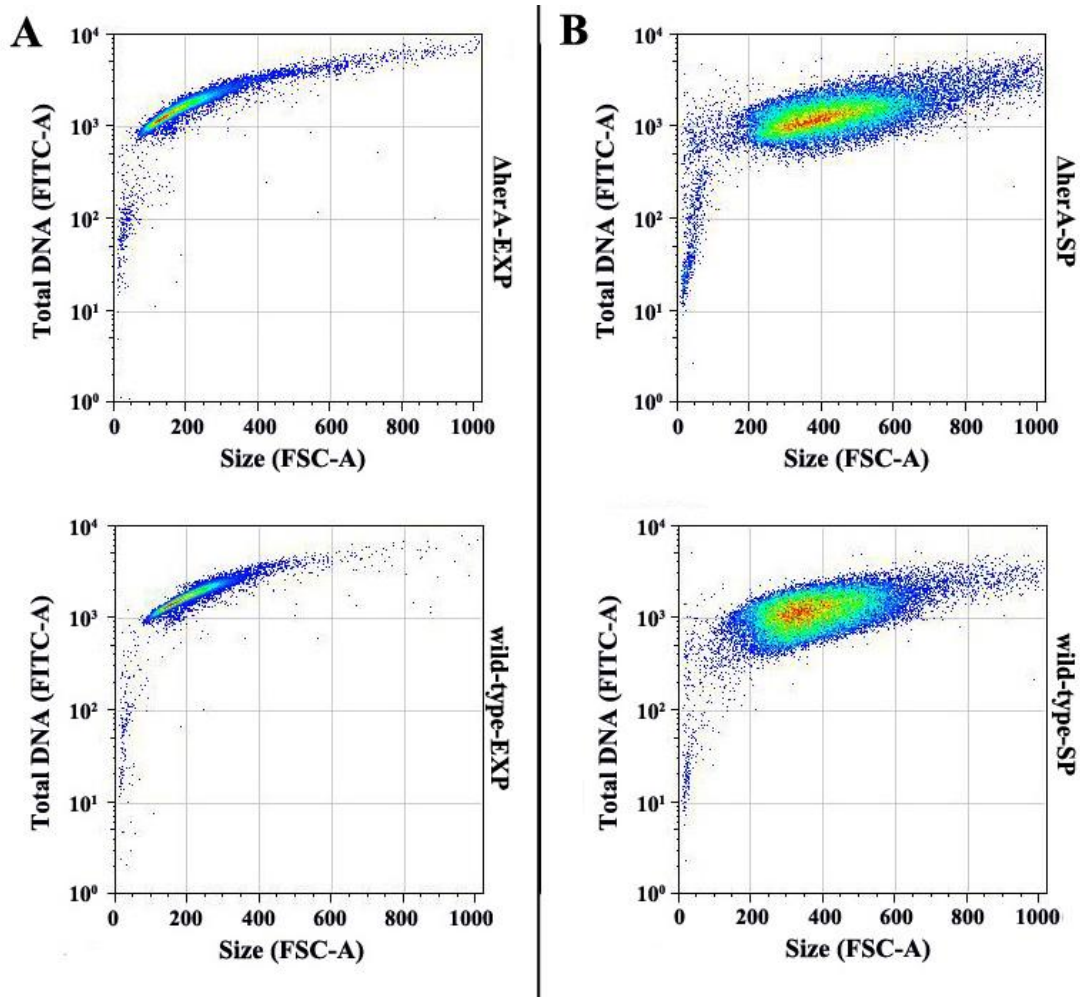


**Figure 3-9: 2-D scatter plots of FSC-A and FITC-A signals from flow cytometry of wild-type and  $\Delta herA$  strains.**

Representative 2-D Scatter plots of SYTO9 fluorescence signal (FITC-A; DNA content) vs. forward-scatter signal (FSC-A; size) from wild-type and  $\Delta herA$  cells (>30,000) in exponential and stationary (>48 hours old) phase of growth. **(A)** Wild-type (bottom) and  $\Delta herA$  cells (top) in exponential phase. **(B)** Wild-type (bottom) and  $\Delta herA$  cells (top) in stationary phase. Cells are larger and contain more DNA from left-to-right, and bottom-to-top, respectively, on the graphs. Scatter plots are shown as density plots where lower concentrations of cells are shown in blue and higher in red

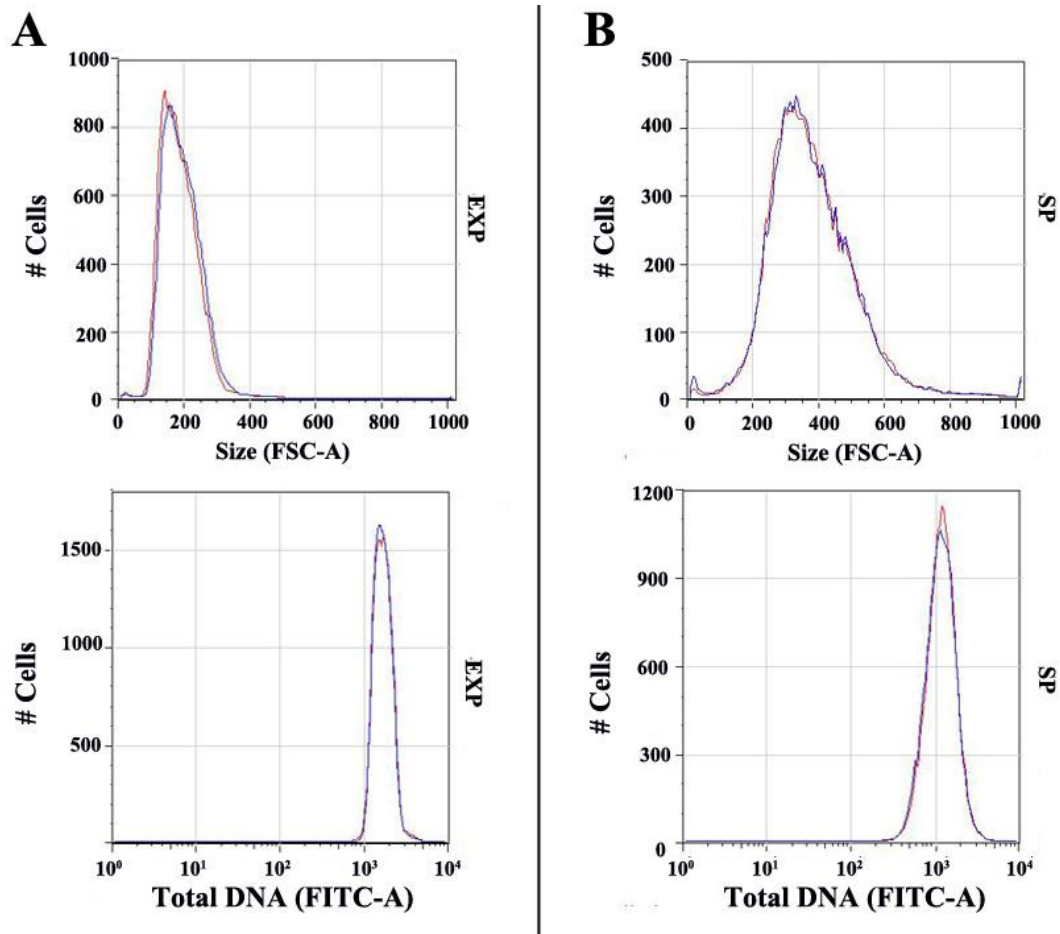


**Figure 3-10: Histogram overlays of FSC-A and FITC-A signals from flow cytometry of wild-type and  $\Delta nurA$  strains.**

(A) Representative histograms showing the distribution of FSC-A signals and FITC-A signals from wild-type and  $\Delta nurA$  cells (>30,000) in exponential phase of growth. Wild-type: blue trace.  $\Delta nurA$ : red trace. (B) Representative histograms showing the distribution of FSC-A and FITC-A signals from wild-type and  $\Delta nurA$  cells (>30,000) in stationary (>48hr) phase of growth. Wild-type: blue trace.  $\Delta nurA$ : red trace.

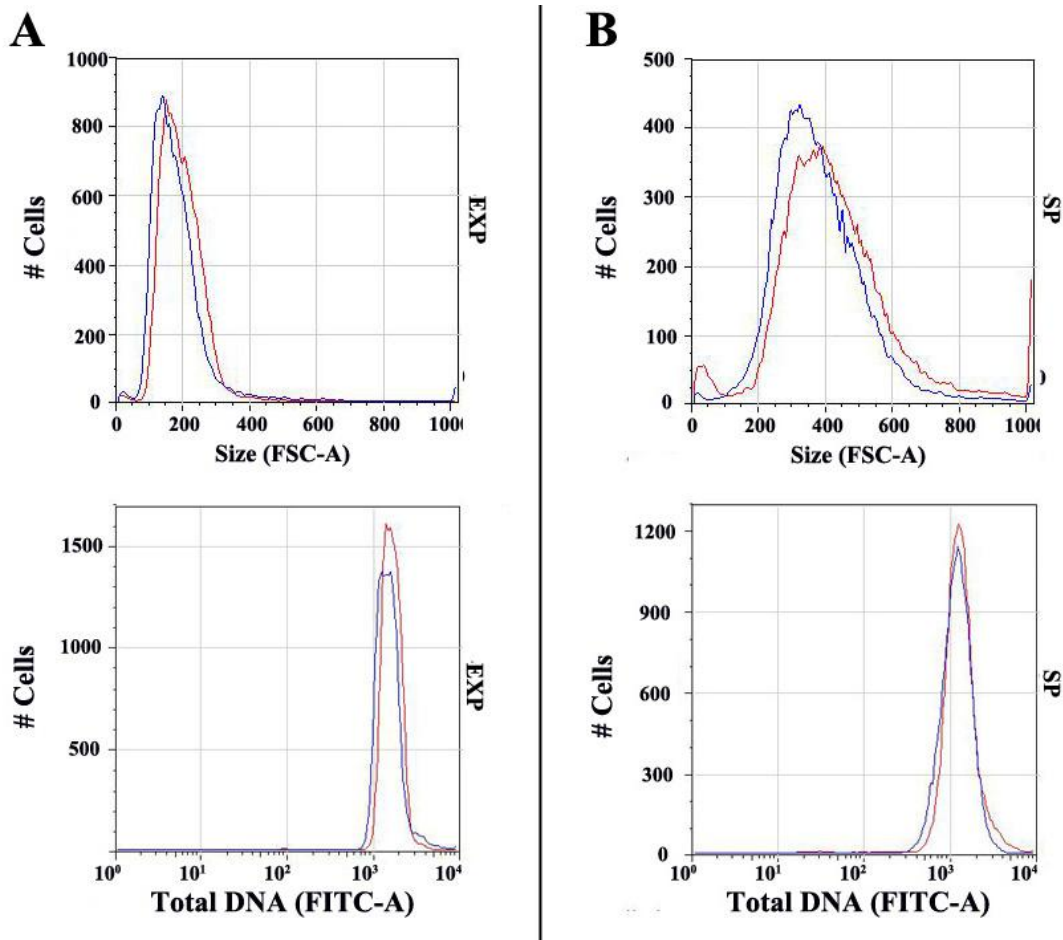


**Figure 3-11: Histogram overlays of FSC-A and FITC-A signals from flow cytometry of wild-type and  $\Delta herA$  strains.**

(A) Representative histograms showing the distribution of FSC-A signals and FITC-A signals from wild-type and  $\Delta herA$  cells (>30,000) in exponential phase of growth. Wild-type: blue trace.  $\Delta herA$ : red trace. (B) Representative histograms showing the distribution of FSC-A and FITC-A signals from wild-type and  $\Delta herA$  cells (>30,000) in stationary (>48hr) phase of growth. Wild-type: blue trace.  $\Delta herA$ : red trace.



### 3.3.4 Effect of *herA* mutation on cell cycle

The results from our growth analyses of the  $\Delta nurA$  and  $\Delta herA$  strains indicated that the  $\Delta nurA$  strain had no detectable growth phenotype, while the  $\Delta herA$  strain had a subtle growth defect accompanied by a shift in the average cell size. For this reason the remaining experiments were performed in order to address the cause of the growth phenotype observed in the  $\Delta herA$  strain.

The growth defect in the  $\Delta herA$  strain implies that something is occurring differently with respect to the cell cycle relative to wild-type. We investigated whether it was possible to inhibit a known pathway in the bacterial cell cycle in wild-type cells and generate growth properties like those seen with the  $\Delta herA$  strain. We monitored changes in growth rates (OD<sub>600</sub> curves) and morphology (microscopy) when wild-type cultures were grown in the presence of various antibiotics. Four antibiotics were chosen to investigate the effects of inhibiting cell wall synthesis (ampicillin, added at 100 and 300 ng/mL), transcription (rifampicin, 1 and 5 µg/mL; GoldBio), translation (chloramphenicol, 500 ng/mL; GoldBio) and DNA synthesis (hydroxyurea, 2, 4 and 14 µg/mL; Sigma-Aldrich). Antibiotics were administered to wild-type cultures during exponential growth. Cell morphology and growth rate properties were evaluated as described above.

Rifampicin, chloramphenicol, and ampicillin caused a reduction in growth rates, but this was not accompanied by a shift in the cell population to larger cell types as assessed by microscopy. In contrast, when hydroxyurea (2, 4 and 14 µg/mL) was added to exponentially-growing wild-type cultures, not only did the growth rate slow, but this was accompanied by a shift to larger cell types, a characteristic also seen with

the  $\Delta herA$  strain in the absence of hydroxyurea. Previous reports have confirmed that treatment of *D. radiodurans* cultures with hydroxyurea causes a decrease in the growth rate due to a decrease in the rate of DNA synthesis (91).

We repeated the experiment with both the wild-type and the  $\Delta herA$  strain using the hydroxyurea dose which caused the wild-type strain to mimic the  $\Delta herA$  phenotype most closely (2  $\mu\text{g}/\text{mL}$ ). We observed roughly the same relative decrease in the growth rate and increase in the size distribution in treated  $\Delta herA$  cultures as we saw for the wild-type culture (**Figure 3-12**). The result indicates that, while a decrease in the DNA synthesis rate caused by hydroxyurea leads to a shift in the cell size distribution and a decrease in the growth rate, the similar effect occurring naturally in the  $\Delta herA$  strain is likely occurring through a mechanism other than inhibition of DNA synthesis. Experiments which looked at the effect of hydroxyurea on septum and nucleoid morphology were not done.

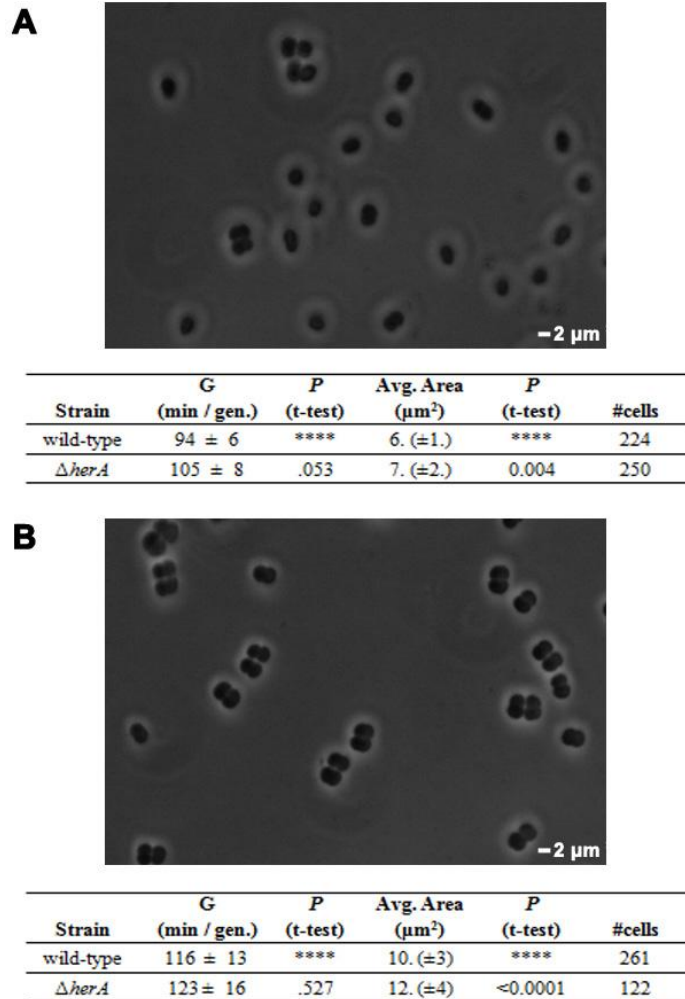


**Figure 3-12: Growth data and representative phase-contrast images of wild-type and  $\Delta herA$  cells upon treatment with hydroxyurea.**

(A) Cultures were grown in 2x TGY medium. Cells were taken from stationary phase cultures and imaged at 400x magnification. (B) Identical to A except cultures were grown in 2x TGY medium supplemented with 2  $\mu\text{g}/\text{mL}$  hydroxyurea. Below images are table summaries of growth and morphology data.

### 3.3.5 Measurement of DNA synthesis rates in $\Delta herA$ strain

The results described above imply that the DNA synthesis rates in the wild-type and the  $\Delta herA$  strain are the same. We measured the rate of DNA synthesis directly by measuring incorporation of  $^3\text{H}$ -thymidine using a pulse label method that allows for determination of the total amount of  $^3\text{H}$ -thymidine incorporated into a population

of cells during a 15 minute incubation period. Experiments were carried out on cells growing in the mid-to-late exponential phase. The average rate of synthesis normalized to the number of cells in solution was  $2.4 (\pm 0.2) \times 10^{-10}$  pmol  $^3\text{H-thy} /(\text{cell}\cdot\text{min})$  for wild-type cultures and  $2.9 (\pm 0.2) \times 10^{-10}$  pmol  $^3\text{H-thy} /(\text{cell}\cdot\text{min})$  for  $\Delta herA$  cultures ( $P = 0.047$ ;  $n=6$ ).

The  $\Delta herA$  strain appears to incorporate the  $^3\text{H-thymidine}$  at a faster rate than the wild-type strain, when the results are normalized to cell concentration. However, knowing that the  $\Delta herA$  strain contained an increased proportion of larger cell types, we rationalized that these larger cells could account for the apparent increase in the amount of incorporated  $^3\text{H-thymidine}$  per cell. To confirm this we normalized the rates to the mass of cells in each aliquot tested. The average rate of synthesis normalized to the mass of cells in solution was  $111. (\pm 7.)$  pmol  $^3\text{H-thy} /(\text{g cells}\cdot\text{min})$  for wild-type cultures and  $115. (\pm 3.)$  pmol  $^3\text{H-thy} /(\text{g cells}\cdot\text{min})$  for  $\Delta herA$  cultures ( $P=0.55$ ;  $n=6$ ). There is virtually no difference between the wild-type and  $\Delta herA$  strains when normalized this way. This supports the conclusion that the decreased growth rate and shift in cell size in the  $\Delta herA$  mutant are not explained by a decrease in its rate of DNA synthesis.

### 3.3.6 Morphology Assessment: High resolution fluorescence microscopy

The resolution in our initial microscopy analysis (**Section 3.3.2**) did not allow us to report on differences in nucleoid morphology and/or localization between the wild-type and  $\Delta herA$  strain. It is possible that the putative HerA is participating in some aspect of chromosome segregation given the fact it is predicted to be part of the FtsK/HerA superfamily of P-loop ATPases, which have been shown to participate in

chromosome segregation (42). We chose to examine the integrity of septa and nucleoid partitioning in wild-type and  $\Delta herA$  cells at a higher resolution using fluorescence microscopes in Dr. Wolniak's lab in the Cell Biology and Molecular Genetics Department at the University of Maryland, College Park.

Using the microscope provided by Dr. Wolniak, we were able to examine cells membranes/septa and nucleoids at a higher resolution (54.2 pixel/ $\mu\text{m}$ ). Overlay composite images of wild-type and  $\Delta herA$  cells were generated as described in **Methods**. These images were used to examine the relationship between the segregating nucleoid and the closing septum in actively growing cells. Using these composite images, a spectrum of the different observed morphologies was created such that cells could be classified into a specific growth state as shown in **Figure 3-13**. Each cell was categorized as being in a growth state from 1 to 9 and its cell area determined.

The  $\Delta herA$  mutant grew at a decreased growth rate which showed that the cell cycle was taking an additional 15 minutes relative to wild-type. Consistent with this finding, we found that the  $\Delta herA$  mutant strain contained more cells in earlier growth states. An entire cell cycle for a particular morphology (a diad) can be observed during the transition of a diad into a tetrad (growth states 2-5). If the wild-type and the  $\Delta herA$  mutant strain were progressing through this transition at the same rate, we'd expect the population distribution of the various states to be the same. The median growth state for wild-type cells during this transition was 4 (n=236), while the median growth state for  $\Delta herA$  cells was 3 (n=223). Statistical analysis on the distribution of growth states using the Mann-Whitney test, which asks what is the

chance any difference in the distribution is due to chance, indicated that these two populations were in fact different ( $p=0.05$ ).

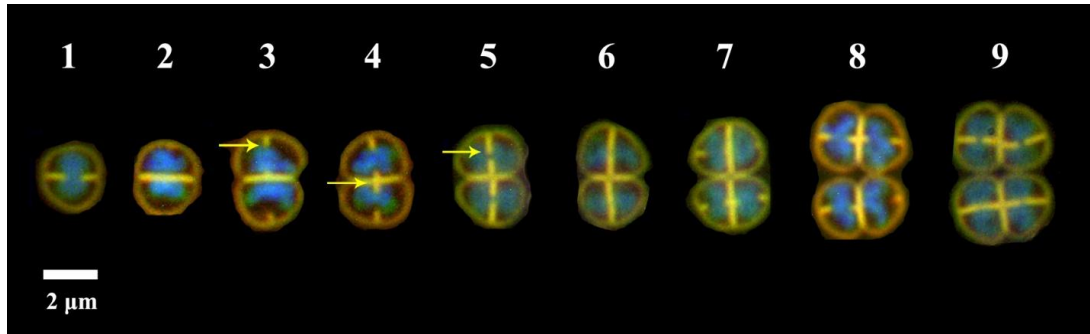


**Figure 3-13: The various growth states of *D. radiodurans*.**

Image shows the progression through the different cellular and nucleoid morphologies observed in wild-type *D. radiodurans* cultures. Images of cells are composite images made from images of cells stained with the cell membrane dye FM1-43FX and the nucleic acid stain DAPI. This image is not a time-lapse image showing the progression of a single cell, but rather these are representative cells found in wild-type images that show the different growth states and morphologies observed. The growth states are described as follows: (1) A monococcus in the mid stages of segregating its nucleoid and closing its septum. (2) A diad (2/2) that has not yet begun to form septa, but has begun segregating its chromosome. (3) A diad that has started to form its new septa [yellow arrow] on the peripheral wall and has yet to segregate nucleoid away from old division plane. (4) A diad that has formed septa at the central wall [yellow arrow] and continues to segregate nucleoid out of cell center. (5) A diad in the final stages of chromosome segregation and septum closure which has almost completely cleared [yellow arrow] the nucleoid from the cell center. (6) A tetrad (4/4) that has not yet begun to form new septa; note at this stage the cell is also capable of splitting along cell the wall of the old division plane resulting in the formation of two diads, essentially sending the cycle back to growth state 2. (7) A tetrad that has not split and begins to divide as two connected diads. Each diad appears to be in growth state 3. (8) A tetrad with each of the two diads it is composed of in growth state 4. (9) A tetrad with each of the two diads it is composed of in growth state 5; almost an (8/8). 86% of wild-type cells in exponential phase are in growth states 1-5 and only 12% of cells are in states 6. The remaining 2% of cells are cells in growth states after 6.

In approximately 80% of wild-type cells, the two dividing halves of a single cell appeared the same and this was taken as an indication that each cell half was progressing through the cell cycle in synchrony. In the other 20% of wild-type cells,

this synchrony appeared to be lost as one half appeared to be different than the other. These irregularities were characterized by noting the extent to which two halves of a cell differed regarding septum and nucleoid morphology (**Figure 3-14**). If the two halves weren't an entire growth state apart, the irregularity was referred to as subtle. When the difference was at least one growth state it was referred to as mild and if it was more than one it was referred to as a severe effect. The majority of irregularities in wild-type were subtle (10.2%) with a small percentage being mild (2.1%) and a very small percentage being severe (0.5%).

In the  $\Delta herA$  strain, approximately 30% of the cells examined had these irregularities. Similar to wild-type, the majority of the irregularities in the  $\Delta herA$  strain were subtle (14.7%) with a smaller percentage being mild (3.1%) and the smallest percentage being severe (1.8%). The wild-type strain experienced the majority of these irregularities in cells in growth states 4 and 5, which are the final stages of chromosome segregation and septation before a diad becomes a tetrad. The mutant strain also had the majority of its irregularities in cells in states 4 and 5, but the mutant strain had a higher percentage of cells in states 4 and 5 experiencing these irregularities.

We also observed a small population (2.1%) of cells in the  $\Delta herA$  strain which displayed what appeared to be a chromosome segregation defect (**Figure 3-14, Pink**). These cells were more spherical and appeared to contain DNA trapped in the division septum or have its nucleoid condensed and unsegregated. No such cell type could be identified in the wild-type strain.

When cells from wild-type and  $\Delta herA$  strains in the same growth state were compared, the  $\Delta herA$  cells were on average larger (**Figure 3-15**). Results from phase contrast microscopy suggested that the  $\Delta herA$  cells were actually larger morphologies, such that their increased size could be explained as an increase in the population of larger morphologies like tetrads. This analysis suggests that the increase in cell size observed from phase contrast microscopy is a result of an increase in the actual cell size for a cell in a particular growth state; that a  $\Delta herA$  cell in growth state 4 is actually a larger version of a wild-type cell in growth state 4 on average.

It is worth noting that when the results obtained via flow cytometry are reexamined with the new information obtained in this analysis in mind, we were unable to detect the unique population of mutant cells that had unusual septum and nucleoid morphologies (~2% population). In these cells, the mutants still retained roughly the same shape as a normal cell its size, but had all of their DNA condensed in the cell center (possibly trapped). The data suggest that the total amount of DNA in these  $\Delta herA$  cells is consistent with what one would expect to find in a normal, wild-type cell of equal size. This is consistent with the finding that DNA replication appears to be occurring at the same rates in both the wild-type and  $\Delta herA$  strains. However, if the difference in DNA content to cell size is subtle, it may be masked in the data by normal cells with similar shapes and DNA content.



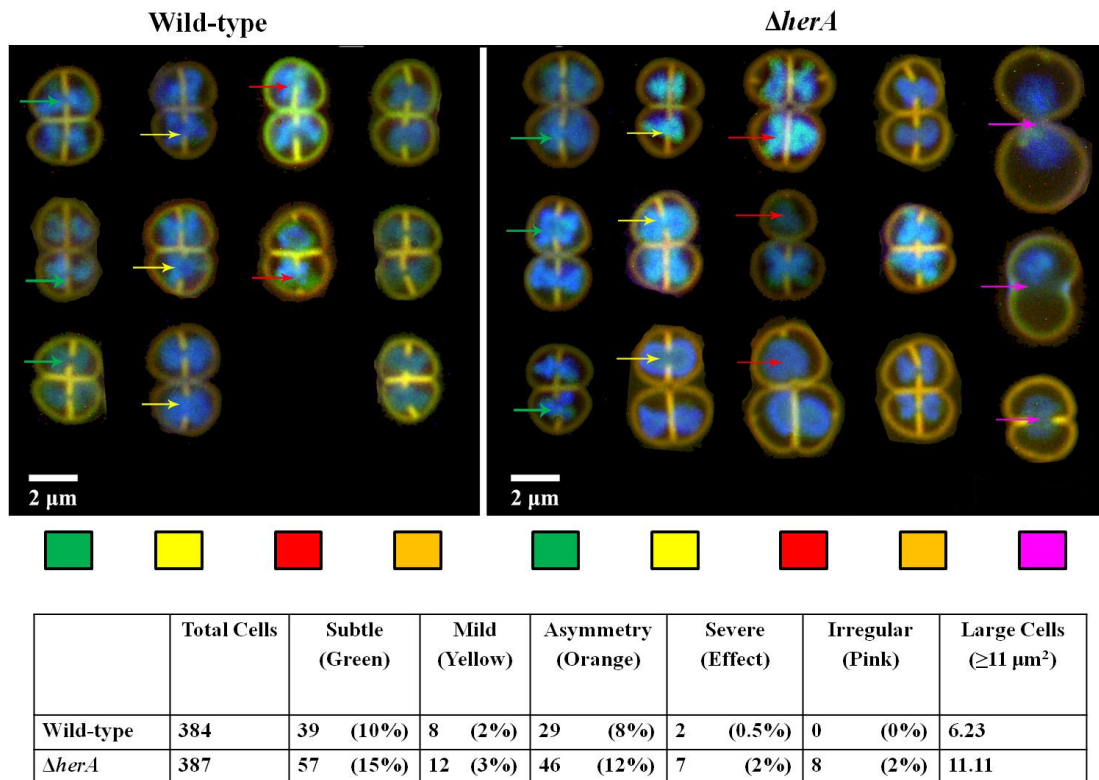
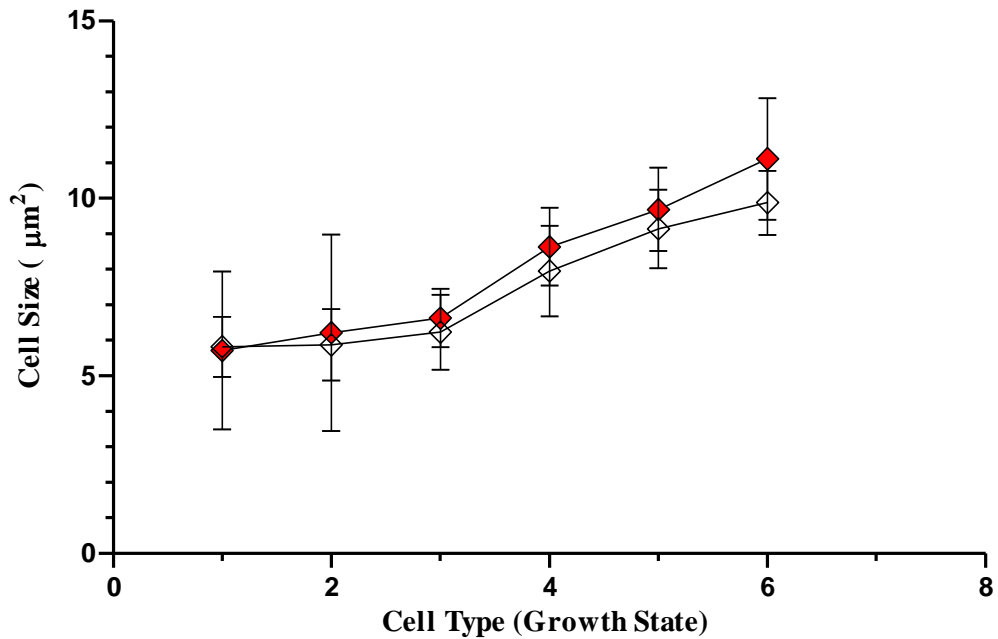


**Figure 3-14: Fluorescence image overlays showing septum and nucleoid abnormalities.**

Cells were imaged using a high resolution fluorescence microscope. Cells were stained with the membrane stain FM1-43FX and the nucleic acid stain DAPI. Image overlays are composite images from individual FM1-43FX and DAPI images. The various septum abnormalities are shown from left to right. The arrows point to the area of the cell which is irregular and the color of the arrow corresponds to the type of irregularity: Green is a subtle timing effect where two halves of the cell appear to be in the same growth state, but are slightly out of sync. Yellow is a mild timing effect where the two halves of the cell appear to be separated by a single growth state. Red is a severe timing defect where the two halves of the cell appear to be separated by a more than a single growth state. Orange indicates an asymmetry within the formation of new septa and/or chromosome segregation patterns, such that new septa are forming at angles, new cellular compartments are asymmetrical. Pink, indicates an irregular morphology that appears more spherical and the nucleoid is seen trapped in the septum or unsegregated. On the left side are representative examples of wild-type cells and on the right are those for *ΔherA*. The table below summarizes the results of the analysis and gives the number of cells and percentages of the total number of cells (in parentheses) which had subtle, mild, asymmetric, and severe effects as well as the % of cells larger than 11 μm<sup>2</sup>.



Average Size						
Strain	1	2	3	4	5	6
Wild-type	6±1	6±1	6±1	8±1	9±1	10±1
<i>ΔherA</i>	6±2	6±3	7±1	9±1	10±1	11±2
p-value (t-test)	0.8	0.4	0.004	0.0002	0.007	0.0003
Median Size						
Strain	1	2	3	4	5	6
Wild-type	5.3	5.8	6.0	7.8	8.9	9.8
<i>ΔherA</i>	5.2	5.8	6.5	8.4	9.6	10.7
p-value (MW)	0.02	0.8	0.001	0.0002	0.001	0.001
Percentage of Total Cells						
Strain	1	2	3	4	5	6
Wild-type	6.4	14.1	28.2	24.7	14.9	11.7
<i>ΔherA</i>	11.4	19.7	23.1	20.8	19.2	5.7

**Figure 3-15: The average cell size per growth state for wild-type and *ΔherA* cells.**

Cell areas and growth states were determined from image overlays of individual FM1-43FX and DAPI images. The graph shows the average cell area for wild-type and *ΔherA* cells in a particular growth state. Standard deviations of averages are shown as error bars. The table below reports the average cell size ( $\mu\text{m}^2$ ), median cell size ( $\mu\text{m}^2$ ) and percentage of total cells for each growth state. Averages are reported with standard deviations and the p-values for t-test comparing the means (t-test) and median distributions (Mann-Whitney) are also given for each growth state.

### 3.4 DISCUSSION

We observed no growth phenotype or change in cellular/nuclear morphology in the  $\Delta nurA$  strain relative to wild-type *D. radiodurans*. In contrast, deletion of *herA* from the *D. radiodurans* genome resulted in a decrease in growth rate accompanied by a shift in the cell size distribution to one favoring larger cells. We did not observe an increase in the number of cells which were anucleate or had abnormal amounts of DNA in the  $\Delta herA$  strain. We did detect a small, unique population of cells (~2%) that had abnormal septum and nucleoid morphologies in the  $\Delta herA$  strain, as well as a larger population of cells experiencing subtle, mild and severe irregularities regarding septum and nucleoid morphology. The slower growth and increased cell size could not be attributed to a decrease in DNA synthesis rate, a phenotype which could be created in the wild-type strain by growing it in the presence of hydroxyurea. The results imply a role in chromosome segregation for the putative HerA in *D. radiodurans*, but we are unable to suggest a corresponding role for the putative NurA.

#### 3.4.1 *Growth and Morphology Analysis*

As described earlier, HerA proteins are close relatives of FtsK proteins and therefore could utilize their C-terminal ATPase activity to perform functions similar to FtsK, such as assisting in segregation of newly replicated DNA and in decatenation and resolution of chromosome dimers (42, 74). *D. radiodurans* has a homolog of *ftsK* which is presumably membrane-bound and insoluble, as are FtsK proteins in other bacteria (92). HerA proteins from *D. radiodurans* and archaea lack the N-terminal transmembrane domain found in FtsK and their sequence similarity is with the ATPase domain in the C-terminal region of FtsK (**Figure 3-1**).

The isolated C-terminal domains of FtsK and archaeal HerA proteins are soluble (46, 48, 93). We have found that the *D. radiodurans* HerA is also expressed as a soluble protein in *E. coli*, and appears to be capable of hydrolyzing ATP, although its precise rate of ATP hydrolysis was not confirmed. These findings suggest that *D. radiodurans* has at least two FtsK-like DNA translocases, one soluble (HerA) and the second membrane-bound (FtsK). *B. subtilis* also has two proteins with amino acid sequence similarity to FtsK, called SpoIIIIE and SftA (referred to in Chapter 3 Introduction). SftA and SpoIIIIE have been proposed to work synergistically in the resolution of chromosome dimers in *B. subtilis* (73, 94). SpoIIIIE is membrane-anchored and involved in the late stages of chromosome segregation, like FtsK in *E. coli*. SftA is a second, soluble, FtsK-like translocase which is involved in the early stages of chromosome segregation (72). The homology between SftA and FtsK is within the C-terminal ATPase domain of FtsK (**Figure 3-1**), and SftA, like HerA, lacks the N-terminal transmembrane domain found in FtsK and in SpoIIIIE (71).

When the ATPase activity in FtsK and FtsK-like proteins is disrupted the mutant cells appear to grow normally, but become defective in chromosome segregation and septation. This leads to an increased population of cells which are larger (having forgone septation) and show asymmetrical nucleoid morphology, and is sometimes accompanied by a slight increase in the frequency of anucleate cells (71, 72, 79, 84, 85). For example, in *E. coli*, disruption of the C-terminal ATPase domain in FtsK leads to an increased population of larger, filamented cells (cells that have forgone septation). In approximately 20% of these mutant cells the nucleoids were positioned asymmetrically and 1% of the mutant cells were anucleate (84). When *sftA* is deleted

from *B. subtilis*, the median cell length distribution increases by about 5% (72) and there is a small increase in the number of cells with chromosome segregation defects (6-8%) characterized by cells with asymmetrical positioning of nucleoids and cells with bisected nucleoids (71).

If HerA in *D. radiodurans* has a role similar to the FtsK and FtsK-like proteins studied in other bacteria, then loss of the activity associated with HerA should produce a phenotype with similarities to those observed in FtsK mutant studies. Deletion of *herA* from *D. radiodurans* caused a small change in the growth rate of the cultures, accompanied by a shift in the average/median cell size indicating an increase in the number of cells which forgo or are delayed in septation. The median cell area was 17% greater in the *herA* deletion strain compared to the wild-type ( $p < 0.0001$ ; Mann-Whitney test). This increase is similar to that observed in the *sftA* deletion strain in *B. subtilis* (5 % increase, see above), given that it is difficult to compare directly the change in cell size in rod-shaped bacteria to that of cocci; rod-shaped bacteria cell size is measured in length (cell-diameter) and area was used for *D. radiodurans*. We were able to determine there was no increase in the population of anucleate cells as a result of the loss of *herA*, a result that is again similar to that reported when *sftA* is deleted from *B. subtilis*.

A delay in chromosome segregation in *sftA* mutant strains in *B. subtilis* was inferred by examining wild-type and *sftA* mutant cells in a similar size range, presumed to be in a similar growth state, and comparing the segregation patterns of the nucleoids in these cells (71). They observed that in cells between 3.7-5.5  $\mu\text{m}$  in diameter, 98% of wild-type cells had two fully segregated nucleoids, but only 72% of

the *sftA* mutant cells had two nucleoids. Since this subset of cells only accounted for 15% of wild-type cells, they concluded that 4.2% of *sftA* mutant cells experience a delay in chromosome segregation.

When *herA* was deleted in *D. radiodurans*, we were able to detect a similar phenotype. When we compared the size of  $\Delta herA$  and wild-type cells at equivalent growth states it was observed that the mutant cells were on average larger. When cells of the same size were compared, we found the  $\Delta herA$  cells were in an earlier growth state than wild-type cells. For example, when average cell size for wild-type was  $\sim 9 \mu\text{m}^2$ , the majority of cells were in growth state 5 (mid-late stages of chromosomes segregation and septation). In contrast, we found the majority of  $\Delta herA$  cells at this average size to be in the growth state of 4 (early-mid stages of chromosome segregation and septation).

Further evidence of a defect in chromosome segregation in the  $\Delta herA$  strain was obtained when we identified a small population of cells ( $\sim 2\%$ ) which were unique to the  $\Delta herA$  strain. These cells appeared to be unable to segregate their chromosomes as the nucleoid was apparently trapped in the newly formed septa or appeared as condensed and unsegregated. These cells apparently continued to expand their cell walls on the anticipation that the chromosomes would eventually be segregated and as a result were a more spherical shape. The finding suggests that some low probability event occurs during the cell cycle that without HerA results in the cell being unable to properly segregate its nucleoid.

It's not clear what the nature of this event is, but it could be something similar to FtsK or SftA's role in the resolution of chromosome dimers. The

frequency at which chromosome dimers occur in *D. radiodurans* is unknown, but in *E. coli* they happen when an uneven number of homologous recombination events occur between newly replicated chromosomes, which is roughly 10% of the time (71, 83). It could be that these abnormal cells are a result of a decreased ability to resolve chromosome dimers or decatenated chromosomes in the  $\Delta herA$  strain, but this result came late in the study and experiments which could have addressed this were not performed. Despite the uncertainty surrounding the biochemical process which results in these abnormal cells, the cellular and nucleoid morphologies of these cells in the  $\Delta herA$  strain are similar to the types of abnormalities reported to occur in *sftA* mutants in *B. subtilis* (72) and *ftsK* mutants in *E. coli* (84) that are attributed to a defect in chromosome segregation.

There is also additional evidence in the literature that suggests these cells (2% abnormal in  $\Delta herA$  strain) are experiencing a chromosome segregation defect. A study which looked at the effects of deleting the genes necessary for the ClpPX protease in *D. radiodurans* found that these mutant strains were unable to properly segregate their chromosomes following radiation induced DNA damage (89). The ClpPX protease is an enzyme apparently important for degradation of damaged proteins following radiation induced DNA damage in *D. radiodurans* and helps regulate the SOS response (89). Without it, cells are unable to properly segregate their chromosomes following DNA repair. When these cells were examined using fluorescence microscopy, the chromosome segregation defects observed were similar to what we observed in the unique 2% population of cells in the  $\Delta herA$  strain; the

cells became larger, formed abnormal septa and had irregular nucleoids (**Figure 3-16**).

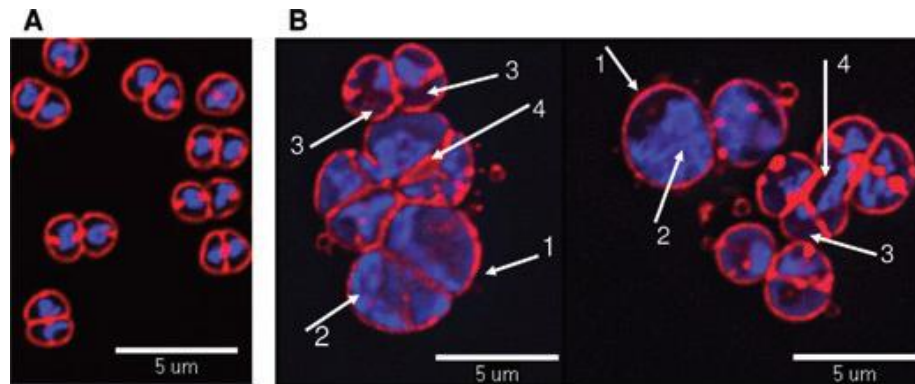


**Figure 3-16: The loss of ClpPX activity results in a chromosome segregation defect following DNA damage in *D. radiodurans*.**

Cells were stained with the nucleic acid stain DAPI and cell membrane stain FM4-64 (A) Normal wild-type cell 5 hours after exposure to 6.8 kGy  $\gamma$ -irradiation (B)  $\Delta$ clpX cells 7 hours after exposure to 6.8  $\gamma$ -irradiation. 1 refers to giant cells, 2 refers to cells with decondensed nucleoids, 3 refers to anucleate or cut nucleoids and 4 refers to cells with abnormal septation. This figure was adapted from Servant 2007 (89).

#### 3.4.2 The *nurA* and *herA* genes in *D. radiodurans*

The genes for the HerA proteins studied thus far in archaea are found in a conserved operon with genes for NurA, Mre11 and Rad50. However, this core orthologous lineage is not the only lineage as archaea contain paralogs of HerA which are found without genes for Mre11 and Rad50, but are found with the genes for a divergent paralog of NurA (42). In bacteria, there is no trace of the four protein conserved operon. The bacterial orthologs of Mre11 and Rad50 are SbcC and SbcD and are typically encoded in a conserved operon themselves. This has led to the idea that SbcC/SbcD and Mre11/Rad50 must have descended from a last universal common ancestor which acted as a nuclease/ATPase. This implies that the four protein conserved operon of NurA/HerA/Mre11/Rad50 did not evolve together, but rather came to be through the fusion of two gene pairs after each had evolved



separately (42). The association of NurA and HerA with Mre11 and Rad50 has been what sparked the speculation that these proteins were involved in the repair of double strand breaks. Therefore, it seems that the conserved two gene operon consisting of only *nurA/herA* contains paralogs of the genes found in the four gene operon consisting of *nurA/herA/mre11/rad50*.

*D. radiodurans* contains only the *nurA/herA* operon and thus it's not obvious that their protein counterparts will have a physical and functional association with SbcC and SbcD as has been shown and was predicted for the NurA and HerA in archaea found within the same operon as Mre11 and Rad50. Rather it appears *D. radiodurans* obtained its homologs of Mre11 and Rad50 prior to the merger of these with NurA and HerA or from species which evolved these two gene pairs differently than the species which fused these gene pairs together. This may help explain the fundamental differences observed when studying the role of *herA* and *nurA* in *D. radiodurans* and their proposed role in archaea.

The presence of homologs of the archaeal *herA* and bacterial *ftsK* in the *D. radiodurans* genome suggests that cell division in *D. radiodurans* may utilize processes unique to both the bacterial and archaeal cell cycle making it an interesting model organism for further study of prokaryotic cell division. Very little is known regarding the complexities surrounding how *D. radiodurans* alternates its division planes perpendicularly with each cell cycle and it seems likely that the mechanism of efficient DNA segregation during this process is equally complex. It could be that *D. radiodurans* utilizes both HerA and FtsK as has been observed for SftA and SpoIIIE in *B. subtilis*, where these two FtsK-like proteins work synergistically to resolve

chromosome dimers and segregate newly replicated chromosomes during division. HerA may function similarly to SftA in *B. subtilis*, assisting chromosome segregation in the early stages of cell division, while FtsK may perform similar functions as those observed for FtsK in other organisms, assisting in chromosome dimer resolution, chromosome decatenation, and segregation of the terminus region. It is unclear if NurA could assist HerA in decatenation of chromosome dimers much like has been observed for FtsK and TopoIV in *E. coli* because of the distinct differences between hydrolases and topoisomerases.

#### 3.4.3 Growth and Morphology Analysis: Future Work

While this study has presented evidence that suggests a role for HerA in chromosome segregation, there are still other experiments which need to be done before its precise role is understood. A more extensive biochemical characterization of the purified HerA and NurA enzyme would be quite beneficial, mostly because all of the knowledge about them is from *in vitro* work in archaea. If it were found that the *D. radiodurans* putative NurA and HerA could demonstrate the same *in vitro* activities as their archaeal counterparts (43, 44, 46, 48) it would provide evidence to suggest their proposed role in archaea in just DNA repair is a red herring for their true role in the cell; that the *in vitro* interpretation of a role in DNA repair is not appropriate for their *in vivo* role in the cell.

Such experiments could also reveal if the *D. radiodurans* putative NurA and HerA physically interact. If it were found they did not, then this could help explain why we saw no phenotype in DNA repair in growth for the  $\Delta nurA$  strain, but did with the  $\Delta herA$  strain. It would imply that over time, the two had lost their physical

association observed in archaea and have begun to evolve their role together in *D. radiodurans* to one which is independent of each other. The apparent lack of NurA involvement in *D. radiodurans* DNA repair or growth could also be a consequence a structural evolutionary change to the putative NurA that rendered its active site inactive. Instead, NurA could be an accessory protein to HerA that has evolved to help HerA recognize certain DNA targets or help facilitate its DNA translocase activity like has been observed when HerA is complexed with a nuclease deficient NurA in *S. solfataricus* (44) and similar to how the RecC domain functions in the RecBCD complex of *E. coli* (17).

Additionally, studies which could probe the localization of HerA inside a *D. radiodurans* cell could help explain the data presented here or may result in a reinterpretation depending on what is observed. If a shuttle plasmid containing a GFP-tag (Green fluorescent protein) fused to the *D. radiodurans herA* gene could be made then it could be possible to determine the circumstances which facilitate its recruitment to a particular region of the cell using high resolution fluorescence microscopy, similar to how has been done for SftA in *B. subtilis* (72). If this GFP-fusion protein also retained wild-type activity, it would be interesting to see if such a shuttle plasmid could rescue the phenotypes observed in the  $\Delta herA$  strain.

Most helpful though would be generating an *ftsK* deletion strain in *D. radiodurans* and comparing its phenotypes to the  $\Delta herA$  strain or even attempting to generate a double knock out strain of *ftsK* and *herA*. Such studies would help elucidate if the two are in fact working together in chromosome segregation in *D. radiodurans*. Similar microscopy studies as those suggested above that utilize a GFP-

fusion tag for the *D. radiodurans* FtsK could help provide information about the timing and localization of FtsK relative to HerA. Doing such studies under normal conditions or even in cells which have been treated with DNA damaging agents, could provide details about their recruitment in the cell under various conditions helping further to understand the chromosome segregation process in *D. radiodurans*.

#### 3.4.4 Concluding Remarks Regarding NurA and HerA in *D. radiodurans*

The goal of this study was to test the hypothesis that the putative HerA and NurA from *D. radiodurans* had a role in DNA processing, like chromosome segregation. Despite a clear argument for a case of HerA participating in chromosome segregation in *D. radiodurans*, the results obtained here do not provide any evidence the putative NurA has such a role. It could be its role is as an accessory protein, with no intrinsic activity, that by physically interacting with HerA helps facilitate its role in chromosome segregation. However, if this were the case and the role of HerA inside the cell was dependent on forming a complex with NurA we would have expected to see similar growth phenotypes in the  $\Delta nurA$  strain as we saw in the  $\Delta herA$  strain.

The NurA superfamily of nucleases are a highly divergent group displaying low levels of sequence similarity between paralogs and even orthologs (42). The authors who detected this superfamily speculated that such divergence within a conserved class of nucleases was similar to restriction endonucleases. They went on to say that it could be that this divergence reflects the ability of the NurA nucleases to recognize specific DNA targets, much like restriction enzymes. So it could be possible that NurA has evolved to be utilized as part of a restriction-modification

system with HerA acting as an accessory helicase or ATPase. Furthermore, it has already been speculated that HerA and NurA could act as a type of protection system from foreign DNA based on the finding that the NurA-HerA complex can digest linear dsDNA (44). No such experiments were designed to test for such a role, but experiments which looked at the transformation efficiency of various types of foreign DNA in the  $\Delta nurA$  strain relative to wild-type could begin to address this possibility.

A role for NurA in *D. radiodurans* seems likely because as said before the *nurA* gene is expressed (56, 57). Even though this study was unable to precisely identify the role for NurA in *D. radiodurans*, it was able to accomplish a better understanding of what roles it likely does not have which will help outline how future studies can better address its true role in *D. radiodurans*.

In contrast to the results obtained with the  $\Delta nurA$  strain, the loss of HerA in *D. radiodurans* did result in a detectable growth phenotype. When all that has been discussed above is taken together, it appears the putative HerA could have a role in chromosome segregation in *D. radiodurans*. If this were the case, this role cannot be essential as total loss of HerA is acceptable in *D. radiodurans*. Instead, it would appear the role exists to increase the efficiency and fidelity of the chromosome segregation process.

The primary pathway for chromosome segregation in *E. coli* is not precisely known. The leading theory is that DNA replication from the cell origin and condensation of this newly replicated DNA, by proteins such as SMC and MukB complexes, provides the necessary forces to facilitate the bulk of chromosome segregation (95-97). It is also believed that DNA replication is regulated by the

concentration of DnaA, which is in turn regulated by the extent of cell wall synthesis and transcription (96, 97). The theory highlights the interconnectedness of the different parts of the bacterial cell cycle. However, when this primary pathway fails or encounters obstacles like chromosome dimers, the process is recovered or completed by proteins like FtsK (98).

It would follow that in wild-type *D. radiodurans* cells the primary mechanism of chromosome segregation works perfectly ~90% (excluding the percentage of cells with asymmetric septa in **Figure 3-15**) of the time and the remaining ~10% of the time a secondary mechanism, possibly consisting of FtsK and HerA working synergistically, is able to restore faithful completion of the segregation process. It is also possible that HerA and FtsK are not an exclusive secondary mechanism, but are an active part of the primary mechanism that makes it more efficient. Assuming they are essentially a backup pathway, in the absence of HerA, this secondary mechanism becomes less efficient and causes certain cells to experience a delay in chromosome segregation, which stalls growth (decreasing growth rate) and causes cells to become larger without impeding DNA replication. Approximately 2% of the time, cells are unable to complete the segregation process during exponential growth and develop severe septa and nucleoid irregularities.

Therefore, it would appear that the acquisition of the archaeal *herA* through horizontal gene transfer from archaea into *D. radiodurans* provided the bacterium with a more efficient chromosome segregation mechanism that also increased the rate at which it could complete its cell cycle (~15 min per cycle). Although this may not seem like much, from an evolutionary standpoint, the ability to increase the efficiency

of any DNA metabolizing process and decrease the time needed to duplicate is beneficial for survival in environmental conditions where such things could be the difference between life and death.

## Appendices

### Appendix 1: Partial In vivo Characterization of the $\Delta herA^*$ Strains

#### Appendix 1.1: Generation of $\Delta herA^*$ mutant strains with *nurA* mutation

The 1050 bp *nurA* gene in *D. radiodurans* is predicted to code for the 339 amino acid NurA nuclease. The upstream fragment for the  $\Delta herA^*$ KO fragment is directly upstream from the *herA* start codon. This region spans approximately 4/5 of the entire *nurA* gene. The original generation of the  $\Delta herA^*$  KO fragment resulted in the introduction of 4 mutations into the *nurA* gene and deletion of the *nurA* stop codon; the mutations were in the UPstream fragment of the  $\Delta herA$  KO fragment (**Figure A-1**). This occurred partly due to an error in design and partly to the method used to generate it. A careless design error in the RHer\_2 primer resulted in the deletion of the *nurA* stop codon. The RHer\_2 primer *nurA* annealing region was 4 nucleotides shorter than it needed to be and thus resulted in the mutation of the last four bases in the *nurA* gene into the bases for the spacer region of the primer which separated the operon binding site from the added restriction sites needed to make the  $\Delta herA^*$ KO fragment.

Additionally, 4 mutations were introduced into the upstream fragment of the  $\Delta herA^*$ KO fragment during its generation, possibly a result of UV damage incurred during excision of the bands from agarose gels. These mutations resulted in 4 amino acid changes to the predicted NurA nuclease: I213T, G237D, A258G, P316S. The removal of the stop codon also resulted in the addition of 18 amino acids to the C-



terminal tail of the predicted NurA Nuclease: STOP350A, D, P, V, R, E, G, L, R, A, M, E, T, E, G, P, G, H, STOP.



**Figure A-1: Alignment of pCRBlunt\_ΔherA\* and nurA from D. radiodurans .**  
 The ΔherA \*KO fragment that was inserted into pCRBlunt was sequenced. The upstream region contained 4 point mutations and deletion of the TGA stop codon. The upstream sequence was aligned with the Genbank (DR\_0837) annotated nurA sequence for D. radiodurans. All changes to the nurA sequence are shown in turquoise, except for the stop codon deletion which is shown in red.

Thus when the herA gene was originally removed from wild-type D. radiodurans, the nurA gene was simultaneously mutated to have 4 different amino acids plus an additional 18 amino acid C-terminal tail.

Appendix 1.2: Summary of all  $\Delta herA^*$  mutant strains

The wild-type strain was transformed 4 different times with this mutated  $\Delta herA^*$ KO, twice with gDNA isolated from  $\Delta herA^*$  mutant strains and 4 times using the  $\Delta herA^*$  KO fragment amplified and isolated from  $\Delta herA^*$  mutants transformed with original  $\Delta herA^*$ KO fragment (**Table A1**). There were 30  $\Delta herA^*$  mutant strains isolated (**Figure A-2**) from these transformations and of these were characterized, several were partially characterized to various degrees. The  $\Delta herA^*$  KO fragments from these 4  $\Delta herA^*$  mutants were sequenced and were found to be the same. These mutant strains also gave the same genotype PCR results (**Figure A-3**)

**Table A1: Summary of  $\Delta herA$ \* Phenotypes**

Transformation	DNA Used	Strain Isolated	Growth Description (Qualitative)	G (Gen./min)	Cell Morphology (Qualitative)	UV Sensitivity	Phleomycin Sensitivity
1 (1 colony)	$\Delta herA$ KO	$\Delta herA1\_1$	Slow	171±4 n=3	Large-Clumpy	-	1000
		$\Delta herA1\_5$	Slow	-	-	-	-
		$\Delta herA1\_10$	Slow	185±9 n=5	Large	10	4300
2 (2 colonies)	$\Delta herA$ KO	$\Delta herA2$	Moderate	144±9 n=2	Normal-Moderate	100	1000
		$\Delta herA3$	Slow	200 ±0 n=1	-	-	-
3 (1 colony)	$\Delta herA1\_1$ gDNA	$\Delta herA1A$	Slow	191±8 n=3	Very Large	5	4700
4 (19 colonies)	$\Delta herA$ KO	$\Delta herA4$	Fast	110±20 n=2	Normal	-	1000
		$\Delta herA14$	Fast	130±30 n=2	-	-	-
		$\Delta herA20$	Fast-Moderate	-	-	-	-
5 (2 colonies)	$\Delta herA1\_10$ gDNA	$\Delta herA1B$	Fast-Moderate	-	-	-	-
		$\Delta herA1C$	Fast-Moderate	-	-	-	-
6 (4 colonies)	$\Delta herA$ KO	$\Delta herA\_23$	Slow	-	Very Large	180	1800
		$\Delta herA\_24$	Moderate	-	Normal	-	-
		$\Delta herA\_25$	Moderate	-	Large-Sheets	18000	5
		$\Delta herA\_26$	Slow	-	Large	-	-
7 (4 colonies)	$\Delta herA\_KO$ from $\Delta herA1A$	$\Delta herA1A\_1$	Fast	-	Normal-Moderate	5	0.5
		$\Delta herA1A\_2$	Fast	-	Normal-Moderate	-	-
		$\Delta herA1A\_3$	Slow	-	Large-Sheets-Clumps	1300	2200
		$\Delta herA1A\_4$	Moderate	-	-	-	-
8 (3 colonies)	$\Delta herA\_KO$ from $\Delta herA1\_10$	$\Delta herA1\_10\_1$	Fast	-	-	-	-
		$\Delta herA1\_10\_2$	Moderate	-	Normal-Moderate	-	-
		$\Delta herA1\_10\_3$	Moderate-Fast	-	Normal	-	-
9 (2 colonies)	$\Delta herA\_KO$ from $\Delta herA2$	$\Delta herA2\_1$	Slow	-	Moderate-Large	-	-
		$\Delta herA2\_2$	Fast	-	Normal-Moderate	-	-
10 (7 colonies)	$\Delta herA\_KO$ from $\Delta herA4$	$\Delta herA4\_1$	Slow	-	Moderate	-	-
		$\Delta herA4\_2$	Fast	-	Normal-Moderate	-	-
		$\Delta herA4\_3$	VERY Slow	-	Small-Normal	5	3900
		$\Delta herA4\_4$	Moderate-Slow	-	Moderate-Large	-	-
		$\Delta herA4\_5$	Slow	-	Moderate-Large	-	-
		$\Delta herA4\_6$	Fast	-	Normal-Moderate	5	0.5
		$\Delta herA4\_7$	Moderate-Slow	-	Large-Sheets	240	1800

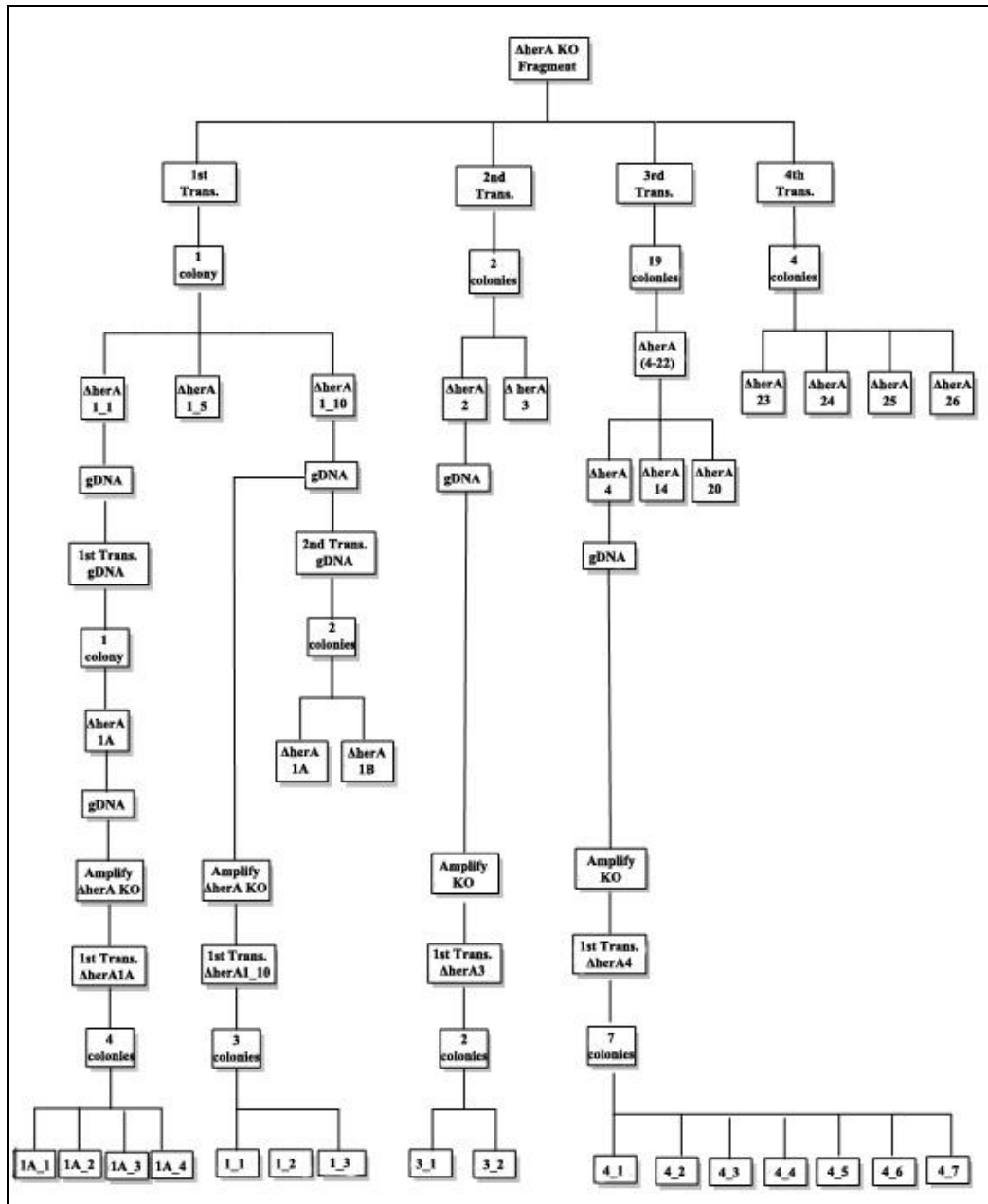


**Figure A-2: A family tree of the  $\Delta herA^*$  strains made from  $\Delta herA^*KO$ .**

All strains are derived from the original  $\Delta herA^*KO$  fragment which contained mutations in the *nurA* gene. Other strains were derived from gDNA or the  $\Delta herA^*KO$  amplified from gDNA of  $\Delta herA^*$  strains. Boxes with  $\Delta herA$  in them indicate a strain which has been isolated. Each colony formed, following transformation, was given a number and all ( $\Delta herA^* \#$ ) are strains derived from the original  $\Delta herA^*KO$  fragment. Strains 1\_1, 1\_5 and 1\_10 are the same strain, but different colonies isolated and kept from the same pass. In all other cases, a number followed by a number ( $\Delta herA^* \# \#$ ) indicates which strains  $\Delta herA^*KO$  fragment was amplified from gDNA and used to transform wild-type cells to give the new strain. A letter following a number indicates the new strain was transformed with gDNA. The number preceding the letter corresponds to the particular  $\Delta herA$  strain gDNA used. The number of colonies following each transformation is given.

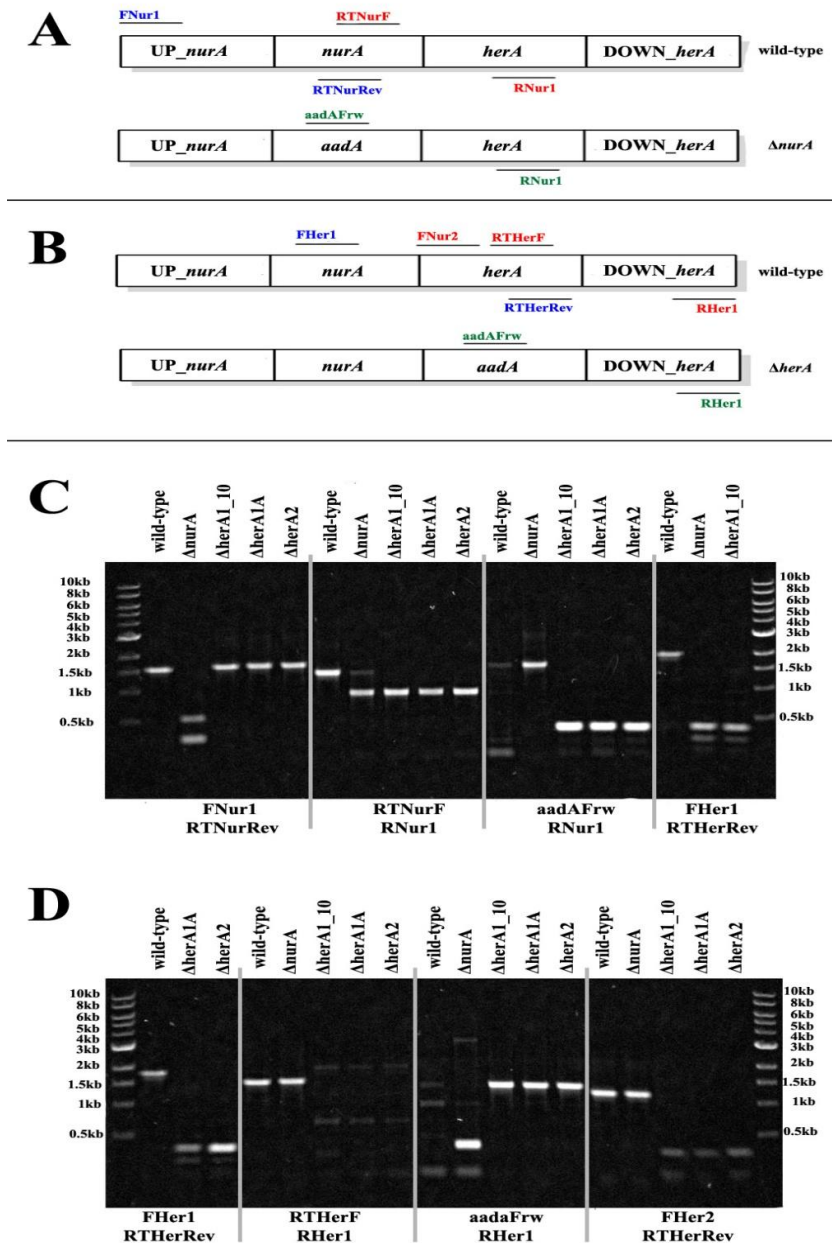


**Figure A-3: PCR Genotype reactions for select  $\Delta herA^*$  strains.**

(A) and (B). Schematic of primer binding sites for  $\Delta nurA$  and  $\Delta herA^*$  genotype PCR reaction. The primer pairs are shown in multiple colors and primers with the same color were used together in the same PCR reaction. (C) Agarose gel image of the PCR reactions performed with WT gDNA,  $\Delta nurA$  gDNA and  $\Delta herA^*$  (1<sub>10</sub>, 1A, 2) gDNA designed originally to test for *nurA* deletion. (D) Agarose gel image of the PCR reactions performed with WT gDNA,  $\Delta nurA$  gDNA and  $\Delta herA^*$  (1<sub>10</sub>, 1A, 2) gDNA designed originally to test for *herA* deletion. The PCR reactions were identical except for primers used. Each lane is identified at the top of the gel and the lanes which show the products from reactions using the same primers are identified at the bottom of the gel.

### Appendix 1.3: Partial growth analysis of selected $\Delta herA^*$ strains

The original transformation with the  $\Delta herA^*$ KO fragment resulted in a single colony on TGY-streptomycin plates. This colony grew slower than the wild-type strain and came up after 72 hours rather than the normal 48. This colony was grown and took almost 48 hours to reach saturation, which was almost twice as long as it took wild-type cultures to reach saturation. The 2<sup>nd</sup> passage of this strain only resulted in 10 colonies and of these 10, three were cultured and isolated ( $\Delta herA1\_1$ , 5, 10). Genetically these three colonies should be identical and thus it was expected that each of the three would display identical phenotypes. All three displayed similar growth properties in that they repeatedly grew slower than wild-type.

The transformation was repeated a second time and this resulted in two colonies;  $\Delta herA2$  and  $\Delta herA3$  strains. The  $\Delta herA2$  strain seemed to always grow a little bit faster than the original  $\Delta herA1$  strains, but still slower than the wild-type strain. This could be qualitatively confirmed by comparing the saturation levels (OD<sub>600</sub>) of liquid cultures started from single colonies following overnight incubation at 30°C (250 rpm shaking). The wild-type strains were always at OD<sub>600</sub> values higher than the  $\Delta herA1$  and  $\Delta herA2$  strains, while the  $\Delta herA2$  was always in between the wild-type and  $\Delta herA1$  strains. This result suggested that the transformation of *D. radiodurans* wild-type with the same  $\Delta herA$  KO fragment produced two strains with different growth phenotypes.

It could be that one of the two strains was a heterozygous mutant and the other a homozygous mutant, but genotype PCR analysis suggested they were both homozygous *herA* deletion strains (**Figure A-3**). Another explanation was that

something had occurred during the transformation causing the two strains to be genetically distinct in a manner distinguishable from being homo/heterozygous. To confirm this, the entire gDNA sequences from the two strains would need to be sequenced and compared, but this was not done.

The transformation was repeated again with the original  $\Delta herA$ \*KO fragment. This transformation resulted in many colonies and three were isolated ( $\Delta herA_{4, 14, 20}$ ). These colonies formed about as quickly on TGY-streptomycin plates as wild-type colonies on TGY plates. This growth phenotype was inconsistent with the other observed phenotypes from the first 3 transformation attempts. These new strains displayed the growth characteristics of the correctly made  $\Delta herA$  strain from Chapter 3. Representative growth curves are shown in **Figure A-4**.

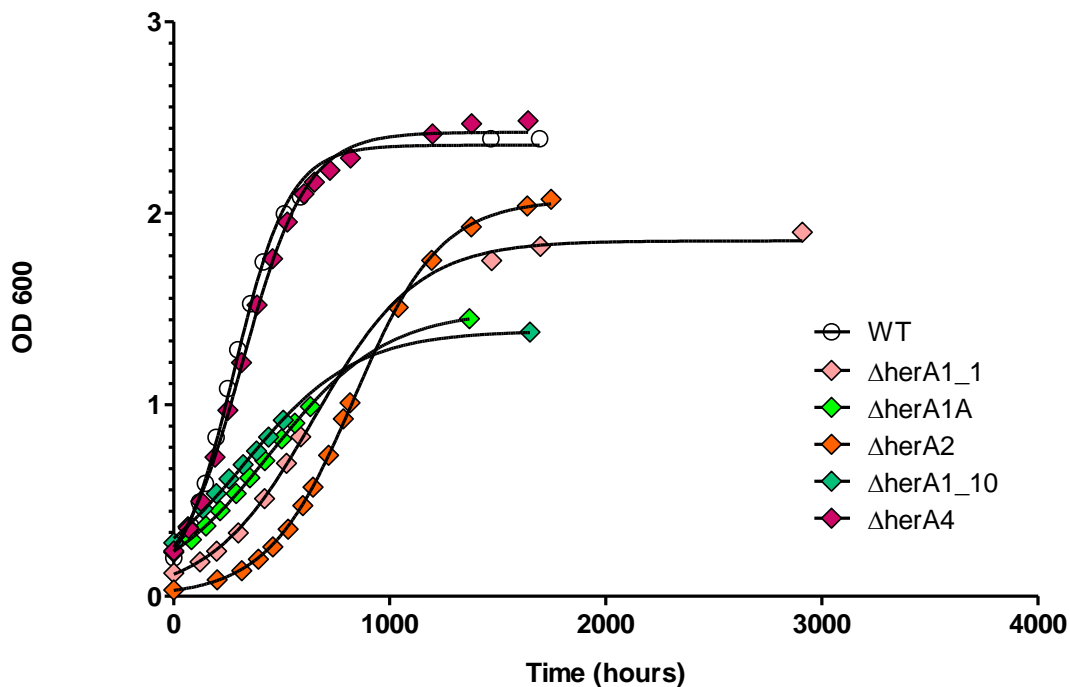


**Figure A-4: Growth Curves for wild-type and  $\Delta herA^*$  strains.**

Stationary-phase cultures were diluted into 2x TGY to an initial  $OD_{600} < 0.3$  and shaken at 250 rpm and 30 °C. Aliquots were removed and the optical density at 600 nm was recorded. Strain identities are displayed in the legend on graph. The solid line is the fit to equation 1 (see Methods, Chapter 1), with  $k = 0.008 \text{ min}^{-1}$ ,  $P = 2.36$ , and  $Y_o = 0.2339$  (wild-type),  $k = 0.004 \text{ min}^{-1}$ ,  $P = 1.86$ , and  $Y_o = 0.1149$  ( $\Delta herA1_1$ ),  $k = 0.004 \text{ min}^{-1}$ ,  $P = 1.494$ , and  $Y_o = 0.2347$  ( $\Delta herA1A$ ),  $k = 0.005 \text{ min}^{-1}$ ,  $P = 2.07$ , and  $Y_o = 0.0311$  ( $\Delta herA2$ ),  $k = 0.004 \text{ min}^{-1}$ ,  $P = 1.39$ , and  $Y_o = 0.2842$  ( $\Delta herA1_10$ ) and  $k = 0.007 \text{ min}^{-1}$ ,  $P = 2.42$ , and  $Y_o = 0.2569$  ( $\Delta herA4$ )

#### Appendix 1.4: Partial morphology assessment of selected $\Delta herA^*$ strains

The morphology of some  $\Delta herA^*$  strains was assessed using phase-contrast microscopy and flow cytometry as described before. Not all assessments were quantitative and rather some were more qualitative because certain strains had very unusual morphologies (**Figure A-5**). It appears that the faster growing cells display cellular morphologies similar to those of WT, although slightly larger and in one particular case, much larger. All of the slow growth mutants appear larger on average



than the WT cells and many times very unusual morphologies are observed such as massive “sheets” of cells and large aggregates, as if the cells are forming colonies in liquid culture. **Figure A-5** shows representative images of the wild-type and unusual  $\Delta herA^*$  morphologies. Flow cytometry confirmed the variable shift in size distributions (**Figures A-6 and A-7**).

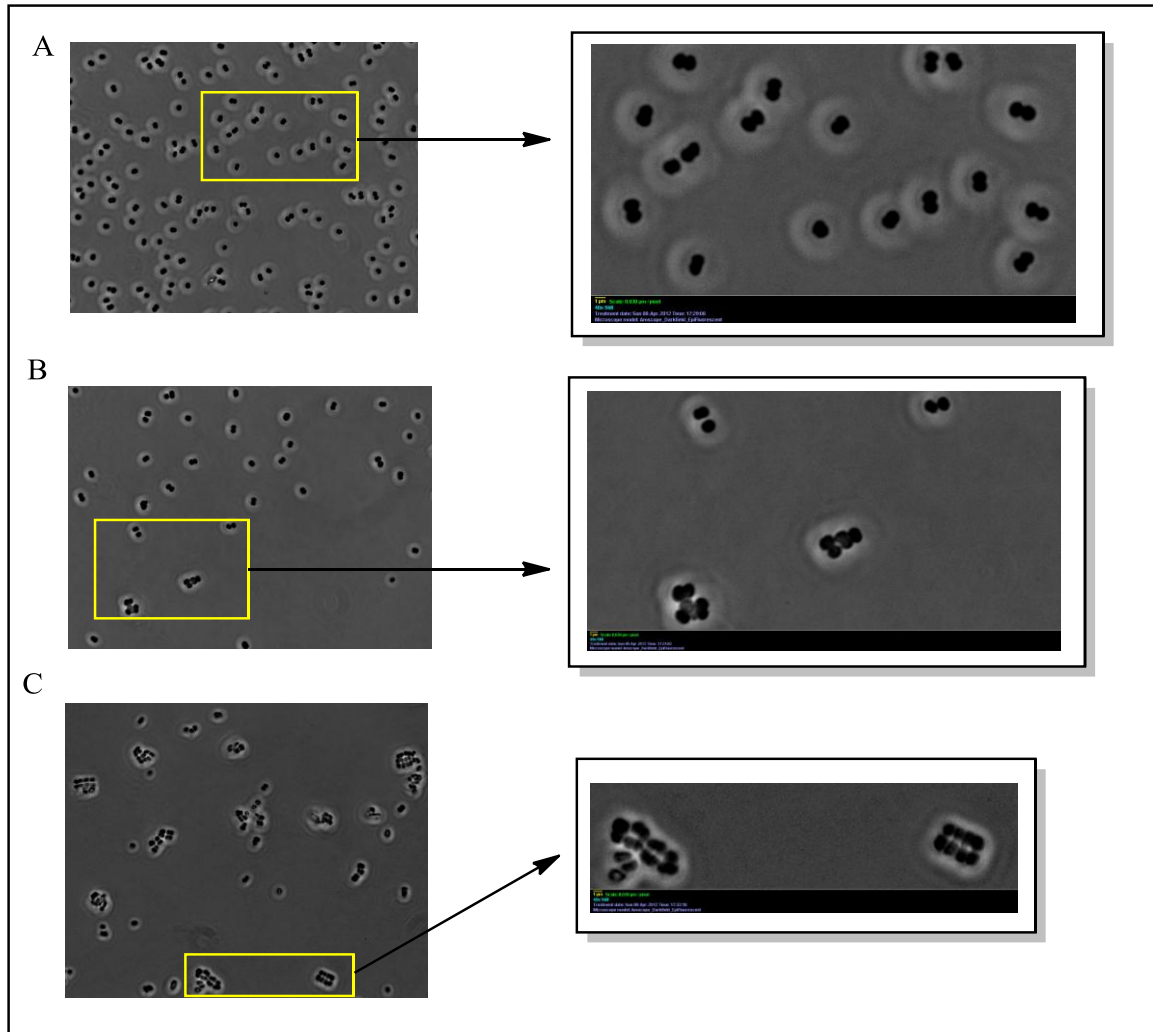


**Figure A-5:** *D. radiodurans* cells imaged at 400x magnification using phase contrast. Shown are cells in the early stationary phase. The yellow boxed area is expanded to the right for easier visualization of cells. (A) Wild-type cells existing mostly as diads and tetrads (B)  $\Delta herA1A$  cells existing mostly as diads, tetrads and larger aggregates. (C)  $\Delta herA25$  cells existing mostly as diads, tetrads and sheets characteristic of cells growing on solid TGY agar plates.

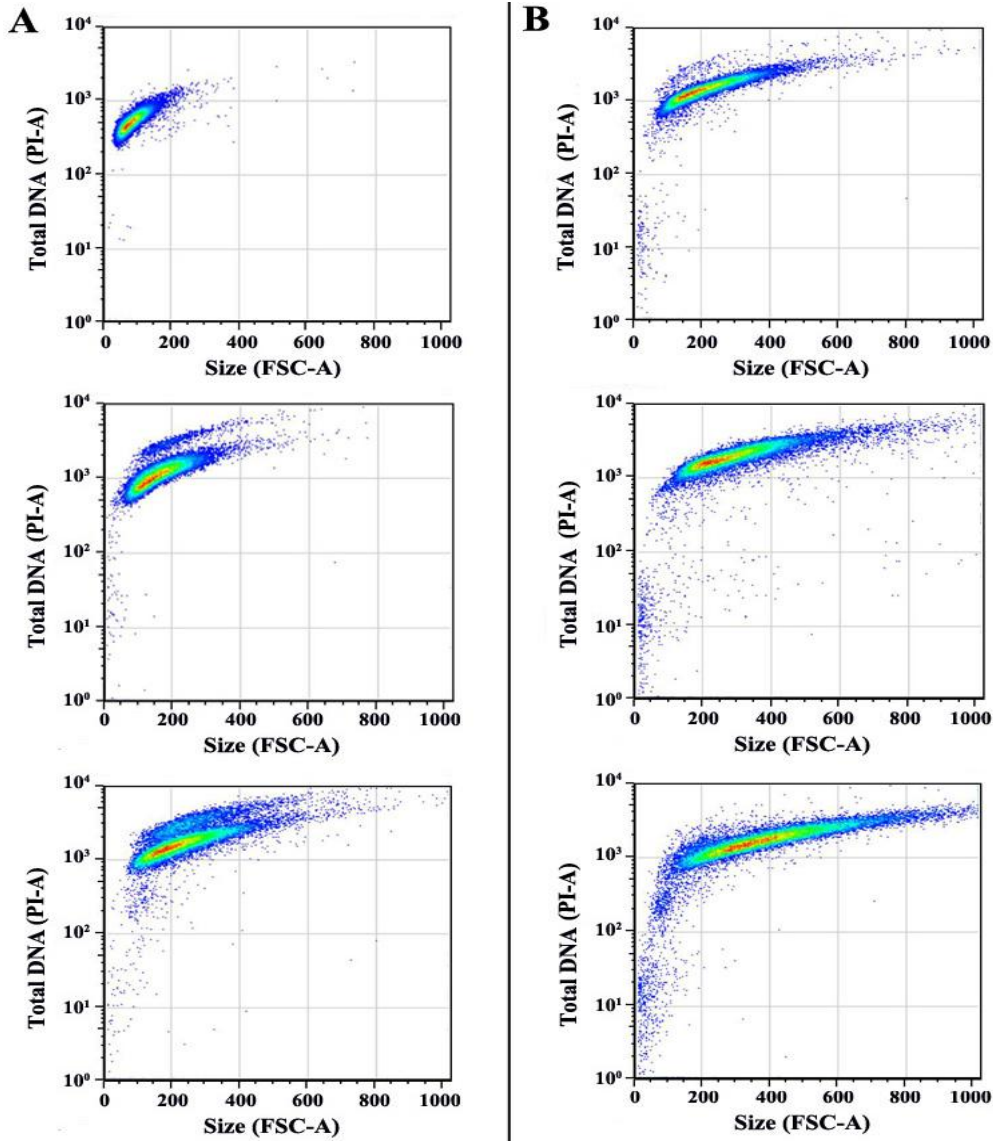


**Figure A-6: 2-D scatter plots of FSC-A and PI-A signals from flow cytometry of wild-type and  $\Delta herA^*$  strains.**

Representative 2-D Scatter plots of PI fluorescence signal (PI-A; DNA content) vs. forward-scatter signal (FSC-A; size) from wild-type and  $\Delta herA^*$  cells (>30,000) in exponential and stationary (>48hr) phase of growth. **(A)** Wild-type (top),  $\Delta herA1$  cells (middle) and  $\Delta herA1A$  (bottom) in exponential phase. **(B)** Wild-type (top),  $\Delta herA1$  cells (middle) and  $\Delta herA1A$  (bottom) in stationary phase. Cells are larger and contain more DNA from left-to-right, and bottom-to-top, respectively, on the graphs. Scatter plots are shown as density plots where lower concentrations of cells are shown in blue and higher in red

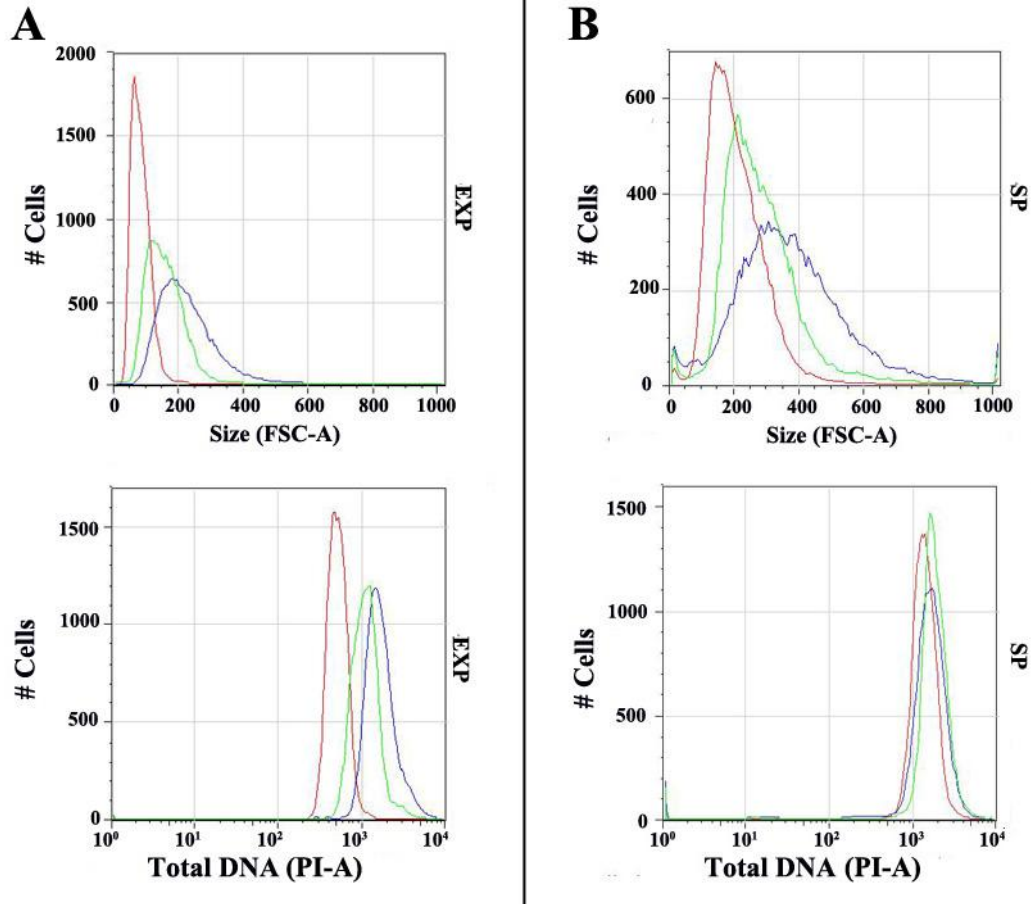


**Figure A-7: Histograms of FSC-A and PI-A signals from flow cytometry of wild-type and  $\Delta herA^*$  strains.**

(A) Representative histograms showing the distribution of FSC-A signals from wild-type and  $\Delta herA^*$  cells (>30,000) in exponential phase of growth. Wild-type: red trace.  $\Delta herA1$ : green trace,  $\Delta herA1A$ : blue trace. (B) Representative histograms showing the distribution of FITC-A signals from wild-type and  $\Delta herA^*$  cells (>30,000) in stationary (>48hr) phase of growth. Wild-type: red trace.  $\Delta herA1$ : green trace,  $\Delta herA1A$ : blue trace

Appendix 1.5: Partial DNA damage sensitivity analysis for selected  $\Delta herA^*$  strains

The most significant deviation of the  $\Delta herA^*$  strains with the *nurA* mutation from the correctly made  $\Delta herA$  strain regarding phenotypes was their difference in sensitivity to the DNA damaging agents phleomycin and UV-C radiation. The

*ΔherA2* and *ΔherA1\_10* strains were assayed as described in previous chapters for sensitivity to UV-C radiation and representative survival curves are shown in **Figure A-8**. Both strains consistently displayed an actual increase in the resistance to the damage induced by UV-C. It was too tedious to test all of the strains, so instead several of the strains were tested simultaneously at one dose point which was shown to kill 99.999% of wild-type cells (Results reported in **Table A1**). All of the strains tested displayed an increase in their resistance relative to wild-type. No obvious correlation between the growth rate, morphology distribution and/or this DNA damage sensitivity phenotype could be established amongst the various *ΔherA\** strains tested.

A similar phenotype for the *ΔherA\** strains was observed when cultures were spotted onto 1xTGY plates containing 5 μg/mL phleomycin in that many more of the *ΔherA\** cells were able to grow on these plates than wild-type for the most part (Results reported in **Table A1**). Again though, it is not clear why this resistance to phleomycin exists within these strains, especially when the *ΔherA* strain lacking the *nurA* mutations was more sensitive than wild-type to this treatment. This comparison suggests that the nature of this increased resistance to UV-C and phleomycin is likely a consequence of the *nurA* mutation. It is unclear why this mutation is able to reverse the phenotype of the *herA* deletion strain.

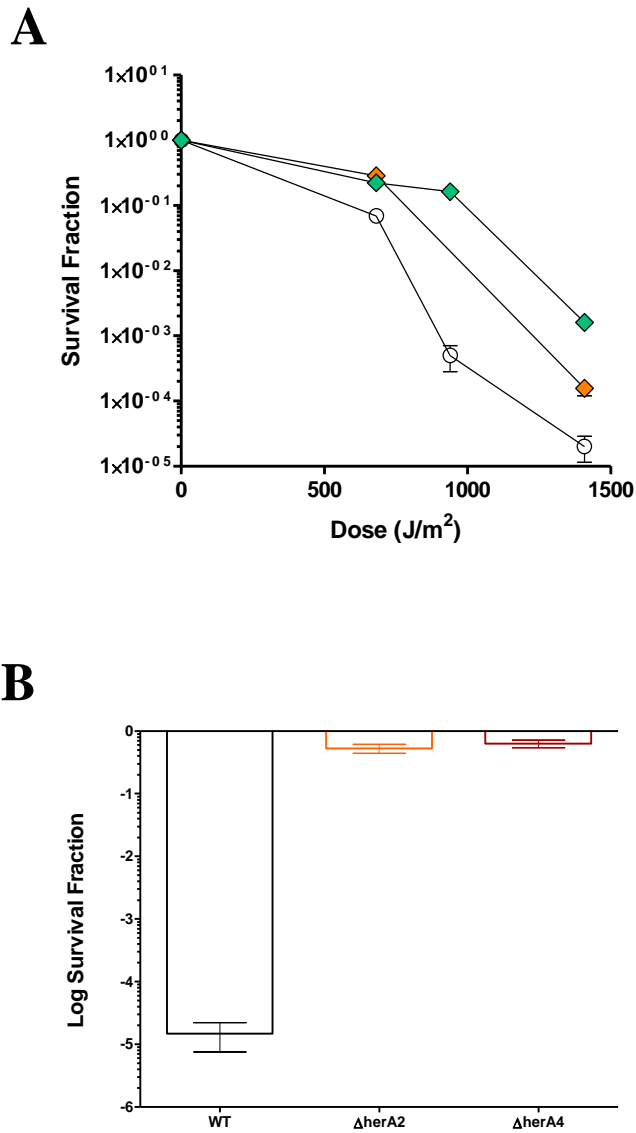


**Figure A-8: Effect of DNA damaging agents on viability of wild-type and  $\Delta herA^*$  cells.** (A) Exponential phase cultures were exposed to the indicated dose of UV light from a germicidal lamp and then spread on 1x TGY plates without antibiotic. Open circles, wild-type. Turquoise diamonds,  $\Delta herA1A$ . Orange diamonds,  $\Delta herA1$ . (B) Exponential phase cultures were spread in triplicate on TGY plates containing 0 and 5 $\mu$ g/mL phleomycin. The plates were incubated for 48 hours in the dark before colonies were counted.

Appendix 1.6: Concluding remarks on  $\Delta herA^*$  strains

There was no obvious explanation for the spectrum of phenotypes observed amongst the  $\Delta herA^*$  strains. If the strains are genetically identical regarding the *nurAherA* operon, but genetically distinct in other regions of the genome, then these unidentified genetic changes could be responsible for the spectrum of phenotypes. However, the only way to confirm this would be to determine the sequence of each mutant strains gDNA. This process is costly and was not performed.

The  $\Delta herA^*$ KO fragment from the  $\Delta herA1_{10}$ ,  $\Delta herA1A$ ,  $\Delta herA2$  and  $\Delta herA4$  strains were amplified via PCR and ligated into pCRBlunt to sequence them to ensure all 4 overlap fragments were the same. If they were not, then maybe this could explain the reason for the various phenotypes. All four overlap fragments contained the same DNA sequence meaning that if the strains were genetically different it had to be changes outside the *nurAherA* operon.

Transformation of the wild-type strain with these 4 identical KO fragments resulted in the same generation of strains with variations in their growth phenotypes. The result confirms that it is not variation in the overlap fragment that is causing the variation in the phenotypes, but it's that the process of transforming this fragment into wild-type cells that results in something else that creates the variation.

It could be that deletion of  $\Delta herA^*$  results in a mutator phenotype such that upon replacement of *herA* with *aadA*, the genome integrity becomes compromised resulting in accumulation of random mutations. Thus the variation in phenotypes among strains could be the fact each contains a unique set of random mutations along with identical *nurAherA* operons. Inconsistent with this hypothesis is the fact that the

phenotypes for each strain were quite stable and displayed the same characteristics over many passes (>10). They had repeatable growth rates, predictable morphology distributions and consistent sensitivities to DNA damage.

Mutator phenotypes can be assessed by determining the number of cells which can grow on TGY-rifampicin plates. Rifampicin is a translation inhibitor which binds to the  $\beta$ -subunit of RNA polymerase and it inhibits it from transcribing DNA. Cells which can acquire a mutation in the  $\beta$ -subunit gene for RNA polymerase which inhibits rifampicin binding can grow on TGY-rifampicin plates. Thus, if the  $\Delta herA^*$  genotype results in a faster accumulation of spontaneous mutations, we might expect more of these cells to be able to grow on TGY-rifampicin plates. When such experiments were performed no difference was observed between the number of cells which could obtain mutations in the  $\beta$ -subunit of RNA polymerase allowing for rifampicin resistance suggesting the rates of mutation are the same and the  $\Delta herA^*$  genotype is not a mutator phenotype.

The observation that knocking out the *herA* gene induces different phenotypes associated with growth, morphology and DNA repair is interesting. Again, assuming that these observations are due to the desired recombination events and not some other event, it suggests that wild-type cells, while having identical genomes, do not “use” this genome identically. The idea of such a circumstance is referred to as penetrance in genetics (99, 100). The concept has to do with how a particular cell orchestrates its transcriptome. Even though two cells may have the same genes, one cell may use a gene that is virtually silent in the other cell. If you remove the gene

from both cells, they may react differently as this removal will have different effects on the transcriptome of the two cells.

This perception could explain the different observed phenotypes and morphologies. Some wild-type cells may have a role in their cell cycle that is dependent on the function of HerA, while others may get along fine without using it. One thought is that since *D. radiodurans* has the *ftsK* gene, some cells may depend on the presence of both FtsK and HerA, just FtsK or just HerA since each has similar folds and predicted functions (42). In order to assess this possibility, a transcriptomic or proteomic analysis of the various strains would have to be done. If they showed clear differences, then maybe there could be something to this idea. However, a simpler way to address this hypothesis would be to analyze the transcriptome and/or proteome of single wild-type *D. radiodurans* cells through something like single-cell microarray (101). If you could detect cells which utilized the *herA* and *ftsK* genes differently, then it may make sense that depending on which type of wild-type cells was transformed with the  $\Delta herA^*$  KO fragment, you would get a particular phenotype.

Inconsistent with this idea are the results using the proper  $\Delta herAKO$  fragment, which in each transformation produced strains with the same properties. Additional studies are needed, such as ones that address the possibilities proposed above, if the true nature of this most bizarre result can be understood.



Appendix 2: References to Work on RecJ Nuclease in *D. radiodurans*

Prior to the start of the work presented in this dissertation I worked in collaboration with Dr. Zheng Cao in his attempt to determine the role of the RecJ nuclease in *D. radiodurans*. The result of our collaboration resulted in a publication in the journal of DNA Repair and the reference is given at the end of this appendix entry.

In this work I was primarily responsible for a two things: 1) I performed the quantitative real time-PCR analysis of the *recJ* mutant strains 2) I developed and implemented a semi-quantitative method for the estimation of genome copy number. The semi-quantitative method essentially applied the same principles used in quantitative real-time PCR except that rather than having the process automated, it was performed by hand.

In addition to this work, I assisted Dr. Cao in the *in vivo* biological assessment of the  $\Delta recJ$  mutants. This required me to work side by side and at times by myself to generate growth curves and survival curves following exposure to DNA damaging agents. I also assisted Dr. Cao and Dr. Julin in the analysis of the data obtained from Dr. Cao's RecJ study and contributed to the actual writing of our publication.

**Cao Z, Mueller CW, Julin DA.** 2009. Analysis of the *recJ* gene and protein from *Deinococcus radiodurans*. DNA Repair **9**:66-75.

## Bibliography

1. **Yeeles JT, Dillingham MS.** 2010. The processing of double-stranded DNA breaks for recombinational repair by helicase-nuclease complexes. *DNA Repair (Amst)* **9**:276-285.
2. **Freidberg EC, Walker GC, Siede W, Wood R, Schultz RA, Ellenberger T.** 2006. *DNA Repair and Mutagenesis*. ASM Press, Washington, D.C.
3. **Dillingham MS, Kowalczykowski SC.** 2008. RecBCD Enzyme and the Repair of Double-Stranded DNA Breaks. *Microbiol. Mol. Biol. Rev.* **72**:642-671.
4. **Kowalczykowski S, Dixon D, Eggleston A, Lauder S, Rehrauer W.** 1994. Biochemistry of homologous recombination in *Escherichia coli*. *Microbiol. Mol. Biol. Rev.* **58**:401-465.
5. **Wigley DB.** 2013. Bacterial DNA repair: recent insights into the mechanism of RecBCD, AddAB and AdnAB. *Nat. Rev. Microbiol.* **11**:9-13.
6. **Dixon DA, Kowalczykowski SC.** 1993. The recombination hotspot chi is a regulatory sequence that acts by attenuating the nuclease activity of the *E. coli* RecBCD enzyme. *Cell* **73**:87-96.
7. **Bianco PR, Tracy RB, Kowalczykowski SC.** 1998. DNA strand exchange proteins: a biochemical and physical comparison. *Frontiers in bioscience : a journal and virtual library* **3**:D570-603.
8. **Cox M, Battista J.** 2005. *Deinococcus radiodurans* - the consummate survivor. *Nat. Rev. Microbiol.* **3**:882-892.
9. **Slade D, Radman M.** 2011. Oxidative stress resistance in *Deinococcus radiodurans*. *Microbiol. Mol. Biol. Rev.* **75**:133-191.
10. **Krasin F, Hutchinson F.** 1977. Repair of DNA double-strand breaks in *Escherichia coli*, which requires recA function and the presence of a duplicate genome. *Journal of molecular biology* **116**:81-98.
11. **Resnick MA.** 1978. Similar responses to ionizing radiation of fungal and vertebrate cells and the importance of DNA doublestrand breaks. *Journal of theoretical biology* **71**:339-346.

12. **Lin J, Qi R, Aston C, Jing J, Anantharaman TS, Mishra B, White O, Daly MJ, Minton KW, Venter JC, Schwartz DC.** 1999. Whole-Genome Shotgun Optical Mapping of *Deinococcus radiodurans*. *Science* **285**:1558-1562.
13. **Makarova KS, Aravind L, Wolf YI, Tatusov RL, Minton KW, Koonin EV, Daly MJ.** 2001. Genome of the Extremely Radiation-Resistant Bacterium *Deinococcus radiodurans* Viewed from the Perspective of Comparative Genomics. *Microbiol. Mol. Biol. Rev.* **65**:44-79.
14. **Rocha EP, Cornet E, Michel B.** 2005. Comparative and Evolutionary Analysis of the Bacterial Homologous Recombination Systems. *PLoS Genet.* **1**:e15.
15. **Blasius M, Hubscher U, Sommer S.** 2008. *Deinococcus radiodurans*: What Belongs to the Survival Kit? *Critical Reviews in Biochemistry and Molecular Biology* **43**:221-238.
16. **Gutman P, Carroll J, Masters I, Minton K.** 1994. Sequencing, targeted mutagenesis and expression of *recA* gene required for the extreme radioresistance of *Deinococcus radiodurans*. *Gene* **141**:31-37.
17. **Spies M, Kowalczykowski SC.** 2005. Homologous recombination by RecBCD and RecF pathways, p. 389-403. *In* Higgins P (ed.), *The bacterial chromosome*. ASM Press, Washington, D.C.
18. **Daly M, Minton K.** 1996. An alternative pathway of recombination of chromosomal fragments precedes *recA*-dependent recombination in the radioresistant bacterium *Deinococcus radiodurans*. *J. Bacteriol.* **178**:4461-4471.
19. **Kim J-I, Cox MM.** 2002. The RecA proteins of *Deinococcus radiodurans* and *Escherichia coli* promote DNA strand exchange via inverse pathways. *Proc. Natl. Acad. Sci. U.S.A.* **99**:7917-7921.
20. **Kim J-I, Sharma AK, Abbott SN, Wood EA, Dwyer DW, Jambura A, Minton KW, Inman RB, Daly MJ, Cox MM.** 2002. RecA Protein from the Extremely Radioresistant Bacterium *Deinococcus radiodurans*: Expression, Purification, and Characterization. *J. Bacteriol.* **184**:1649-1660.
21. **Morimatsu K, Kowalczykowski SC.** 2003. RecFOR Proteins Load RecA Protein onto Gapped DNA to Accelerate DNA Strand Exchange: A Universal Step of Recombinational Repair. *Molecular Cell* **11**:1337-1347.

22. **Jolivet E, Lecointe F, Coste G, Satoh K, Narumi I, Bailone A, Sommer S.** 2006. Limited concentration of RecA delays DNA double-strand break repair in *Deinococcus radiodurans* R1. *Molecular microbiology* **59**:338-349.
23. **Repar J, Cvjetan S, Slade D, Radman M, Zahradka D, Zahradka K.** 2010. RecA protein assures fidelity of DNA repair and genome stability in *Deinococcus radiodurans*. *DNA Repair (Amst)* **9**:1151-1161.
24. **Norais CA, Chitteni-Pattu S, Wood EA, Inman RB, Cox MM.** 2009. DdrB Protein, an Alternative *Deinococcus radiodurans* SSB Induced by Ionizing Radiation. *J. Biol. Chem.* **284**:21402-21411.
25. **Wang J, Julin D.** 2004. DNA helicase activity of the RecD protein from *Deinococcus radiodurans*. *J. Biol. Chem.* **279**:52024-52032.
26. **Servinsky M, Julin D.** 2007. Effect of a recD mutation on DNA damage resistance and transformation in *Deinococcus radiodurans*. *J. Bacteriol.* **189**:5101-5107.
27. **Shadrick WR, Julin DA.** 2010. Kinetics of DNA unwinding by the RecD2 helicase from *Deinococcus radiodurans*. *J. Biol. Chem.* **285**:17292-17300.
28. **Bentchikou E, Servant P, Coste G, Sommer S.** 2010. A Major Role of the RecFOR Pathway in DNA Double-Strand-Break Repair through ESDSA in *Deinococcus radiodurans*. *PLoS Genet.* **6**:e1000774.
29. **Satoh K, Kikuchi M, Ishaque AM, Ohba H, Yamada M, Tejima K, Onodera T, Narumi I.** 2012. The role of *Deinococcus radiodurans* RecFOR proteins in homologous recombination. *DNA Repair (Amst)* **11**:410-418.
30. **Cao Z, Mueller CW, Julin DA.** 2009. Analysis of the recJ gene and protein from *Deinococcus radiodurans*. *DNA Repair (Amst)* **9**:66-75.
31. **Huang L, Hua X, Lu H, Gao G, Tian B, Shen B, Hua Y.** 2007. Three tandem HRDC domains have synergistic effect on the RecQ functions in *Deinococcus radiodurans*. *DNA Repair (Amst)* **6**:167 - 176.
32. **Kitayama S, Kohoroku M, Takagi A, Itoh H.** 1997. Mutation of *D. radiodurans* in a gene homologous to *ruvB* of *E. coli*. *Mutation research* **385**:151-157.
33. **Lloyd RG, Evans NP, Buckman C.** 1987. Formation of recombinant lacZ+ DNA in conjugal crosses with a recB mutant of *Escherichia coli* K12 depends on recF, recJ, and recO. *Molecular & general genetics : MGG* **209**:135-141.

34. **Matson SW, Robertson AB.** 2006. The UvrD helicase and its modulation by the mismatch repair protein MutL. *Nucleic acids research* **34**:4089-4097.
35. **Cao Z, Julin DA.** 2009. Characterization in vitro and in vivo of the DNA helicase encoded by *Deinococcus radiodurans* locus DR1572. *DNA Repair (Amst)* **8**:612-619.
36. **Zahradka K, Slade D, Bailone A, Sommer S, Averbeck D, Petranovic M, Lindner A, Radman M.** 2006. Reassembly of shattered chromosomes in *Deinococcus radiodurans*. *Nature* **443**:569-573.
37. **Barry ER, Bell SD.** 2006. DNA replication in the archaea. *Microbiology and molecular biology reviews* : MMBR **70**:876-887.
38. **Bell SD, Jackson SP.** 1998. Transcription and translation in Archaea: a mosaic of eukaryal and bacterial features. *Trends in microbiology* **6**:222-228.
39. **Kelman Z, White MF.** 2005. Archaeal DNA replication and repair. *Current opinion in microbiology* **8**:669-676.
40. **Blackwood JK, Rzechorzek NJ, Bray SM, Maman JD, Pellegrini L, Robinson NP.** 2013. End-resection at DNA double-strand breaks in the three domains of life. *Biochem. Soc. Trans.* **41**:314-320.
41. **Stracker TH, Petrini JH.** 2011. The MRE11 complex: starting from the ends. *Nature reviews. Molecular cell biology* **12**:90-103.
42. **Iyer LM, Makarova KS, Koonin EV, Aravind L.** 2004. Comparative genomics of the FtsK-HerA superfamily of pumping ATPases: implications for the origins of chromosome segregation, cell division and viral capsid packaging. *Nucleic Acids Res.* **32**:5260-5279.
43. **Constantinesco F, Forterre P, Elie C.** 2002. NurA, a novel 5'-3' nuclease gene linked to rad50 and mre11 homologs of thermophilic Archaea *EMBO reports* **3**:537-542.
44. **Blackwood JK, Rzechorzek NJ, Abrams AS, Maman JD, Pellegrini L, Robinson NP.** 2012. Structural and functional insights into DNA-end processing by the archaeal HerA helicase-NurA nuclease complex. *Nucleic Acids Res.* **40**:3183-3196.
45. **Chae J, Kim YC, Cho Y.** 2012. Crystal structure of the NurA-dAMP-Mn<sup>2+</sup> complex. *Nucleic Acids Res.* **40**:2258-2270.

46. **Constantinesco F, Forterre P, Koonin E, Aravind L, Elie C.** 2004. A bipolar DNA helicase gene, *herA*, clusters with *rad50*, *mre11* and *nurA* genes in thermophilic archaea. *Nucleic Acids Res.* **32**:1439-1447.
47. **Hopkins BB, Paull TT.** 2008. The *P. furiosus* Mre11/Rad50 Complex Promotes 5' Strand Resection at a DNA Double-Strand Break. *Cell* **135**:250-260.
48. **Zhang S, Wei T, Hou G, Zhang C, Liang P, Ni J, Sheng D, Shen Y.** 2008. Archaeal DNA helicase HerA interacts with Mre11 homologue and unwinds blunt-ended double-stranded DNA and recombination intermediates. *DNA Repair (Amst.)* **7**:380-391.
49. **Zhang C, Tian B, Li S, Ao X, Dalgaard K, Gokce S, Liang Y, She Q.** 2013. Genetic manipulation in *Sulfolobus islandicus* and functional analysis of DNA repair genes. *Biochem. Soc. Trans.* **41**:405-410.
50. **Fujikane R, Ishino S, Ishino Y, Forterre P.** 2010. Genetic analysis of DNA repair in the hyperthermophilic archaeon, *Thermococcus kodakaraensis*. *Genes Genet. Syst.* **85**:243-257.
51. **Takahashi NK, Kusano K, Yokochi T, Kitamura Y, Yoshikura H, Kobayashi I.** 1993. Genetic analysis of double-strand break repair in *Escherichia coli*. *J. Bacteriol.* **175**:5176-5185.
52. **Quaiser A, Constantinesco F, White MF, Forterre P, Elie C.** 2008. The Mre11 protein interacts with both Rad50 and the HerA bipolar helicase and is recruited to DNA following gamma irradiation in the archaeon *Sulfolobus acidocaldarius*. *BMC Mol. Biol.* **9**:25.
53. **Lundgren M, Bernander R.** 2007. Genome-wide transcription map of an archaeal cell cycle. *Proc. Natl. Acad. Sci. U.S.A.* **104**:2939-2944.
54. **Mimitou EP, Symington LS.** 2009. DNA end resection: Many nucleases make light work. *DNA Repair (Amst)* **8**:983-995.
55. **Wei T, Zhang S, Zhu S, Sheng D, Ni J, Shen Y.** 2008. Physical and functional interaction between archaeal single-stranded DNA-binding protein and the 5'-3' nuclease NurA. *Biochemical and Biophysical Research Communications* **367**:523-529.
56. **Tanaka M, Earl A, Howell H, Park M, Eisen J, Peterson S, Battista J.** 2004. Analysis of *Deinococcus radiodurans*'s transcriptional response to ionizing radiation and desiccation reveals novel proteins that contribute to extreme radioresistance. *Genetics* **168**:21-33.

57. **Lipton MS, Pasa-Tolic L, Anderson GA, Anderson DJ, Auberry DL, Battista JR, Daly MJ, Fredrickson J, Hixson KK, Kostandarithes H, Masselon C, Markillie LM, Moore RJ, Romine MF, Shen Y, Stritmatter E, Tolic N, Udseth HR, Venkateswaran A, Wong KK, Zhao R, Smith RD.** 2002. Global analysis of the *Deinococcus radiodurans* proteome by using accurate mass tags. Proc. Natl. Acad. Sci. U.S.A. **99**:11049-11054.
58. **Earl AM, Mohundro MM, Mian IS, Battista JR.** 2002. The IrrE Protein of *Deinococcus radiodurans* R1 Is a Novel Regulator of recA Expression. J. Bacteriol. **184**:6216-6224.
59. **Bergmans HE, van Die IM, Hoekstra WP.** 1981. Transformation in *Escherichia coli*: stages in the process. J. Bacteriol. **146**:564-570.
60. **Tirgari S, Moseley BEB.** 1980. Transformation in *Micrococcus radiodurans*: Measurement of Various Parameters and Evidence for Multiple, Independently Segregating Genomes per Cell. Journal of General Microbiology **119**:287-296.
61. **Davidson RC, Blankenship JR, Kraus PR, de Jesus Berrios M, Hull CM, D'Souza C, Wang P, Heitman J.** 2002. A PCR-based strategy to generate integrative targeting alleles with large regions of homology. Microbiology **148**:2607-2615.
62. **Bonura T, Smith KC.** 1975. Enzymatic production of deoxyribonucleic acid double-strand breaks after ultraviolet irradiation of *Escherichia coli* K-12. J. Bacteriol. **121**:511-517.
63. **Farrell L, Reiter H.** 1973. Phleomycin-Stimulated Degradation of Deoxyribonucleic Acid in *Escherichia coli*. Antimicrob. Agents Chemother. **4**:320-326.
64. **Moore CW.** 1989. Cleavage of Cellular and Extracellular *Saccharomyces cerevisiae* DNA by Bleomycin and Phleomycin. Cancer Res. **49**:6935-6940.
65. **Pan SS, Iracki T, Bachur NR.** 1986. DNA alkylation by enzyme-activated mitomycin C. Molecular pharmacology **29**:622-628.
66. **Tomasz M, Lipman R, Chowdary D, Pawlak J, Verdine GL, Nakanishi K.** 1987. Isolation and structure of a covalent cross-link adduct between mitomycin C and DNA. Science **235**:1204-1208.
67. **Imlay JA, Chin SM, Linn S.** 1988. Toxic DNA damage by hydrogen peroxide through the Fenton reaction in vivo and in vitro. Science **240**:640-642.

68. **Breen AP, Murphy JA.** 1995. Reactions of oxyl radicals with DNA. Free radical biology & medicine **18**:1033-1077.
69. **Lloyd RG, Porton MC, Buckman C.** 1988. Effect of recF, recJ, recN, recO and ruv mutations on ultraviolet survival and genetic recombination in a recD strain of *Escherichia coli* K12. Molecular & general genetics : MGG **212**:317-324.
70. **Kuzminov A.** 1999. Recombinational Repair of DNA Damage in *Escherichia coli* and Bacteriophage  $\lambda$ . Microbiology and Molecular Biology Reviews **63**:751-813.
71. **Kaimer C, Gonzalez-Pastor JE, Graumann PL.** 2009. SpoIIIE and a novel type of DNA translocase, SftA, couple chromosome segregation with cell division in *Bacillus subtilis*. Molecular microbiology **74**:810-825.
72. **Biller SJ, Burkholder WF.** 2009. The *Bacillus subtilis* SftA (YtpS) and SpoIIIE DNA translocases play distinct roles in growing cells to ensure faithful chromosome partitioning. Molecular microbiology **74**:790-809.
73. **Kaimer C, Schenk K, Graumann PL.** 2011. Two DNA Translocases Synergistically Affect Chromosome Dimer Resolution in *Bacillus subtilis*. J. Bacteriol. **193**:1334-1340.
74. **Sherratt DJ, Arciszewska LK, Crozat E, Graham JE, Grainge I.** 2010. The *Escherichia coli* DNA translocase FtsK. Biochem. Soc. Trans. **038**:395-398.
75. **Grenga L, Luzzi G, Paolozzi L, Ghelardini P.** 2008. The *Escherichia coli* FtsK functional domains involved in its interaction with its divisome protein partners. FEMS Microbiol. Lett. **287**:163-167.
76. **Wang X, Possoz C, Sherratt DJ.** 2005. Dancing around the divisome: asymmetric chromosome segregation in *Escherichia coli*. Genes Dev. **19**:2367-2377.
77. **Wang L, Lutkenhaus J.** 1998. FtsK is an essential cell division protein that is localized to the septum and induced as part of the SOS response. Molecular microbiology **29**:731-740.
78. **Yu XC, Tran AH, Sun Q, Margolin W.** 1998. Localization of cell division protein FtsK to the *Escherichia coli* septum and identification of a potential N-terminal targeting domain. J. Bacteriol. **180**:1296-1304.



79. **Stouf M, Meile JC, Cornet F.** 2013. FtsK actively segregates sister chromosomes in *Escherichia coli*. *Proc. Natl. Acad. Sci. U.S.A.* **110**:11157-11162.
80. **Val ME, Kennedy SP, El Karoui M, Bonne L, Chevalier F, Barre FX.** 2008. FtsK-dependent dimer resolution on multiple chromosomes in the pathogen *Vibrio cholerae*. *PLoS Genet.* **4**:e1000201.
81. **Wang SC, West L, Shapiro L.** 2006. The bifunctional FtsK protein mediates chromosome partitioning and cell division in *Caulobacter*. *J. Bacteriol.* **188**:1497-1508.
82. **Espeli O, Lee C, Marians KJ.** 2003. A physical and functional interaction between *Escherichia coli* FtsK and topoisomerase IV. *J. Biol. Chem.* **278**:44639-44644.
83. **Steiner W, Liu G, Donachie WD, Kuempel P.** 1999. The cytoplasmic domain of FtsK protein is required for resolution of chromosome dimers. *Molecular microbiology* **31**:579-583.
84. **Yu XC, Weihe EK, Margolin W.** 1998. Role of the C terminus of FtsK in *Escherichia coli* chromosome segregation. *J. Bacteriol.* **180**:6424-6428.
85. **Diez AA, Farewell A, Nannmark U, Nystrom T.** 1997. A mutation in the *ftsK* gene of *Escherichia coli* affects cell-cell separation, stationary-phase survival, stress adaptation, and expression of the gene encoding the stress protein UspA. *J. Bacteriol.* **179**:5878-5883.
86. **Shimokawa K, Ishihara K, Grainge I, Sherratt DJ, Vazquez M.** 2013. FtsK-dependent XerCD-dif recombination unlinks replication catenanes in a stepwise manner. *Proc. Natl. Acad. Sci. U.S.A.* **110**:20906-20911.
87. **Eggington JM, Haruta N, Wood EA, Cox MM.** 2004. The single-stranded DNA-binding protein of *Deinococcus radiodurans*. *BMC Microbiol* **4**:2.
88. **Mennecier S, Coste G, Servant P, Bailone A, Sommer S.** 2004. Mismatch repair ensures fidelity of replication and recombination in the radioresistant organism *Deinococcus radiodurans*. *Mol Genet Genomics* **272**:460-469.
89. **Servant P, Jolivet E, Bentchikou E, Mennecier S, Bailone A, Sommer S.** 2007. The ClpPX protease is required for radioresistance and regulates cell division after gamma-irradiation in *Deinococcus radiodurans*. *Molecular microbiology* **66**:1231-1239.

90. **Pearl R, Reed LJ.** 1920. On the Rate of Growth of the Population of the United States since 1790 and Its Mathematical Representation. Proc. Natl. Acad. Sci. U.S.A. **6**:275-288.
91. **Slade D, Lindner AB, Paul G, Radman M.** 2009. Recombination and Replication in DNA Repair of Heavily Irradiated *Deinococcus radiodurans*. Cell **136**:1044-1055.
92. **Burton B, Dubnau D.** 2010. Membrane-associated DNA transport machines. Cold Spring Harb Perspect Biol **2**:a000406.
93. **Aussel L, Barre FX, Aroyo M, Stasiak A, Stasiak AZ, Sherratt D.** 2002. FtsK Is a DNA motor protein that activates chromosome dimer resolution by switching the catalytic state of the XerC and XerD recombinases. Cell **108**:195-205.
94. **Kaimer C, Graumann PL.** 2011. Players between the worlds: multifunctional DNA translocases. Current opinion in microbiology **14**:719-725.
95. **Wang X, Montero Llopis P, Rudner DZ.** 2013. Organization and segregation of bacterial chromosomes. Nature reviews. Genetics **14**:191-203.
96. **Thanbichler M.** 2010. Synchronization of chromosome dynamics and cell division in bacteria. Cold Spring Harb Perspect Biol **2**:a000331.
97. **Reyes-Lamothe R, Nicolas E, Sherratt DJ.** 2012. Chromosome replication and segregation in bacteria. Annu Rev Genet **46**:121-143.
98. **Sherratt DJ, Arciszewska LK, Crozat E, Graham JE, Grainge I.** 2010. The Escherichia coli DNA translocase FtsK. Biochemical Society Transactions **038**:395-398.
99. **Lidstrom ME, Konopka MC.** 2010. The role of physiological heterogeneity in microbial population behavior. Nat Chem Biol **6**:705-712.
100. **Lobo I.** 2008. Same Genetic Mutation, Different Genetic Disease Phenotype. Nature Education **1**:1.
101. **Kurimoto K, Saitou M.** 2011. A global single-cell cDNA amplification method for quantitative microarray analysis. Methods in molecular biology (Clifton, N.J.) **687**:91-111.